Journal Pre-proofs

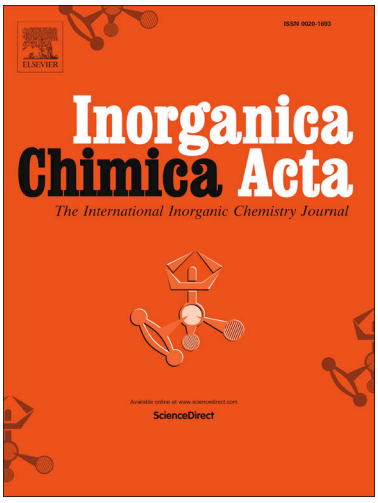

Review article

Photofunctional Metal-Organic Framework thin films for sensing, catalysis and device fabrication

Germán E. Gomez, Federico Roncaroli

PII: S0020-1693(20)31126-9
DOI: https://doi.org/10.1016/j.ica.2020.119926
Reference: ICA 119926

To appear in: *Inorganica Chimica Acta*

Received Date: 30 March 2020
Revised Date: 9 July 2020
Accepted Date: 22 July 2020

Please cite this article as: G.E. Gomez, F. Roncaroli, Photofunctional Metal-Organic Framework thin films for sensing, catalysis and device fabrication, *Inorganica Chimica Acta* (2020), doi: https://doi.org/10.1016/j.ica.2020.119926

Photofunctional Metal-Organic Framework thin films for sensing, catalysis and device fabrication

Germán E. Gomez[a,c] and Federico Roncaroli[b,c]*

[a]Instituto de Investigaciones en Tecnología Química (INTEQUI), área de Química General e Inorgánica, Facultad de Química, Bioquímica y Farmacia, Chacabuco y Pedernera, Universidad Nacional de San Luis, Almirante Brown 1455,

5700 San Luis, Argentina

[b]Departamento de Física de la Materia Condensada, Instituto de Nanociencia y Nanotecnología, Centro Atómico Constituyentes, Comisión Nacional de Energía Atómica (CNEA), Avenida General Paz 1499, (1650) San Martín, Buenos Aires, Argentina.

[c]Consejo Nacional de Investigaciones Científicas y Técnicas-CONICET. Godoy Cruz 2290 (1425), Ciudad de Buenos Aires, Argentina

*Corresponding author: email: roncaroli@cnea.gov.ar,

Tel: +54-11-6772-7681; fax: +54-11-6772-7121

Abstract

Metal Organic Frameworks (MOFs) constitute a developing class of materials constructed by metallic ions or inorganic clusters bridged by organic ligands, generating 2D or 3D extended porous crystalline structures. Their physical and chemical properties can be dramatically changed since the huge database of metal centers and type of ligands available for the design and construction MOFs. Besides,

the implementation of anchored MOF onto different substrates opens up to an emerging field of device fabrication for specific applications.

In this review we surveyed the recent progress and developments on MOF for sensing, catalylisis, photovoltaics, up conversion, and LED fabrication.

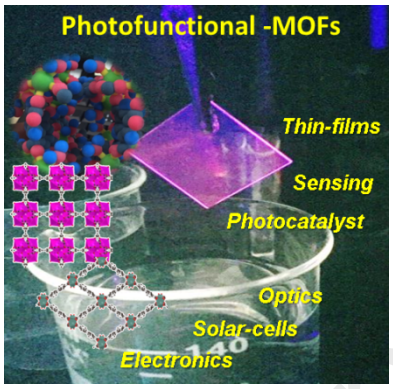

Keywords: sensing, luminescence, catalysis, solar cell, light emitting device, up conversion.

1. Introduction.

According to IUPAC recommendations of 2013 [1], a Coordination Polymer (CP) is defined as a coordination compound composed by repeating inorganic entities extending in one, two or three space dimensions. In addition, a Coordination Network can be extended in two or three dimensions. Moreover, a Metal-Organic Framework (MOF) is a coordination network where inorganic ions or clusters are coordinated by organic ligands giving rise supramolecular crystalline structures containing potential voids [1, 2]. Besides, the great possibility to choose the organic ligands and the metal ions allows the synthetic chemist to tune their structures, pore size, surface area and multiple functionalities in a rational way for a specific property [2, 3]. The inorganic units can be metal ions or oxo-clusters; the latter are widely designated as secondary building units (SBUs) [4], meanwhile the organic units (linkers/bridging-ligands) are commonly carboxylates, phosphonates, sulfonates, and heterocyclic compounds. In

this direction, promising and exciting applications of MOFs have been proposed for gas storage and separation [5, 6] , drug delivery [7], sensing [8], energy conversion and storage [9], catalysis [10-12] optoelectronic devices [13, 14] and water harvesting from air [15], among others.

The MOF science represents, in some way, an evolution of both the coordination chemistry and solid state chemistry. The coordination chemistry has a huge history devoted to Coordination Polymer research [16], and they can be formed by the *self-assembly* and chemical recognition processes between metallic ions and organic ligands (Figure 1). The most popular explored methodology to synthesize MOFs has been the conventional heating route by hidro/solvothermal approach; nevertheless there are other possibilities depending on the textural and crystalline properties for a desired material. The synthetic methodologies include the sonochemistry, microwave-assisted synthesis, electrochemistry, mechanochemistry, spray-dry aerosol and so on [17].

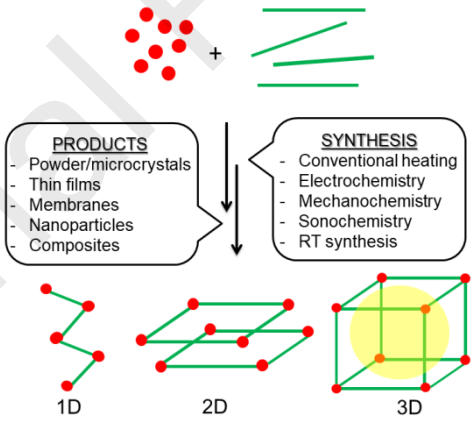

Figure 1. Scheme of the *self-assembly* process in MOFs synthesis. The green bars represent organic ligands meanwhile red circles represent metallic nodes. Traditional synthetic routes and potential products are highlighted.

Besides, many companies around the world paid attention in using MOFs for improving processes or developing prototypes of novel composites [18]. The interest for industrial applications of this type of materials started when the first patent entitled as "*Crystalline*

metalorganic microporous materials for purification of liquids and gases", was registered in 1995 and assigned to NALCO Chemical Company and the pioneer scientist Omar Yaghi [19]. Also, the german company BASF (Badische Anilin- und Soda-Fabrik) is other example of MOF production in large scale and, it has also patents for industrial applications (Basolite A100 [MIL-53-Al]), Basolite C300 (HKUST-1 or Cu-BTC), Basolite Z100H (MOF-5) and Basolite Z1200 (ZIF)).

Moreover, the term "MOF" was popularized by Prof. O. Yaghi by first time, when the laminar cobalt trimesate was reported exhibiting adsorptive properties [20, 21]. After this pioneer work, Yaghi and many other groups around the world obtained MOFs with particular crystalline open architectures with high porosities and surface area, such as IRMOF-n (isoreticular MOFs, n=0-16) [22], HKUST-1 (Hong Kong University of Science and Technology) [23], MIL-47 [24], MIL-53/MIL-88 (Materials Institute Lavoisier) [25], UiO-66 (University of Oslo) [26], ZIFs (Zeolitic Imidazolate Frameworks) [27] among others. Most of them are used as "benchmark structures" to demonstrate new synthetic routes as well as modifications to improve textural properties related to desired applications. A selection of most common MOFs studied in the field is shown in Figure 2.

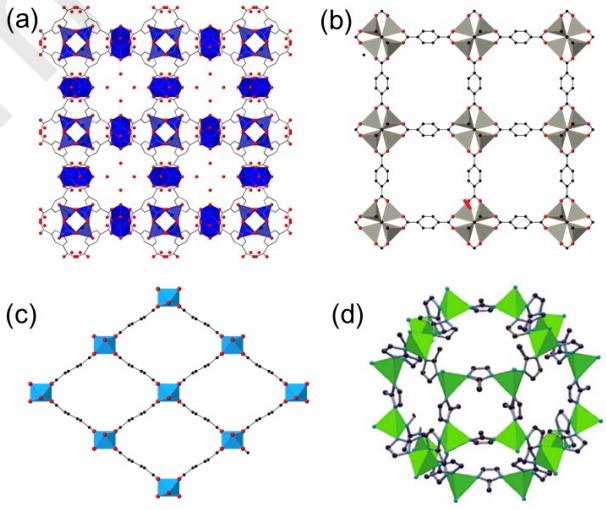

Figure 2. Representations of the most common studied MOFs in the literature: a) HKUST-1, b) MOF-5, c) MIL-53 and d) ZIF-8.

Due to the versatility of MOFs as tunable materials, they have been involved in plenty of modifications in order to explore novel applications. The *miniaturization* of crystals towards the micro or nano-scale has been a concept applied by MOF community during last decade [28] to study drug-delivery [29], bioimaging [30] and also for the construction of thin films [31]. Another methodology implemented in these materials is the post-synthesis modification [32] that allows to functionalize or chemically decorate MOFs structures with available groups useful for a particular property in powder MOFs, and even in thin films [33, 34].

Moreover, for uses in nanotechnology, it is mandatory that MOFs (usually obtained in the form of powders or crystals), are deposited on solid substrates, being particularly evident in the case of electrical applications [35]. According to specialized reviews [36, 37], it is distinguishable four types of MOF thin films:

1. SURMOFs (Surface-supported Metal–Organic Frameworks) fabricated using layer-by-layer (LBL) methodologies, where the orientation and film thickness can be well-controlled,

2. Electrochemically deposited MOF thin films,

3. MOF thin films made by using chemical vapor deposition and,

4. Casted MOF thin films, where nanosized crystalline powders produced by solvothermal synthesis are casted onto a pretreated substrate.

Comparing to the conventional solvothermal methods, the MOF thin film fabrication offers the possibility to obtain functional coatings at mild temperature conditions. Also, a number of factors impact the final thickness and quality of anchored MOF devices. In principle, the selection of the surface and further functionalization will determine the deposition on planar solid (e.g. Au, Si, Cu, ITO, FTO, etc), plastic or nonplanar substrates.

Chemical vapor deposition of films involves the adsorption and subsequent chemical reaction of gases with the surface of a substrate [38]. This approach offers the advantage of implement the deposition on curved or inner surfaces such as inside tubes.

Meanwhile, casted MOF thin films are fabricated from nanosized particles (typically colloids) previously obtained from solvothermal synthesis. By this approach, spin- or dip-coating can be used from suspensions containing nanoparticles. However, the challenge of this methodology is the correct election of molecular modulators in order to achieve MOF nanocrystals (20-100 nm) and then producing homogeneous coatings [39]. Besides, in electrochemically deposits, a metal electrode is oxidized to provide metal ions in a solution containing the ligand. The first case was explored with HKUST-1 resulting in films with remarkable homogeneity [40]. Most of the reported protocols for the deposition of MOF thin films involve chemical reactions occurring in organic solvents. However, solution-based fabrication of MOF thin films (LBL) has severe disadvantages due to potential contamination from the MOF reactant solutions [41]. This issue could be avoided in vacuum-based thin film deposition techniques (chemical vapor deposition and atomic layer deposition).

In spite of the fact that MOF thin films retain the intrinsic properties of the corresponding bulk MOFs, the possibility of also realizing multi-heteroepitaxy with a step-by-step layer by layer technique (see Figure 3), opens up additional architectures, including the creation of well-defined organic–inorganic interfaces [42]. Therefore SURMOFs allow the design of novel crystalline architectures that cannot be achieved using MOF powders.

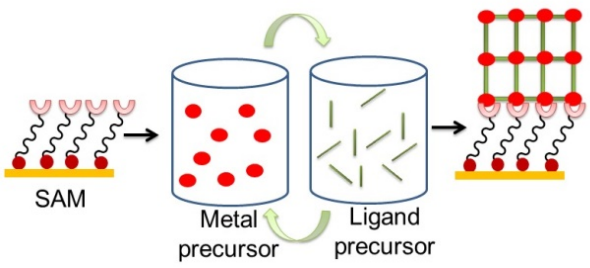

Figure 3. Schematic step-by-step approach for the growth of SURMOFs on a SAM-functionalized substrate. The approach involves repeated cycles of immersion in solutions of the metal precursor and solutions of an organic ligand. Between steps, the material is rinsed with solvent. [42] Reproduced by permission of The Royal Society of Chemistry.

A couple of groups have developed the basis for the construction of MOFs anchored onto substrates as devices for CO_2 reduction, water splitting, electronic, memristors, dielectrics, field-effect transistors, supercapacitors, batteries, membranes [36]. These novel systems were named as SURMOFs and consist onto MOF grown on chemically attached SAMs (Self-Assembly Monolayers) on solid substrates (see Figure 4). The nature of the SAMs depends on the length of the carbon backbone and also, by the terminal functional organic group (-COOH, $-NH_2$, $-CH_3$) that coordinates the metal centers of the MOF itself. For example, the iconic article reporting the synthesis of the first SURMOF [43], when a patterned SAM of 16-mercaptohexadecanoic acid and 1H,1H,2H,2H-perfluorododecane thiol on Au(111) was immersed into a clear reaction mixture typically used for synthesis of MOF-5 macrocrystals, a thin film of MOF-5 nanoparticles was obtained and selectively anchored at the carboxylate-terminated areas of the SAM, as shown in Figure 4.

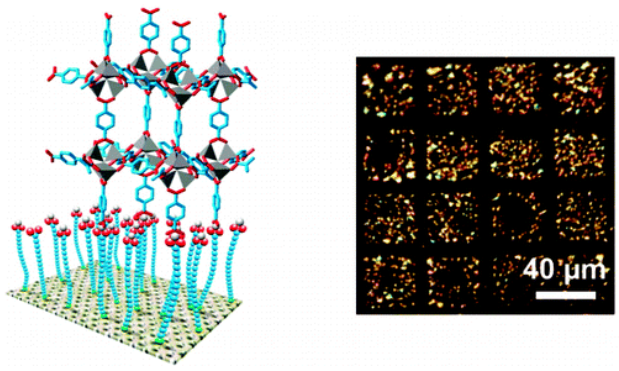

Figure 4. Conceptual representation of the SURMOF based on MOF-5 grown on a carboxylic acid-terminated SAM. The AFM figure reveals that virtually no crystallization

takes place on the CF_3- terminated stripes. Reprinted with permission from Reference [43]. Copyright 2005 American Chemical Society.

1.1. Generalities of luminescence.

In general, Photoluminescence or Luminescence is the process in which light is produced by photon absorption. Depending on multiple spin states during the radiative relaxation process, photoluminescence contains two basic forms, fluorescence and phosphorescence. The former refers to the emitting of light between energy states of the same spin multiplicity, and the process generally lasts no more than about 10 nanoseconds. However, the later refers to the emission of light between states with difference spin multiplicity, and the process lasts microseconds to seconds. All the absorption and emission processes between a ligand and an emitting center can be simplified in the Jablonski energy diagram shown in Figure 5. Photoluminescence can arise from direct organic ligand excitation, metal-centered emission (widely observed in lanthanide-MOFs through the so-called *antenna effect* or by direct excitation into the 4f levels) [44], or energy migration such as ligand-to-metal charge transfer (LMCT) and metal-to-ligand charge transfer (MLCT). In heterometallic systems is also found metal-to-metal charge transfer (MMCT) or, if there are aromatic ligands, ligand to ligand charge transfer (LLCT) can take place. Besides, guest molecules can also result in photoluminescence onto MOFs [45]. A representation of the diverse energy pathways in luminescent MOFs (LMOFs) can be found in Figure 6.

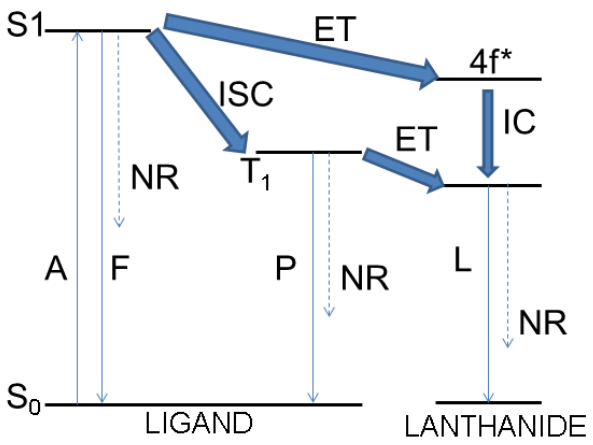

Figure 5. Jablonski diagram that summarizes the energy processes in MOFs. (L = lanthanide-centered luminescence; A=absorption; ISC = intersystem crossing; ET = energy transfer; IC = internal conversion; S = singlet; T = triplet; F=fluorescence; P=phosphorescence, NR = non radiative). Adapted with permission from Reference [44]. Copyright American Chemical Society.

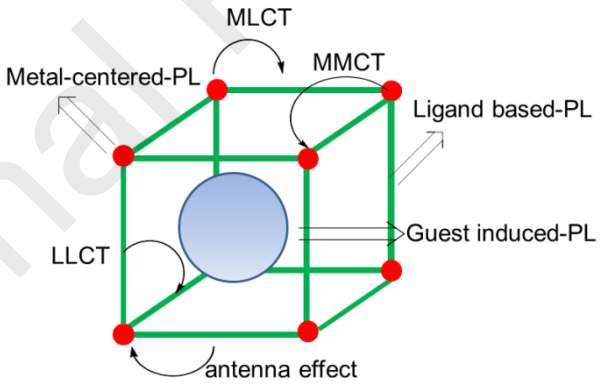

Figure 6. Scheme of the diverse mechanisms presented in luminescent-MOFs.

The nature of the building blocks as well as the structural features of a particular luminescent-MOF will determine the energy processes towards a major efficiency. In general, for an efficient energy transfer from the ligand to the metal (LMCT), a proper "antenna" ligand accompanied by a close excited state (singlet, S_1, or triplet, T_1 states) should match well to the emissive levels of the metal centers [46]. The antenna can be

any aromatic or hetero-aromatic highly π-conjugated system characterized by high capability of light absorption and high efficiencies of intersystem crossing and energy transfer processes. In order to ensure fast energy transfer in Ln-MOFs, a short distance between the antenna and the Ln^{3+} cations is advantageous; the best results can be obtained when the antenna directly coordinates the metal center. Another suitable situation of "antenna-effect" could be seen in chromophores contained within the luminescent-MOFs pores. In addition, the reversible uptake of aromatic molecules is an interesting feature for sensing applications. Nevertheless, the non-radiative processes are incremented with the presence of water molecules in the structure, as well as the proximity of the emissive centers that can quench the overall emission through non-radiative mechanisms [46].

In efforts to develop better photonic functional materials, MOFs have attracted much attention and achieved great experimental success, thus leading the MOF community to propose the concept of ''multiple photonic units'' [47] to highlight this unique feature of MOFs in photonics field. These components refer to the photo-responsive building blocks taking different forms, including organic ligands, metal ions or inorganic clusters, and guest species (dyes, QDs, etc) (Figure 7). Generally, photonic MOFs can be easily synthesized by selecting photo-responsive metal ions/clusters and organic ligands as building blocks.

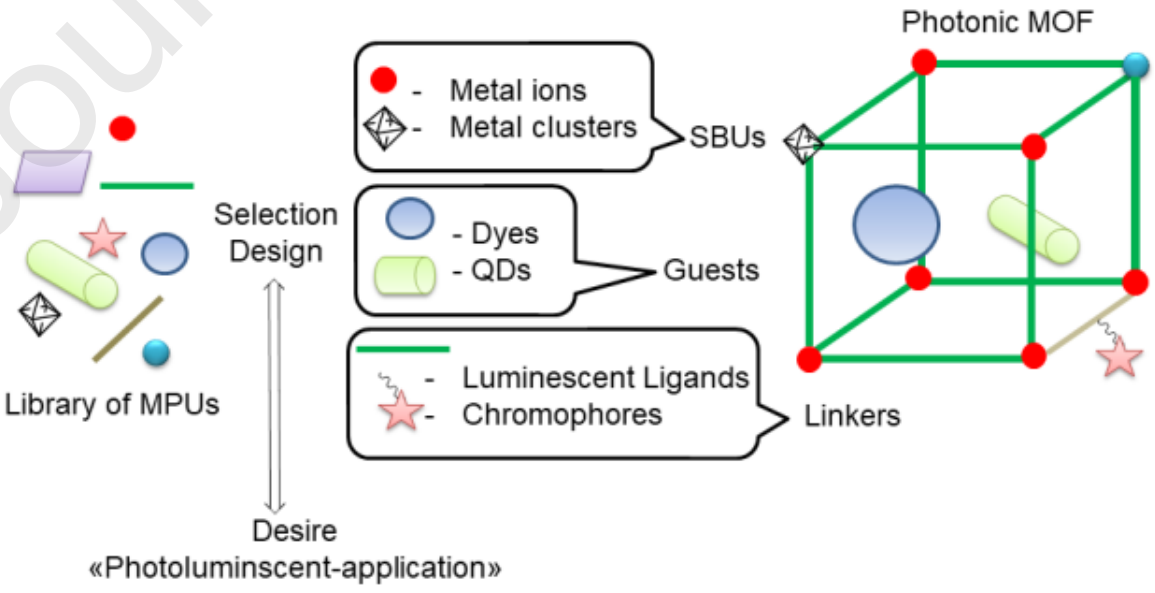

Figure 7. Representation of photo-responsive building blocks toward photonic MOFs.

Moreover, for a particular photonic application, it is relevant the use of computational techniques that support the experimental data and plausible mechanisms. Density function theory (DFT), a theoretical method applied for multi-electron system, presents an enormous potential in quantum chemical calculation domain and have been applied in research areas such as optimization of molecular structures, spectral analysis, energy spectrum interpretation, and calculation of activation barriers and LUMO/HOMO (Lowest Unoccupied Molecular Orbital/Highest Occupied Molecular Orbital) levels in luminescent MOFs [48]].

According to specialized reviews [44, 47, 49, 50] the photoluminescent properties from optical materials can be characterized by the following measurements:

- Luminescence spectra, which refers to the graph of luminescence intensity *vs* wavelength, I=f(λ).
- Overall quantum yield, $QY_{overall}$ (which gives the efficiency of the luminescence process and is defined as the ratio of the number of emitted photons released in the process of luminescence to the number of absorbed photons),

$$QY_{overall} = \frac{emitted\ photons}{absorbed\ photons} \qquad (1)$$

and,

- the observed lifetime (τ_{obs}). The τ_{obs} refers to the average time the molecule stays in its excited state before emitting a photon and is determined to be inversely proportional to the sum of the rate constants of the radiative (k^{rad}) and the non-radiative (k^{nr}) processes:

$$\tau_{obs} = \frac{1}{k^{rad} + \sum_n k_n^{nr}} \qquad (2)$$

The comprehensive analysis of these parameters in the context of the structural features corresponds to a common practice in reports devoted to luminescent-MOFs.

At this point, all the optical properties depend on the number of solvent molecules, the chemical environment, type of luminescent inorganic centers, the presence of aromatic moieties (from the ligand or molecules as guest molecules) and structural features.

2. Applications.

2.1. Solid-State Photoluminescence in MOFs.

The richness of metal ions/clusters and the large number of organic linkers have endowed great promise to explore sophisticated compounds with tunable photoluminescent properties [51]. Taking advantages of their high porosities, MOFs have also unique properties to serve as rigid/flexible hosts for the encapsulation of guest optical species such as dyes [52], lanthanide ions [53], quantum dots (QDs) [54], among others. As a consequence, hundreds of luminescent-MOFs have been synthesized and widely explored in recent years for their potential emerging applications such as solid-state light-emitting devices (LEDs) for white light and near infrared light emission, nonlinear optics (NLO) and 3D patterning and data storage.

From the material design point of view, lanthanides are exceptional candidates to obtain luminescent-MOFs, due to their electronic properties derived from the richness of the electronic levels, resulting in interesting optical properties [55]. Among lanthanides ions, Sm^{3+}, Eu^{3+}, Tb^{3+} and Dy^{3+} [56] are preferred for optical/optoelectronic device implementation due to their frequently long-lived intense and line-like emissions in the visible (orange, red, green and yellow respectively) and near-infrared region

(Nd^{3+}, Yb^{3+}, Er^{3+}, Ho^{3+}) [57]. For sensing properties, the luminescent-MOF has to exhibit promising solid state lighting *per se*. Depending on the nature of luminescent signal, the luminescent MOF could be classified in the following groups: metal centered emission, ligand centered emission and guest induced mission.

2.1.1. Metal centered emission.

In this case, the emission originates from electronic transitions of lanthanide metallic centers. Most lanthanide-MOFs have been tested for optical applications, due to their f-f transitions [58]. Besides, metal emission mediated by LMCT pathways is also a common route to evidence metal centered emission by employing aromatic ligands that could match the emitting levels from the metal centers. This cooperative process is commonly known as "antenna effect". This is the case of the family of compound $[Ln_2(BDC)_3(H_2O)_4]$ (BDC=1,4-benzenedicarboxylate; Ln= Y, La-Tm, except Pm) exhibiting a maximum $QY_{overall}$ of 43% for the Tb-compound [59].

On the other hand, the use of aliphatic ligands provides suitable platforms for metal centered emission through directly lanthanide excitation. We have reported luminescent MOFs constructed by our group [60-62], confirming that those containing Eu^{3+} and Tb^{3+} ions exhibit strong red ($^5D_0 \rightarrow ^7F_2$) and green ($^5D_4 \rightarrow ^7F_5$) emissions, respectively by direct excitation into the $^{2S+1}L_J$ electronic energy levels.

Moreover, during the last two decades there was an increased interest in exploring new luminescent-MOFs based on actinides such us U and Th from depleted nitrates or chlorides. U(VI) luminescent emission originates from a LMCT that excites an electron from nonbonding $5f_\delta$, $5f_\varphi$ uranyl orbitals to uranyl−oxygen bonding orbitals (σ_u, σ_g, π_u, π_g) [63], which is further coupled to "yl" vibrational ($S_{11} \rightarrow S_{01}$ and $S_{10} \rightarrow S_{0\nu}$ [ν = 0−4]) states of the U=O axial bond. In this sense, Gomez et al. [64] have obtained a new set of coordination polymers based on $[UO_2]^{2+}$ and 2,2'-bipyridine-3,3'-dicarboxylate and 2,2′:6′,2″-terpyridine ligands exhibiting optical properties. One of them exhibited a MOF structure with novel *geg1* topology (Figure 8). The suitable combination of two antenna

molecules and uranyl ions made possible to have green emission, with a maximum τ_{obs}=0.979 ms.

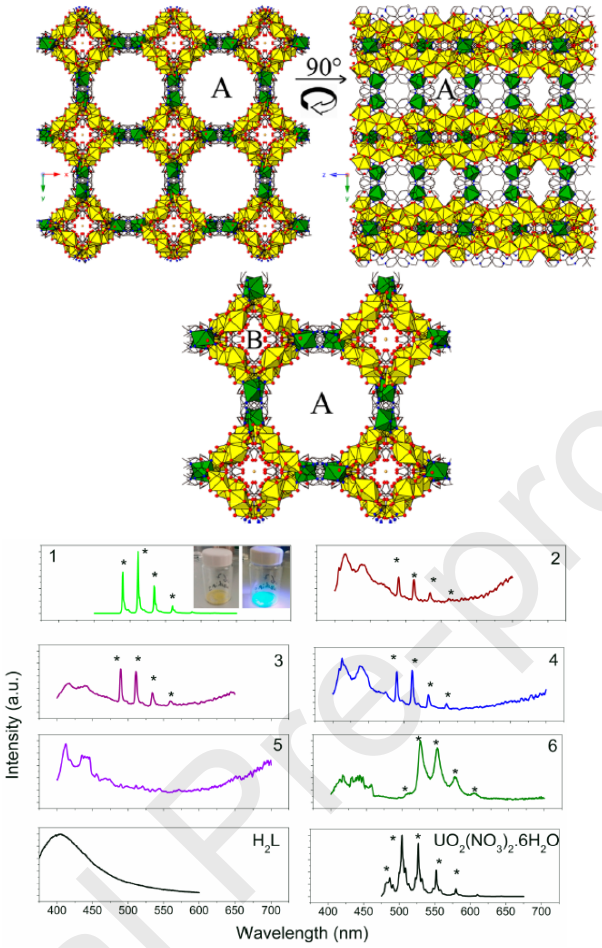

Figure 8. Crystalline structure (top) and solid-state luminescence (bottom) of a novel U(VI)-MOFs under direct ligand excitation (2,2'-bipyridine-3,3'-dicarboxylate and 2,2′:6′,2″-terpyridine). Reprinted with permission from Reference [64]. Copyright 2019 American Chemical Society.

In the field of photonics, solid state lighting is of importance for sensing in general. Thin films and SURMOFs have been constructed with this purpose, mainly based on lanthanide-MOFs. Guo and colleagues have reported a family of thin films based on co-doped $Eu_{1-x}Tb_x$-BTC nanoparticles [65] (see Figure 9). Firstly, the nanoparticles were prepared by coordination modulation employing acetate and oxalate to prevent the crystal growth. Small crystals, 90 ± 15 nm in length and 75 ± 10 nm in width were

obtained when sodium acetate was used as additive. After that, the nano-crystals were deposited by spin-coating at 4000 rpm, producing homogeneous thin films with thickness of ~ 8 μm. Thin films with diverse Eu/Tb ratio originated different luminescent response according the intensity variation of the $^5D_0 \rightarrow {}^7F_2$ (Eu^{3+}) and $^5D_4 \rightarrow {}^7F_5$ (Tb^{3+}) transitions (see Figure 9).

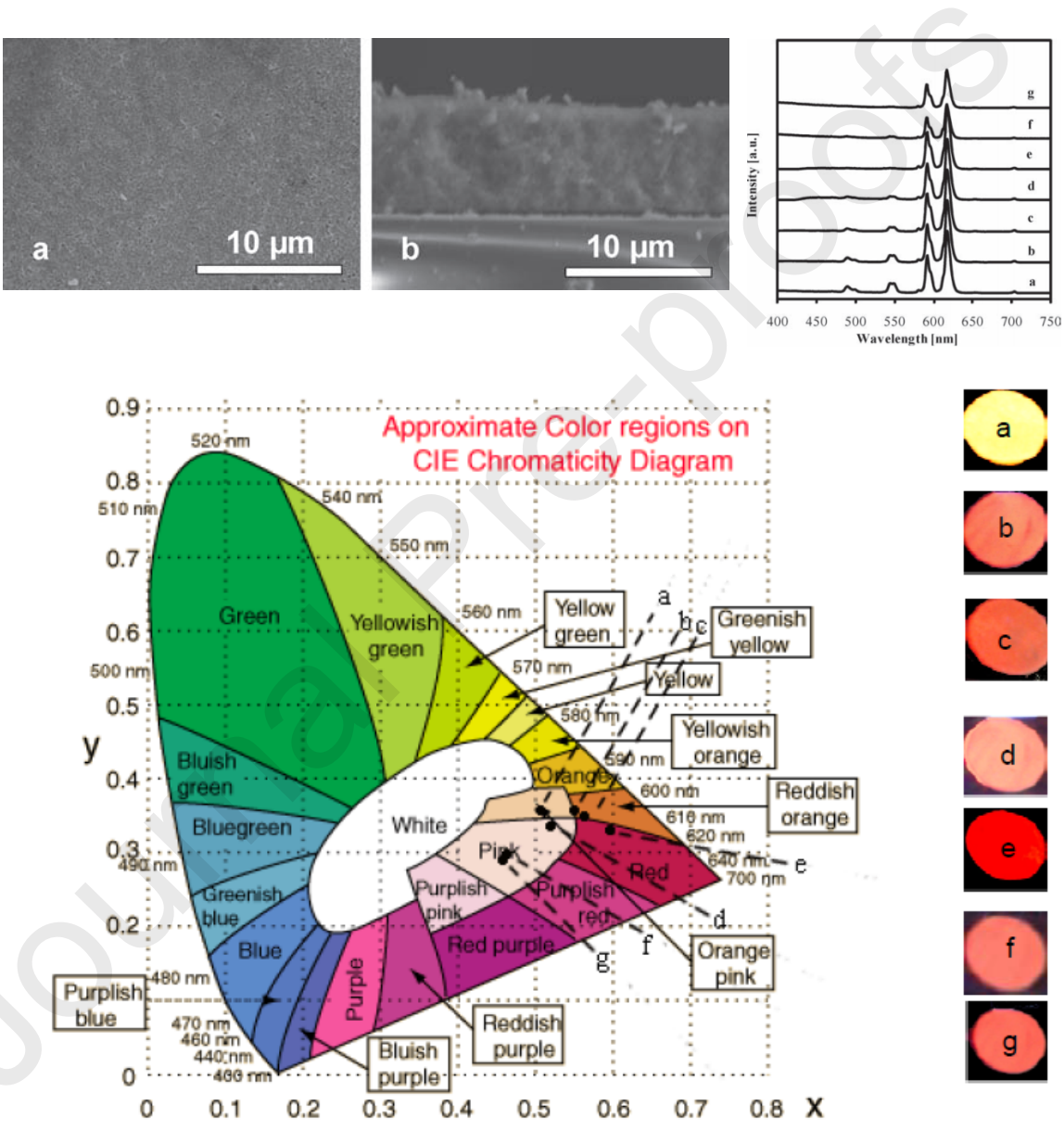

Figure 9. Top left: SEM images of $Tb_{0.5}Eu_{0.5}$-MOF film viewed from: (a) the surface and (b) the cross section. Top right: Luminescent spectra and CIE diagram of as-prepared $Eu_{1-x}Tb_x$-MOF films with Tb^{3+}/Eu^{3+} ratio of: (a) 2.75, (b) 2.44, (c) 1.95 (d) 1.46, (e) 1.02,

(f) 0.40 and (g) 0.30. Reprinted with permission from Reference [65]. Copyright 2010 Wiley-VCH.

Recently, Redel and Wöll et al. have successfully anchored the first Ln-MOF onto silicon and quartz substrates [66], demonstrating that heteroepitaxial Eu^{3+}/Tb^{3+} layer by layer approach produces ordered crystalline materials with desirable luminescent response, in comparison to the classic doping method with powders (Figure 10). These set of luminescent devices with a thickness of ~50 nm corresponding to the first type of SURMOF based on lanthanides with potential applications in photonics, optics and optoelectronics.

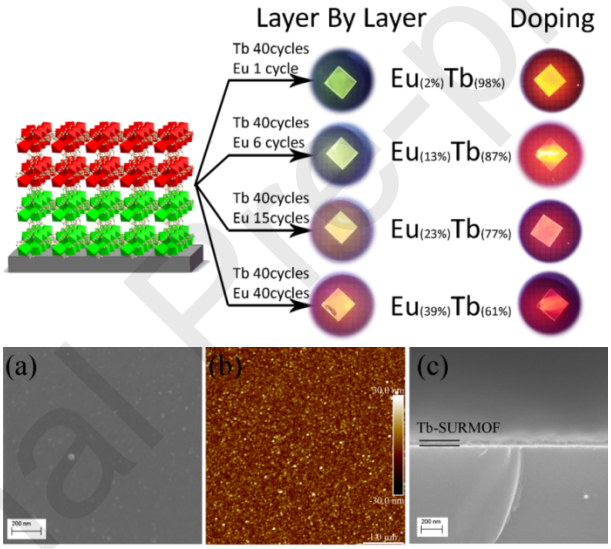

Figure 10. Top: Structure of Eu/Tb-SURMOF and tailorable emission colors' comparison between the thin films fabricated by the layer by layer approach as well as the doping method. Bottom: a) Top view of Tb-SURMOF (10 layers) recorded by SEM; b) AFM image of Tb-SURMOF (10 layers); c) Cross section of Tb-SURMOF (40 layers) recorded by SEM. Reprinted with permission from ref. [66]. Copyright 2019 Wiley-VCH.

2.1.2. Ligand centered emission.

This type of emission takes place when an organic molecule absorbs a photon of certain energy to produce fluorescence or phosphorescence (Figure 5). Generally, the

fluorescence emission from organic ligands corresponds to the transition from the lowest excited singlet state to the singlet ground state, and the transitions are either $\pi^* \rightarrow \pi$ or n $\rightarrow \pi$ transitions in nature, yielding bluish emissions. Nevertheless, the fluorescence parameters such as maximum emission wavelength and lifetime of organic linkers incorporated into the MOFs are often shifted from those of the free molecules. Also, there are luminescent-MOFs which exhibit ligand centered emission, characterized by blue-green light, being the cases of some d-block or main-group element based MOFs (Zn-MOFs and Bi-MOF) [67]. Moreover, compounds based on non-luminescent lanthanide ions such Ce^{3+}, Gd^{3+}, Y^{3+} and La^{3+} exhibits ligand centered emissions [68].

2.1.3. Guest induced mission.

Due to the highly regular channel structures and tunable pore sizes, MOFs can also be used as rigid or flexible hosts for the encapsulation of the guest luminescent species such as lanthanide ions and fluorescent dyes (see Figure 11). A series of lanthanide ion doped systems, Ln^{3+}@bio-MOF-1 (Ln^{3+} = Tb, Sm, Eu, or Yb), obtained from the as-synthesized bio-MOF-1 *via* cation exchange process (bio-MOF= Zn^{2+} 4,4'-benzenedicarboxylate) [53]. Besides, under excitation wavelength of 365 nm, the doped MOFs emitted their characteristic colors in the visible region (see Figure 11).

Moreover, the fluorescent dye rhodamine 6G, (Rh6G) (Figure 12) has been encapsulated into a large porous MOF, exhibiting temperature-dependent luminescent properties [69]. The guest-induced luminescence makes some MOF materials suitable for molecular detection and environmental probing.

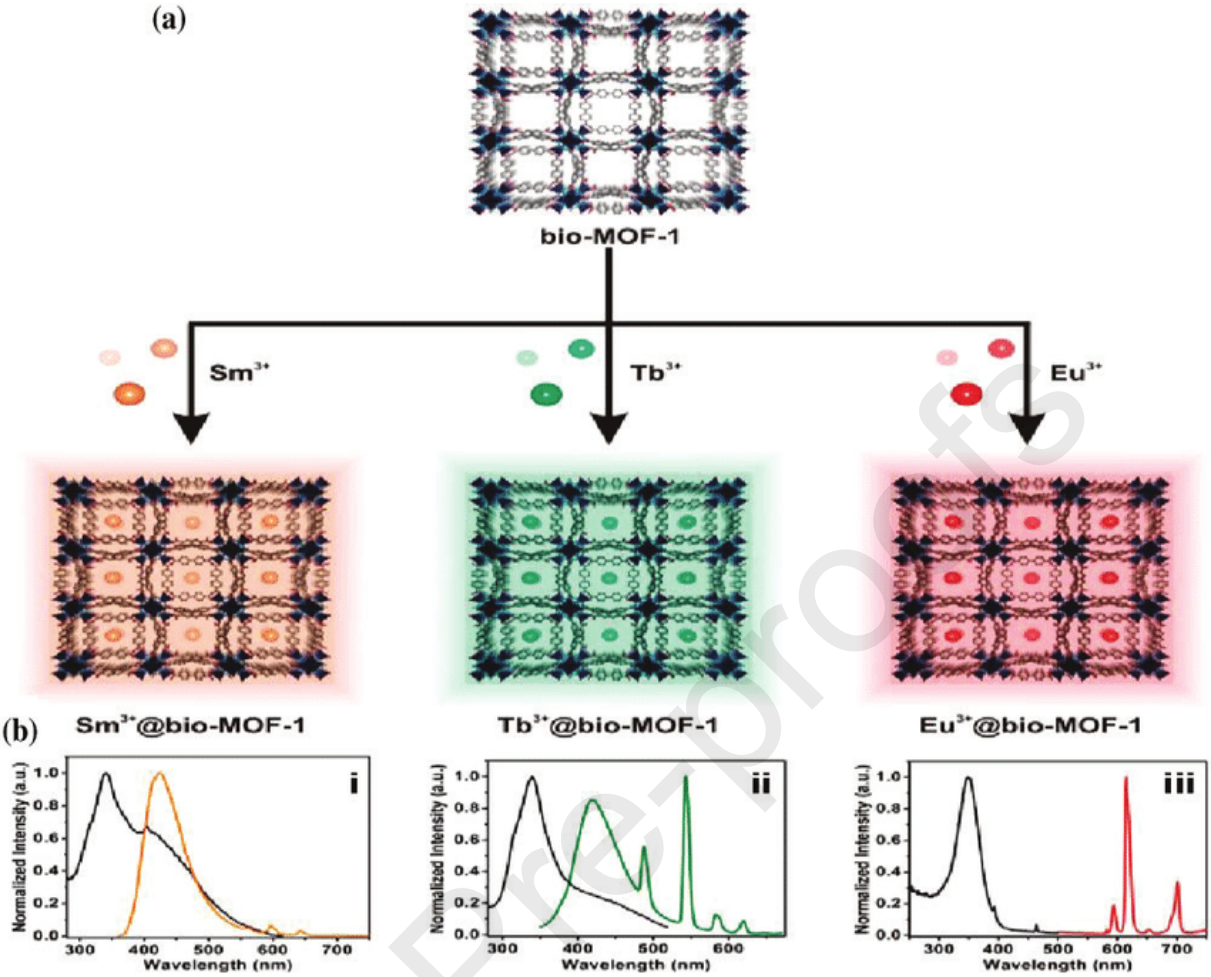

Figure 11. a) and b) Crystalline structure of Ln@bio-MOF-1 compounds (Ln^{3+}=Eu, Tb, Sm). c) Excitation (black traces) and emission spectra (colored lines) of Ln@bio-MOF-1 compounds. Reprinted with permission from Reference [53]. Copyright 2011 American Chemical Society.

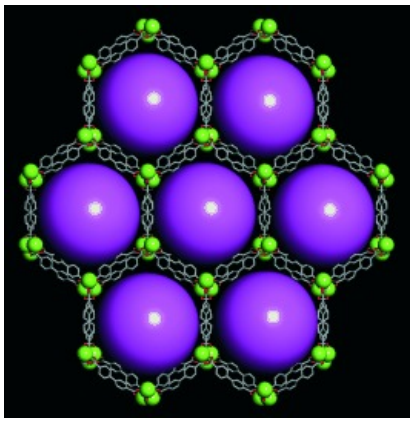

Figure 12. Representation of Rh6G@MOF. Reprinted with permission from ref. [69] Copyright 2007 Wiley-VCH

An interesting case was presented by Adachi and co-workers, in which a coronene molecule was encapsulated within the pores of a ZIF-8. This host–guest system shows phosphorescence with an exceptional large lifetime of 22 s at room temperature (Figure 13) [70]. In this work, the encapsulated coronene dyes are isolated in ZIF-8 pores, and the absence of direct coronene–coronene interactions strongly reduced quenching effects. In a related approach, guest-based emission in a SURMOF was explored by Baroni and colleagues [71]. In this work, an alternative strategy to enhance fluorescence from the tetraphenylethylene chromophores was developed. A chromophore with a tetraphenylethylene core was loaded as a guest into a porous Zn-BDC SURMOF so that the phenyl ring rotations were restricted, incrementing the rigido-chromism resulting in a bright green emission accompanied with a $QY_{overall}$ of ~50%. Moreover, the emissive regions could be patterned by inkjet printing.

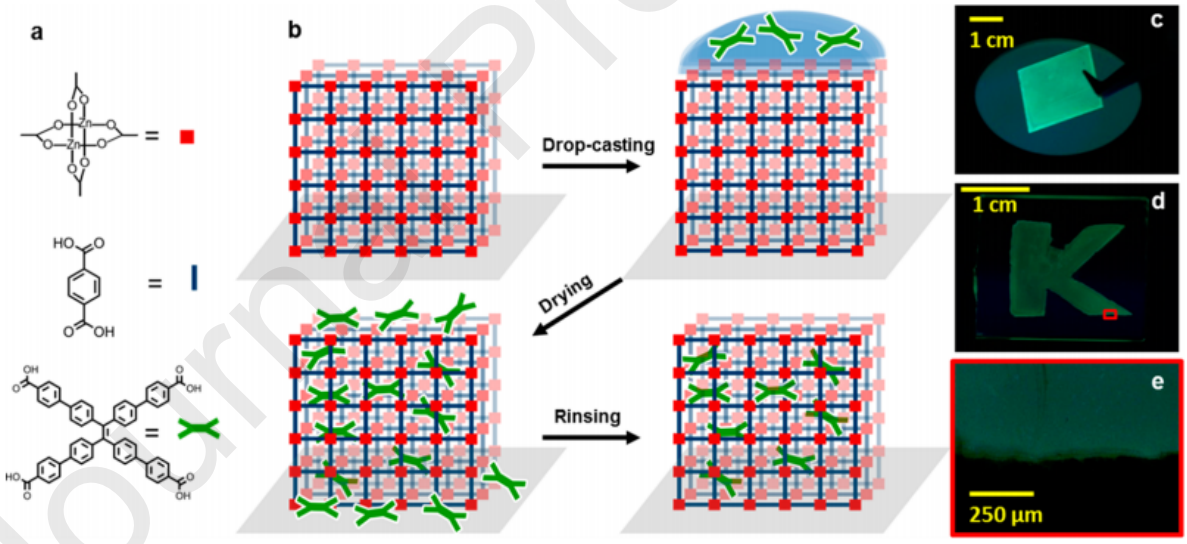

Figure 13. a) Chemical structures of the zinc cluster nodes (red square) and BDC linker (blue line) used to create the Zn-BDC structure as well as the tetraphenylethylene-based chromophore (green bow tie) that is loaded into the SURMOF. b) The process of postfabrication SURMOF loading by drop-casting with the chromophore. A SURMOF is fabricated on a substrate. c) A uniform SURMOF thin film

loaded with the chromophore exhibiting bright emission under UV light. d) and e) patterned SURMOF film with a "K"-shape loaded with the chromophore under UV excitation. Reproduced with permission from reference [71]. Copyright 2018 American Chemical Society.

Moreover, white light-emission can be achieved in luminescent MOFs by modulating factors such as lanthanide concentration, guest species, ligand structure or physical parameters (excitation wavelength and temperature) [72, 73]. A combinatorial approach is an effective strategy not only to achieve white light, but also to tune the characteristic emissions over a broad landscape of mixed lanthanide combinations in ternary lanthanide luminescent-MOFs [74]. The efficacy of the approach is exemplified by the great variety of emission colors showed in an extended family of isostructural luminescent-MOFs with the general formula, $[(Ce_{2-x-y}Eu_xTb_y(BDC)_3(H_2O)_4]$ [75].

One example of white light emissive device corresponds to Tb^{3+}@MOF thin films prepared by spin coating. The thin films were loaded with Tb^{3+} ions into the pores of Zn-based MOF. Also, the study showed that bi-metal-loaded Eu^{3+}/Tb^{3+}@MOF exhibited a Tb^{3+} induced luminescence of Eu^{3+} ions, and the resultant emissions fell in the white region by altering the ratio of Eu^{3+}/Tb^{3+} ions and the excitation wavelengths (Figure 14). A kind of white-lighting thin film based on Eu^{3+}/Tb^{3+}@MOF exhibited a chromaticity coordinate (0.338,0.323) was very close to the standard white light (0.333, 0.333) with a $QY_{overall}$ value of 10.03 % [76], upon excitation at 295 nm.

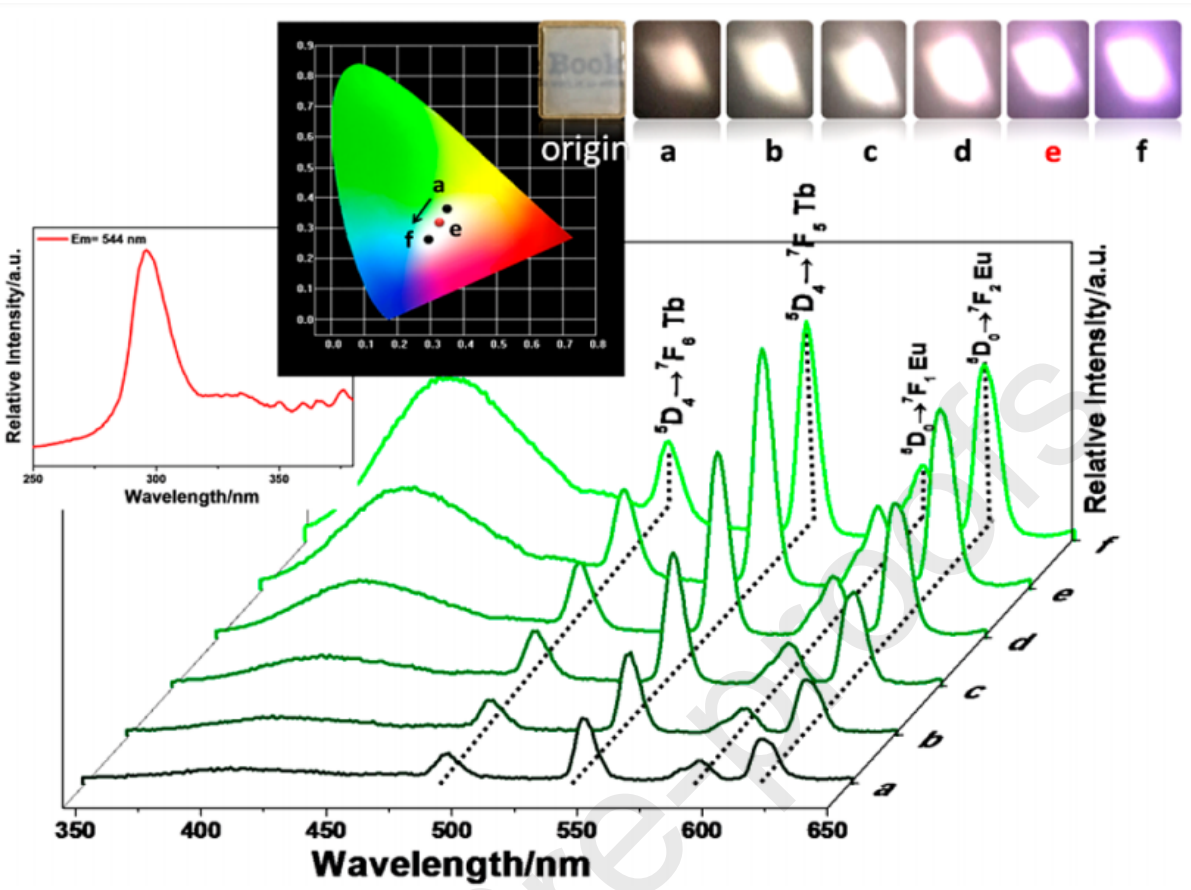

Figure 14. Emission spectra of a Tb^{3+}/Eu^{3+}@MOF thin film at different excitation wavelengths: a) 275 nm, b) 280 nm, c) 285 nm, d) 291 nm, e) 295 nm, f) 300 nm. Inset: CIE chromaticity diagram, the excitation spectrum of the thin film and images under different excitation wavelengths. Reproduced with permission from reference [76]. Copyright 2018 American Chemical Society.

2.2. Sensing properties.

In the case of MOF sensors, photoluminescence continues being the most preferred and easier property to study and interpret the interaction between the analyte and the sensor. The general pathways to construct or use sensors based on luminescent-MOFs are briefly described as follows [45]:

1. *Choice of target analyte*. Features such as size, charge and aggregation (vapor or liquid) will determine the further election of the luminescent-MOF.

2. *Choice of MOF-sensor*. Some research groups reproduce the synthesis of well-known open structures from the literature to ensure a correct guest-MOF interaction. However, for a new structure, if some of its building blocks are sensible under analyte exposition, some dense lanthanide-Coordination Compounds can be used for this application. This last feature is seen particularly in thermal-sensing.

3. *Physical/electrostatic interaction studies*. Once both the sensor and the analyte are selected, the influence of the target molecule on the luminescent signal is studied. Also, relevant parameters including the selectivity, sensitivity, response time and reproducibility are studied in order to establish the efficiency of the MOF-sensor.

In the present review, selected thermal and chemical sensing properties of luminescent-MOFs will be discussed.

2.2.1. Thermal-Sensing properties.

Thermal sensing and mapping in an accurate and non-invasive way are important features for the development of devices with applications in nano-science [77], especially in the optimization of photodynamic therapy. Also, for practical applications it is desirable to develop a sensor anchored onto a solid substrate, so thin films and SURMOFs have a prospective future in this emerging field.

Specific requirements for temperature monitoring in hardly accessible environments have prompted the development of several non-contact methods for temperature measurements, exploiting a change of optical properties, i.e. refractive index, emission intensity, wavelength shift, luminescence decay time, etc., with temperature [78].

In this context, lanthanide-MOFs have attracted particular interest, mainly for the possibility of tuning the color and spectroscopy by controlling the lanthanide doping, this being a “key” factor for thermo-sensor designing. In this sense, Eu^{3+} and Tb^{3+} ions [79] are useful for the development of physical and chemical heterometallic sensors based on the fluorescence intensity ratio (FIR) (equation 3) dependence along a

temperature range. For dual-center thermometers, the commonly used conversion of integrated intensity into temperature is made via the thermometric parameter, Δ:

$$FIR = \frac{I_1}{I_2} \quad (3)$$

where I_1 and I_2 are the integrated intensities of the two transitions. In this context, the thermometric parameter Δ takes the figure of the fluorescence intensity ratio (FIR) from two emission signals.

Also, the performance of luminescence thermometers is compared using the following parameters: 1) Relative thermal sensitivity, 2) Temperature uncertainty, 3) Spatial and temporal resolution and 4) Repeatability and reproducibility.

The relative thermal sensitivity S_r indicates the relative change of the thermometric parameter per degree of temperature change (equation 4):

$$S_r = \frac{1}{\Delta}\left|\frac{\partial \Delta}{\delta T}\right| \quad (4)$$

which can be calculated as the slope of the FIR curve *vs*. T. This parameter (expressed in units of % change per Kelvin of temperature change, $\%\cdot K^{-1}$) was defined by first time in 2003 in the context of optical fiber point temperature sensing [80] and has been used since 2012 as a figure of merit to compare different thermometers [77].

In the beginning of 2010 decade, the pioneer works of Cui et al. [81] have been the first in reporting a ratiometric thermometer employing a heterometallic 3D MOF platform based on DMBDC, $Eu_{0.0069}Tb_{0.9931}$-DMBDC (Figures 15 and 16). Similar studies were carried out by comparing the thermal response of Eu-DMBDC and Tb-DMBDC. The linear trend for the mixed MOF in the 50-200 K range was T = 287.09 − 263.85 (I_{Tb}/I_{Eu}). After this report, there was an intense study regarding to the design of new thermometers based on luminescent-MOFs. The table 1 shows selected MOF-thermometers reported.

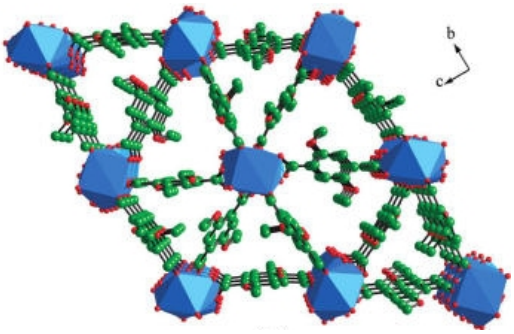

Figure 15. Crystal structure of Tb-DMBDC indicating the crystal packing viewed along the *a* crystallographic direction (Tb, blue polyhedra; C, green; O, red; H atoms are omitted for clarity). Reproduced with permission from Reference [81]. Copyright 2012 American Chemical Society.

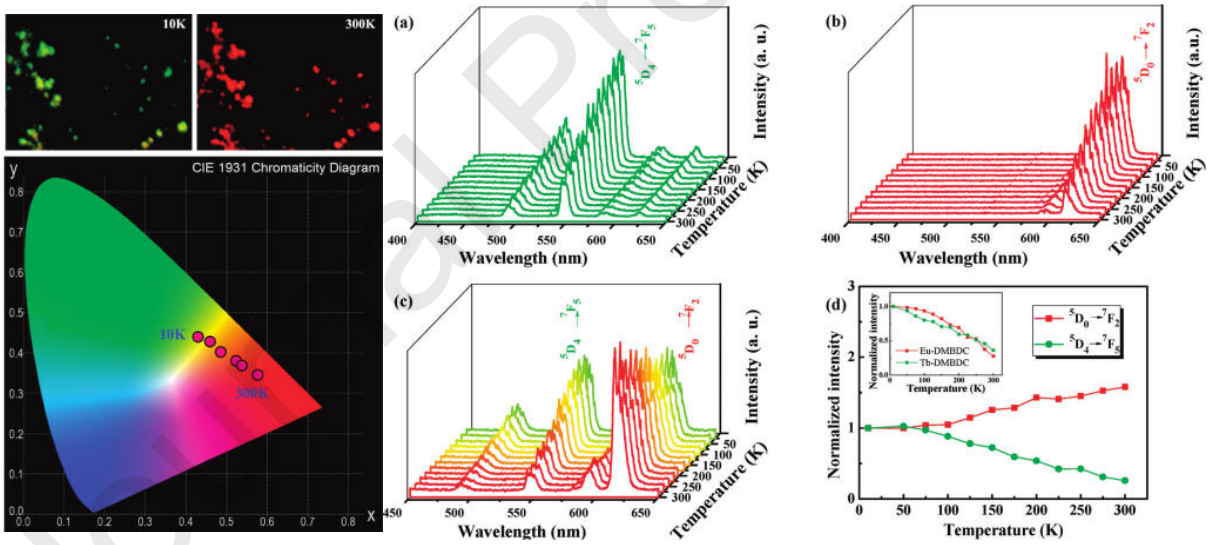

Figure 16. Left: Photograph of the luminescence of the co-doped $Eu_{0.0069}Tb_{0.9931}$-DMBDC powders between 10 K and 300 K (λ_{exc}= 312 nm). CIE chromaticity diagram showing the color luminescence of $Eu_{0.0069}Tb_{0.9931}$-DMBDC at different temperatures. **Right:** Emission spectra of (a) Tb-DMBDC, (b) Eu-DMBDC, (c) $Eu_{0.0069}Tb_{0.9931}$-DMBDC recorded in the 10-300 K range, and (d) temperature dependence of integrated intensities of the $^5D_4 \rightarrow {}^7F_5$ and $^5D_0 \rightarrow {}^7F_2$ transitions for $Eu_{0.0069}Tb_{0.9931}$-DMBDC. (Inset)

Temperature-dependent integrated intensity of the $^5D_4 \rightarrow {}^7F_5$ transition of Tb-DMBDC and $^5D_0 \rightarrow {}^7F_2$ transition of Eu-DMBDC. Reproduced with permission from Reference

MOF thermal sensor	ΔT (K)	S% (%intensity/K)	Ref.
$[(Eu_{0.0138}Tb_{1.9862})(DMBDC)_3(H_2O)_4]\cdot DMF\cdot H_2O$	50-200	0.38	[81]
$[Eu_{0.1}Tb_{0.9}(PIA)(HPIA)(H_2O)_{2.5}]$	100-300	3.53	[83]
$[Eu_{0.043}Tb_{0.957}(H_2cpda)(Hcpda)(H_2O)]\cdot 6H_2O$	40-300	not reported	[84]
$[Eu_2(QPTCA)(NO_3)_2(DMF)_4]\cdot(EtOH)_3 \supset$perylene	293-353	1.28	[85]
$[Eu_{0.025}Tb_{0.024}\ Y_{0.951}\ (succ)_{0.5}(slc)(H_2O)]$	10-270	0.43, 0.361	[58]
$[Eu_{0.01}Tb_{0.99}(BDC)_{1.5}(H_2O)_2]$	298-318	0.31	[86]
$[Eu_{0.086}Tb_{0.914}(pda)_3(H_2O)]\cdot 2H_2O$	10-325	5.96	[87]
$[Eu_{0.102}Tb_{0.898}(notpH_4)(NO_3)(H_2O)_2]\cdot 8H_2O$	20-300	3.9	[88]
$[Ln_{0.14}Gd_{6.86}(3,5\text{-}DSB)_4(OH)_9(H_2O)_{15}]\cdot 4H_2O$	10-300	32	[89]
$[Eu_{0.01}Tb_{0.99}(hfa)_3(dpbp)]$	200-450	0.83	[90]

[81] Copyright 2012 American Chemical Society.

In our context, Y-succ-slc compounds [58], the photoluminescence activity from cryogenic to room temperature was explored for Eu^{3+}/Tb^{3+} co-doped phases in terms of FIR, considering the $^5D_4 \rightarrow {}^7F_5$ Tb^{3+} hypersensitive transition. The resulting performance gave rise to linear or exponential decay behaviors. Therefore thermal sensitivity for one of the compounds was 0.43 $\%\cdot K^{-1}$ calculated in the 10–110 K range. Similar value (0.366% K^{-1}) was found for EuTb-PSA [82], whose FIR exhibited an exponential decay in the 13.5–313.5 K (in this case, the $^5D_0 \rightarrow {}^7F_2$ Eu^{3+} hypersensitive transition).

Table 1. Selected MOF thermal sensors based on FIR algorithms and parameters of interest: operating temperature range (ΔT), maximum sensitivity (S%).

$[Eu^{3+},Tb^{3+}@In(OH)(bpydc)]$	283-333	4.97	[91]
$[Eu_{0.2}Tb_{0.8}(L1)_2(COO)(H_2O)_2]\cdot H_2O$	40-300	0.17	[92]
$[Eu_{0.01}Tb_{0.99}(BDC)_{0,5}(DSTP)]\cdot 2H_2O$	77-275	3.9	[93]
$[Eu_{0.001}Tb_{0.999}$-BPDC-ad]	100-300	1.23	[94]
$Eu^{3+}@[Zr_6(\mu^3\text{-}O)_4(OH)_4(bpydc)_{12}]$	293-353	2.99	[95]
$[Eu_{0.13}Tb_{1.87}(HL_2)_2(H_2O)_3]\cdot 5.5H_2O$	4-50	31	[96]
$[Eu_{0.8}Tb_{1.2}(PSA)_3(H_2O)]$	13.5-313.5	0.366	[82]

Note: DMBDC=2,5-dimethoxy-1,4-benzenedicarboxylate; PIA=5-(pyridine-4-yl)isophthalate; EtOH=ethanol; DMF=N,N'-dimethylformamide; H_3cpda=5-(4-carboxyphenyl)-2,6-pyridinedicarboxylic acid; QPTCA=1,1':4',1'':4'',1'''-quaterphenyl-3,3''',5,5'''-tetracarboxylate; succ= succinate; slc= salicylate; BDC=1,4-benzenedicarboxylate; notpH_6=1,4,7-triazacyclononane-1,4,7-triyl-tris(methylenephosphoniacid); 3,5-DSB=disulfobenzoate; hfa=hexafluoro-acetylacetonate; bpydc=2,2'-bipyridine-5,5'-dicarboxylate; L1= 1,3-bis(4-carboxyphenyl)imidazolium; dpbp=4,4'-bis(diphenylphosphoryl) biphenyl; H_2DSTP= 2,4-(2,2':6',2''-terpyridin-4'-yl)-benzenedisulfonic acid; BPDC= 4,4'-bipheyldicarboxylate; ad = adeninate; L_2=5-hydroxy-1,2,4-benzenetricarboxylate; PSA= 2-phenylsuccinate.

2.2.2. Chemical Sensing properties.

Since the first work on chemical sensing using an open luminescent-MOF (Tb-BTC, BTC=1,3,5-benzenetricarboxylate) [97] based on the hypersensitive lanthanide transition towards fluoride detection, several Eu and Tb-MOFs have been extensively employed as unique platforms for sensing humidity [98], ions [99] and organics [100-102], as well as for detecting explosives as hazardous molecules [103] (see Figure 17). Besides, some sensing studies regarding the detection of explosives by luminescent-MOFs have emerged in the last five years, mainly motivated by finding new procedures and requiring more efficient methods. Employing luminescent-MOF sensors for the detection of highly explosive compounds is maybe one of their most promising

applications. Detection of these life-threatening materials plays a key role in homeland security, civilian safety and anti-terrorism operations, and thus has the ability to directly save human lives and protect the environment. The readers could check the very introductive review of Hu et al. where they can see many examples of explosive detection by employing luminescent-MOFs [104], which is not the main focus of the present contribution.

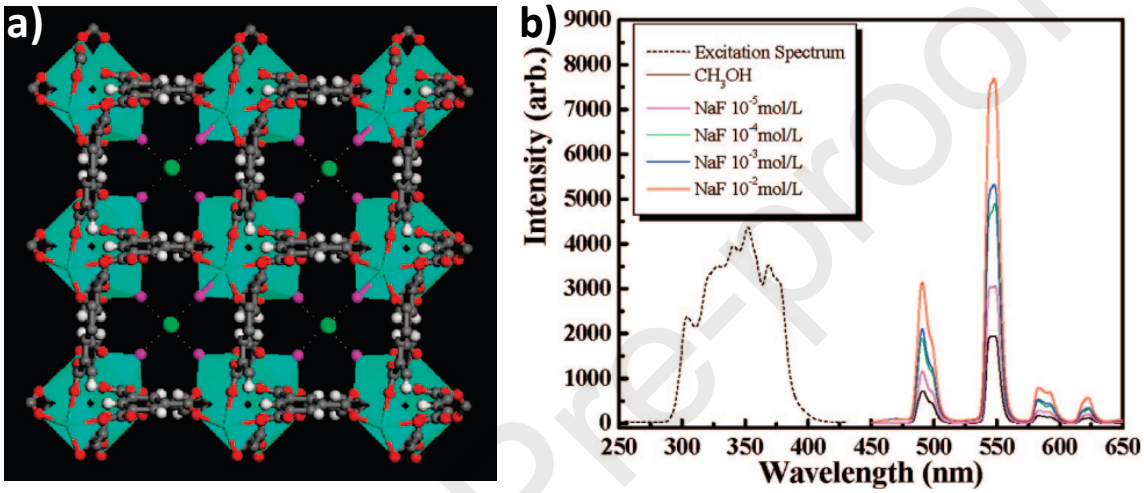

Figure 17. a) Crystalline structure of anion incorporated Tb-BTC activated in NaF with the model of fluoride (green) at the center of the channel. b) Photoluminescence spectra (solid) of anion incorporated Tb-BTC in different concentrations of NaF methanol solution. Reproduced with permission from Reference [97]. Copyright 2008 American Chemical Society.

Moreover, it is absolutely important to know the physicochemical nature of a given analyte for the consequent design of an effective MOF-sensor. In this sense, the LUMO energy from both the analyte and the sensor, determines the direction of electron transfer upon photoexcitation. This is especially useful in understanding the form of the luminescent response, whether it is quenching or enhancement [103]. Quantitative analysis of the quenching efficiency of a sensor can be achieved using Stern–Volmer equation (equation 5) [105]. In this relation I_0 is the emission intensity of the sensor

material before the addition of the quencher (analyte), and I_f is the intensity after the quencher is added. K_{SV} is the Stern–Volmer constant, usually associated with efficiency of the sensor.

$$\frac{I_0}{I_f} = 1 + K_{SV}[Q] \qquad (5)$$

Motivated by these attractive applications, our group has been studying some luminescent-MOFs for chemical sensing. First at all, Eu-msucc (msucc=2-methylsuccinate) was tested for sensing protic and aprotic solvents, basing on its strong luminescence due to the $^5D_0 \rightarrow {}^7F_2$ transition [62]. A dependence of the FIR values with the nature of the solvent was observed in the emission spectra; being particularly marked in the case of water exposition, producing a significant quenching effect (Figure 18). A solvent-size dependence of the quenching process was observed given that the feasibility of solvents to interact with the lanthanide centers is conditioned by the accessible volume of the 1D-channels. Analyte-lanthanide ion interactions may be inferred from the determination of energy transfer efficiency (η_{ET}) within the frame of Förster's dipole-dipole mechanism. In those cases, the following equation is useful to estimate the efficiency of transfer between the donor and the acceptor as equation (6).

$$\eta_{ET} = 1 - \left(\frac{\tau_{obs}}{\tau_0}\right) \qquad (6)$$

where τ_{obs} and τ_0 are the average lifetimes of the donor (Eu-msucc) in presence and in absence of the acceptor agents (solvents), respectively. The mechanism of photoluminescence quenching by vibrational coupling is based on the ability of certain atomic groups to consume part of the energy during the energy transfer (ET) process. Moreover, the chemo-sensing performance of the Tb/Y-succ-slc was tested employing protic and aprotic solvents [58], being the FIR and τ_{obs} the sensing parameters. The emissions suffered quenching when the material was suspended into acetone, n-hexane and toluene. In this case, acetone behaved as the most efficient quencher from

the employed aprotic solvents (Quenching Efficiency, QE = $(I_0 - I)/I_0$, of 98%). As it is expected, regarding protic solvents, water demonstrated to be the most efficient quencher (QE of 50%). The decrease in lifetime is consistent with the increase of the QE% values, where the sensor experiments a prominent quenching effect in solvents containing C–H and C=O groups compared with those containing O–H groups. These preliminary results set the basis for the elaboration of solvato-sensors containing lanthanide luminescent-MOFs devices.

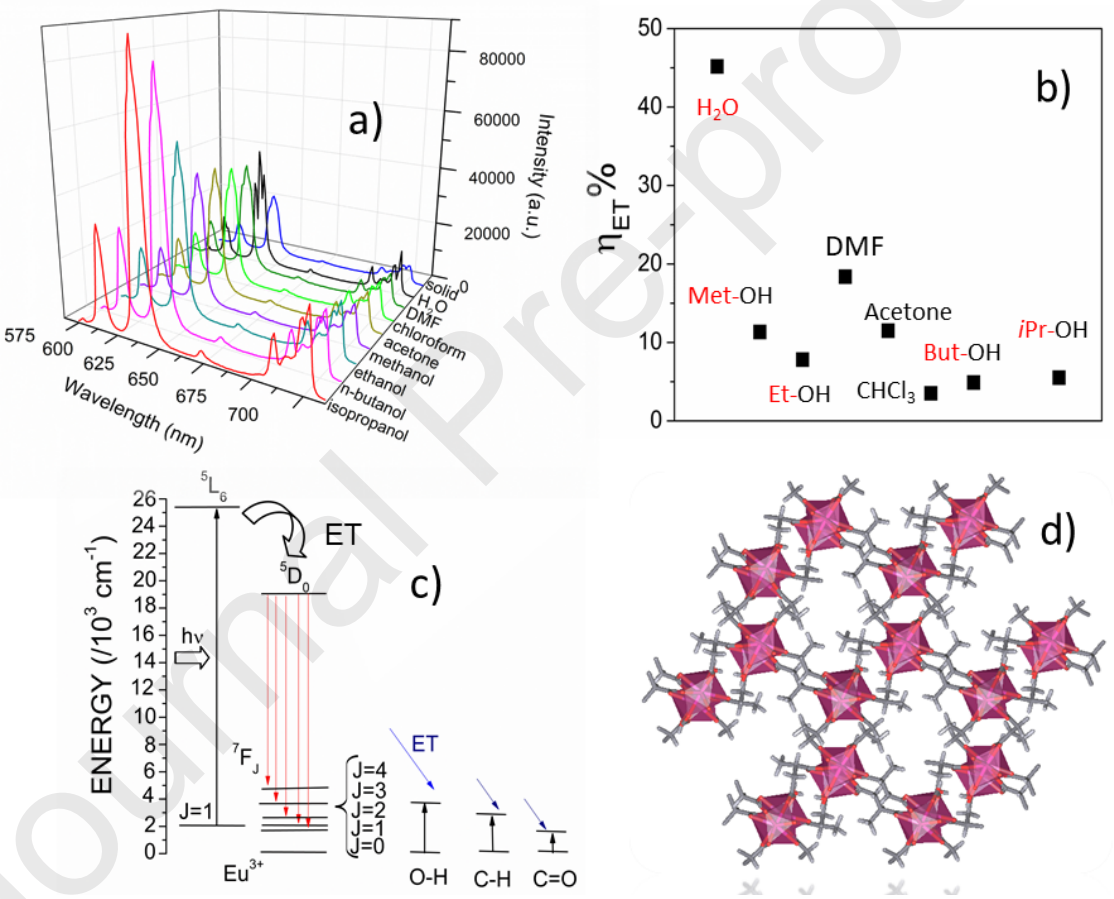

Figure 18. a) Emission spectra and b) energy transfer efficiency of Eu-msucc in different solvents. c) The mechanism of sensing and view of the Eu-msucc structure. Reproduced with permission from Reference [62]. Copyright 2017 Wiley-VCH.

Besides, it is worthy to mention that quantum chemistry is an excellent tool to study the diverse interaction between luminescent MOFs and the analytes. By this approach,

it is not only feasible to get the LUMO/HOMO energies from the different parts, but it is also possible to identify the sites of interaction in the MOFs. Recently a family of luminescent MOFs were reported as chemical sensors towards agrochemicals and ionic species derived from nuclear activity such as U(VI). The report presented the synthesis of Ln-BTC, Ln-BPDC and Ln-PSA (BTC=1,3,5-benzetricarboxylate, BPDC=4,4'-biphenyldicarboxylate, PSA=2-phenylsuccinate) for the detection of metsulfuron chlorpyrifos, chlorimuron, imazalil and uranyl in aqueous media [106]. By quantum chemistry calculations it was possible to characterize the sites from the herbicides interacting with the lanthanide centers (see Figure 19), and predict and justifying the energy transfer inside the MOFs.

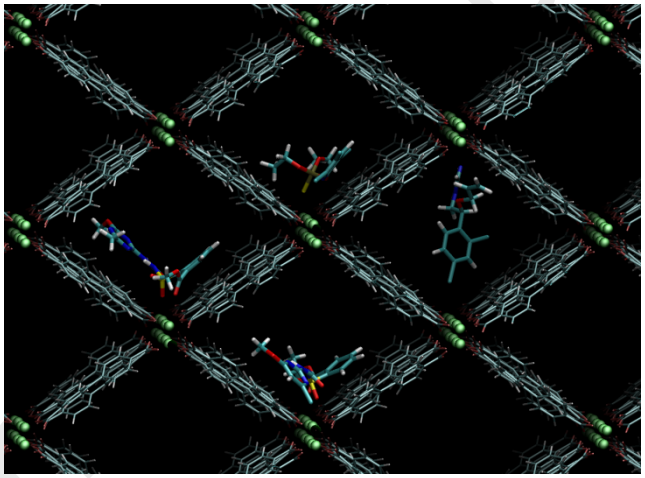

Figure 19. Model system of host–guest interaction constructed by Amber program, employing Eu-BPDC as sensor. (MOF dimensions (x,y,z): 100 Å × 60 Å × 58 Å). Reproduced with permission from Reference [106], published by MDPI, 2019.

The application of MOF optical films in sensing is accomplished following the changes in optical properties, typically changes in the reflectance spectra (or colors) caused by the interaction with target molecules [107].

Moreover, SURMOFs devices are suitable platforms for the fabrication of sensors, due the possibility of anchoring the MOFs onto diverse substrates, controlling the

thickness and then, the optical properties. This is the case of ZIF-8 thin film-based Fabry−Pérot device that was fabricated as a selective sensor for chemical vapors and gases (Figure 20). The ZIF-8 film was prepared by layer-by-layer approach employing silicon substrates yielding nanodevices of around 50 nm of cross section. Under different vapors exposure, the films exhibited a selective sensing towards n-propane. It could also detect the ethanol from water/ethanol system with a limit as low as 0.3 vol%, corresponding to an ethanol vapor concentration of ca. 100 ppm. The mechanism of sensor-analyte interaction is based on steric effect of analytes within the ZIF-8 pores [108].

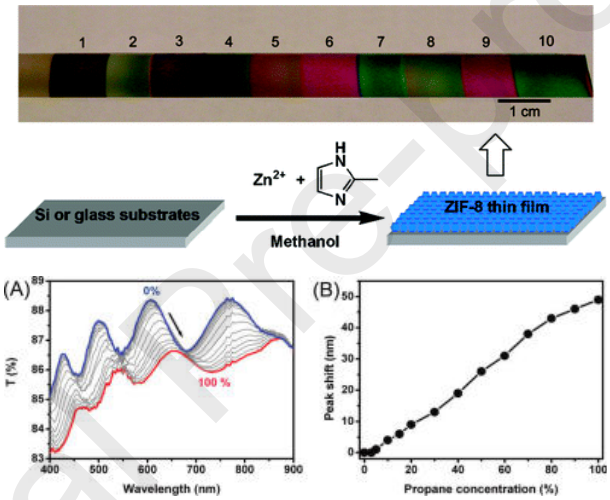

Figure 20. Top: Photograph of a series of ZIF-8 films of various thicknesses grown on silicon substrates. Bottom: A) UV-vis transmission spectra of 10-cycle ZIF-8 film grown on glass substrate after exposure to propane of various concentrations and B) corresponding interference peak shift (originally at 612 nm) versus propane concentration. Reproduced with permission from Reference [108]. Copyright 2010 American Chemical Society.

Compared with the rigid pore structure of ZIF-8, the pore structure of flexible MOFs can change more significantly after adsorbing water or organic vapors. Hu et al. chose the flexible NH_2-MIL-88B to fabricate a Fabry-Pérot device by spin-coating method [109].

The NH_2-MIL-88B photonic film displayed high chemical selectivity, i.e. acetone induced 380 nm red-shifts, while water only led to a red-shift of about 50 nm. Remarkably, the color change after absorbing the water or organic vapors (Figure 21) could be observed by the "naked eye". Depending on the nature of the organic solvent and their interaction with NH_2-MIL-88B, the selective "breathing behavior" of NH_2-MIL-88B promoted the excellent selectivity of the optical films.

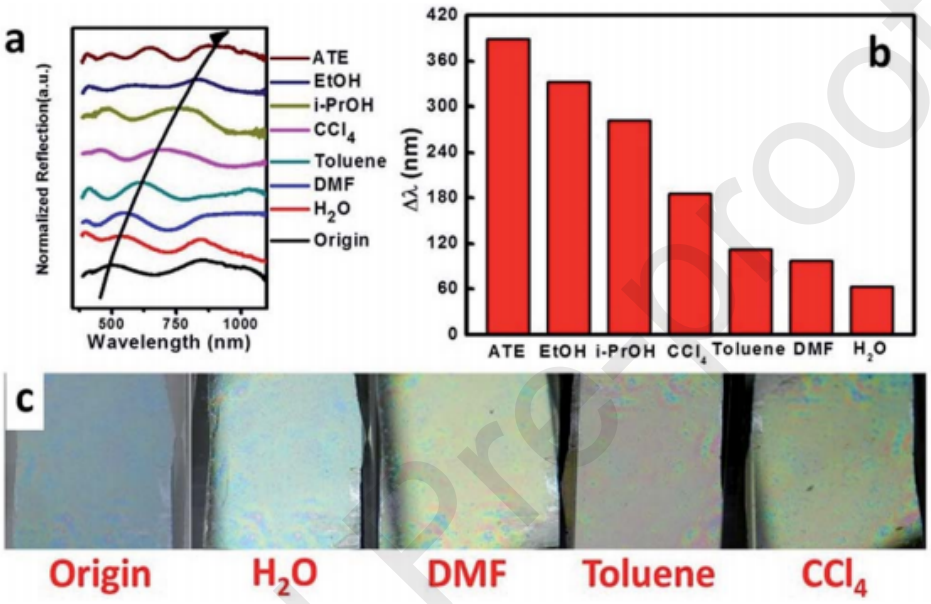

Figure 21. a) UV-Vis reflection spectra of the 4 wt% NH_2-MIL-88B photonic film deposited on a silicon wafer exposed to various vapors. b) Red-shift in film peak position upon exposure to various analytes. c) Photographs of the film upon exposure to various organic vapors. From Reference [109].Reproduced by permission of The Royal Society of Chemistry.

2.3. Photocatalysis.

The presence of metal sites, unsaturated in many cases, together with the presence of tunable pore sizes, make MOFs very suitable for catalysis of different reactions [110, 111]. However, only photocatalyzed reactions will be discussed within this review, particularly water reduction (H_2 evolution reaction, HER), water oxidation (O_2 evolution reaction, OER) and CO_2 reduction. The two first reactions constitute the water splitting.

On the other hand, the CO_2 reduction coupled to the O_2 evolution, represents the artificial photosynthesis [112]. Both water splitting and artificial photosynthesis are environmental and technological relevant in order to obtain solar fuels (H_2, methanol, methane, etc) in a sustainable way and reduce the amount on green-house effect gases, particularly CO_2 [112, 113]. Other photocatalyzed reactions, like organic transformations [114, 115] or pollutant degradation [116] will not be discussed in this review, although they are very relevant from an industrial and environmental point of view, the reader is directed to specialized literature [114, 115].

MOFs exhibit a very limited degree of delocalization over the extended structure, i.e.: orbitals are mainly localized. In this way, they behave more like molecular solids than actual semiconductors, where larger degree of delocalization is observed [117]. However, since the research on photocatalysis was initially developed with semiconductors like TiO_2, many of the concepts like valence band (VB) or conduction band (CB) are still used and extended to MOFs. Upon photon absorption in a semiconductor, one electron is promoted from the VB to the CB, an electron-hole pair is generated (e^--h^+) [113, 118]. From a molecular point of view, probably more accurate for MOFs, the electron would be promoted from the (HOMO) to the (LUMO). In many cases, these transitions have been proposed to be LMCT (or ligand to cluster charge transfer particularly for MOF-5 (Zn), MIL-125 (Ti), NH_2-MIL-125 (Ti)) [118]. The unwanted e^- -h^+ recombination would release the absorbed energy as heat to the environment. However, the energetic electron thus generated, could be employed in a reduction, for example to generate H_2. Usually, the electron has to be transferred to a co-catalyst, typically Pt or metallic nanoparticles, to improve the kinetics of H_2 evolution [113, 119, 120]. On the other hand, the photogenerated h^+ can be used to perform an oxidation reaction, for example organic molecules or water to O_2 [113]. In this last case, oxides or polyoxometalates (POM) are usually used as co-catalysts [120]. The transfer of the e^- to a metal or the h^+ to an oxide prevents e^- -h^+ recombination and drives unidirectionally the charge flow improving the photocatalytic efficiency [121].

Additionally, a sensitizer can be adsorbed on the semiconductor. It can be a dye, a complex or a MOF, which absorbs photons in the visible region and transfers the e^- to the semiconductor (see Figure 22). Photo oxidations and reductions have been extensively studied employing suspended MOFs in water, employing sacrificial reagents, typically triethanolamine for the reduction of water, or potassium persulfate for the oxidation of water [122], which will not be discussed in this work, since they were not deposited as films. Electrocatalyzed water splitting (electrolysis) has been successfully done with MOFs and materials derived from them, however, this is outside the scope of this revision [123].

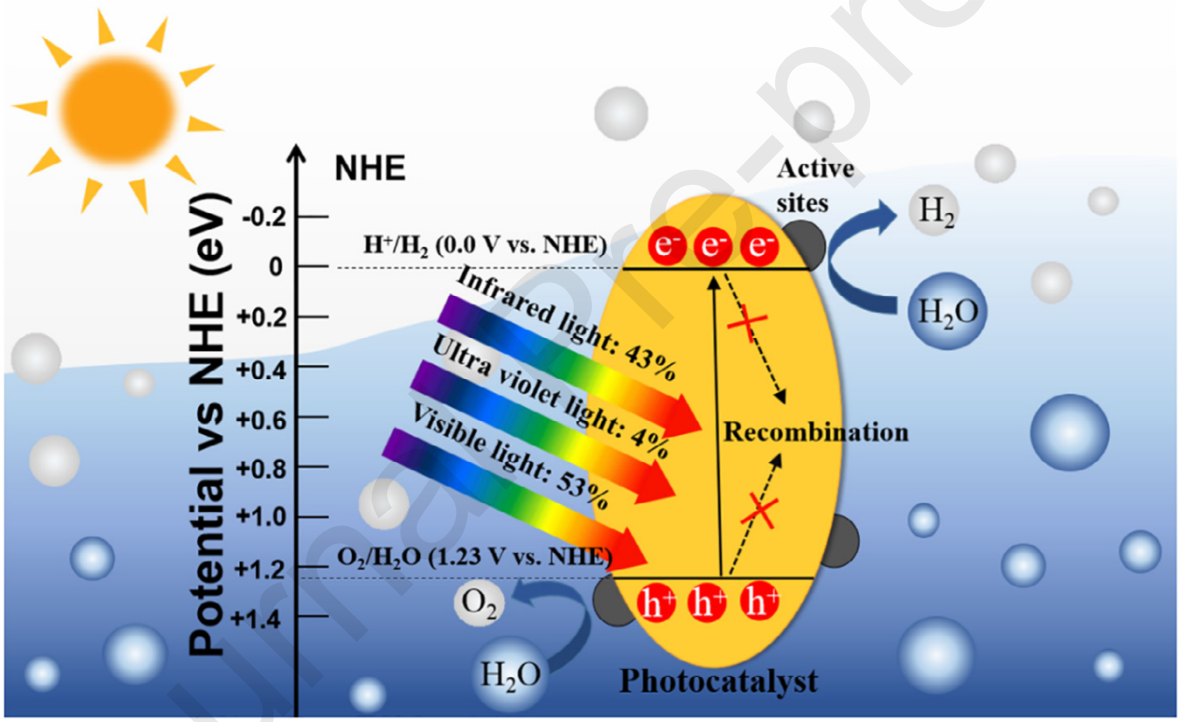

Figure 22. Scheme of the photocatalytic water splitting, employing co-catalyst for OER and HER. Reproduced with permission from [122]. Copyright 2020 ELSEVIER.

Catalyst deposition on substrates avoids its removal from the reaction medium at the end of reaction and they are more suitable for continuous processes in reactors, sensors, etc. [124]. However, MOF deposition as films for photocatalytic water splitting has been studied in much less extent than with suspended samples. For example, 2D

MOF nanosheets were grown using Pt(II) tetrakis(4-carboxyphenyl)porphyrin (Pt-TCPP) as the linker and Cu_2-$(COO)_4$ paddle-wheel clusters as the metal nodes. Employing polyvinyl pyrrolidone as surfactant allowed growing 2D MOF nanosheets instead of bulk crystals. They were drop-casted on glass or silicon wafers and ascorbic acid was used as sacrificial reagent. As a result of the presence of single atom active sites, the obtained films exhibited outstanding photocatalytic activity for H_2 evolution (11320 μmol g^{-1} h^{-1}) via water splitting under visible-light irradiation (λ>420 nm) and high cycling stability [125].

POM@MOF films (polyoxometalate $[(PW_9O_{34})_2Co_4(H_2O)_2]^{10-}$ on the porphyrinic MOF−545) have been deposited on Fluorine-doped Tin Oxide (FTO) substrates using electrophoretic or drop-casting techniques (see Figure 23). These films were tested for photocatalytic water oxidation, using persulfate as sacrificial oxidant. They exhibited turnover numbers of 1600 (drop-casting) and 403 (electrophoresis), which were higher than the one obtained with the bulk material suspended in water (70). This difference in catalytic activities was ascribed to the different proportion of efficiently illuminated crystallites. In this way, the POM catalyzed the water oxidation while the porphyrinic MOF was responsible for the high photon absorption [126]. For comparison, a metal free photocatalyst for overall water splitting (Cdot $–C_3N_4$) exhibited yields of 105 μmol g^{-1} h^{-1} for H_2 and 51.2 μmol g^{-1} h^{-1} for O_2, (quantum efficiency 6.3 % at 580 nm) and excellent stability. Higher yields and efficiencies were reported for other catalysts employing UV light [127]. This shows the potential that MOFs have as photocatalysts for water splitting, particularly employing visible light.

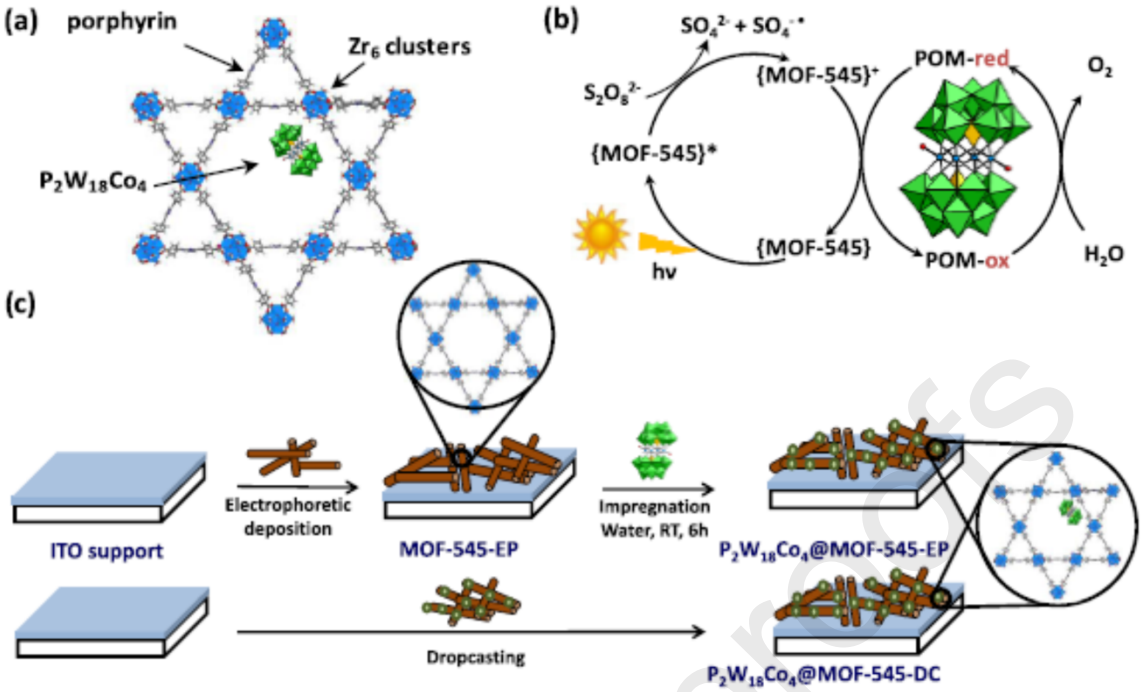

Figure 23. POM@MOF photocatalyst for O_2 evolution reaction. a) Scheme representing the composite with porous channels, POM catalyst and MOF (porphyrinic) sensitizer. b) Proposed mechanism for the photocatalytic O_2 evolution reaction. Reprinted in part with permission from [128]. Copyright 2018 American Chemical Society. c) Scheme of the photocatalyst deposition. Reprinted with permission from [126]. Copyright 2019 American Chemical Society.

The photoelectrochemical water splitting, i.e.: decomposition of water into H_2 and O_2 driven by both light and electricity has been studied quite extensively [129]. Typically, the photoelectrochemical cell consists in a photoanode, i.e. a transparent electrode (ITO = Indium Tin Oxide or FTO) covered by a semiconducting material (TiO_2, ZnO, $BiVO_4$, hematite, etc.) or a MOF (UiO-67, porphyrin based MOFs), on which a sensitizer or co-catalyst is usually grown (Ru-polypyridyl complexes, MIL-125(Ti) (see Table 2 and Figure 23), which would facilitate h^+ capture (i.e. charge separation) and avoid e^--h^+ recombination. The h^+ would oxidize the metal centers of the MOF to higher oxidation states capable of oxidizing water to O_2 [129]. Electrons generated in the semiconductor upon light absorption are transferred through the external circuit to the

cathode or counter electrode, usually made of Pt, on which the water reduction takes place. A bias potential has to be applied in order to make the reaction spontaneous. A third electrode is usually employed as reference electrode.

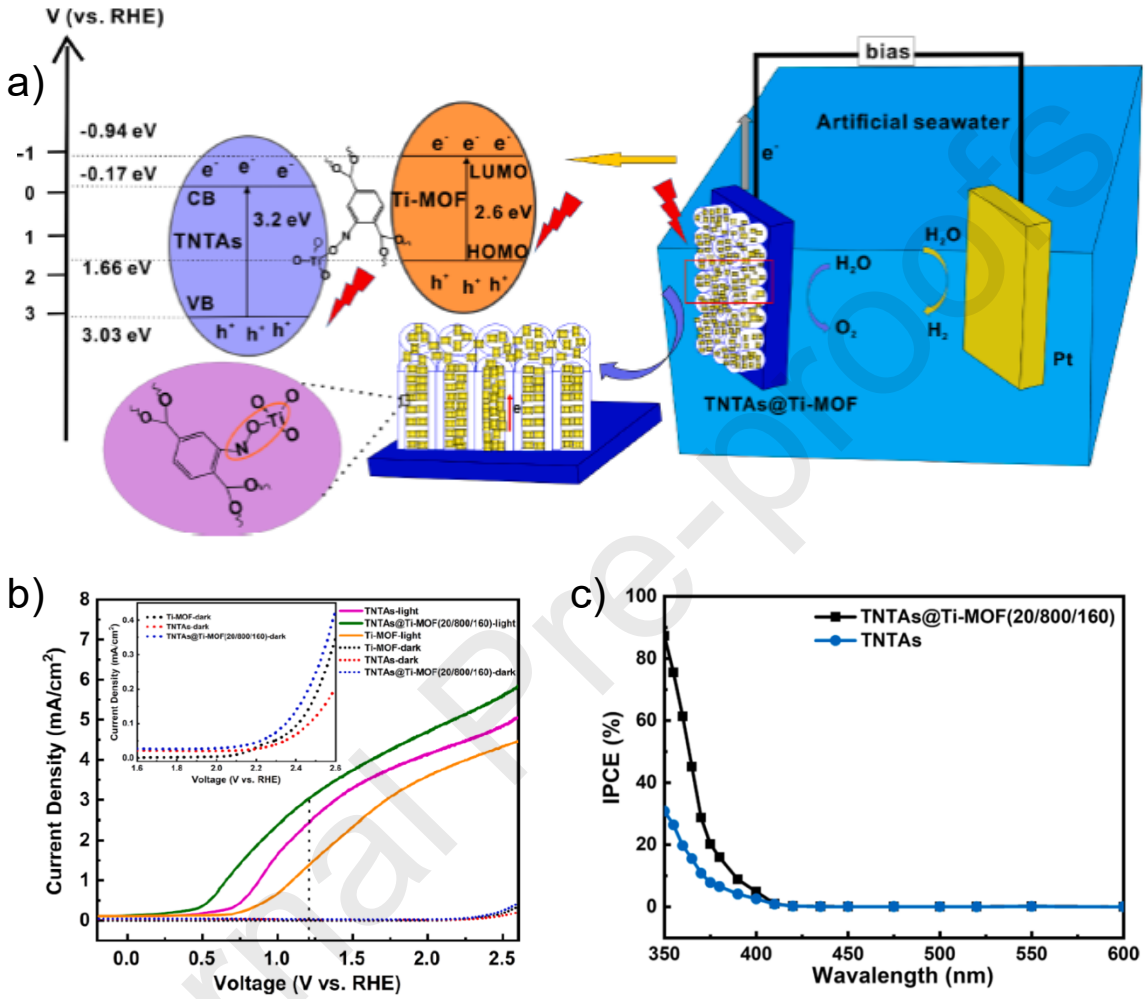

Figure 24. a) Scheme of the photoelectroncatalytic water splitting on the heterostructure of TiO_2 nanotubes@ MIL-125(NH_2)(Ti) composite photoanode. b) Linear sweep voltammogram of TiO_2 nanotubes assemblies with and without MIL-125(NH_2)(Ti), under illumination (solid line) and in darkness (dotted line). c) The incident photon-to-current conversion efficiency (IPCE) plot under monochromatic irradiation. Reprinted with permission from [130]. Copyright 2019 Elsevier.

The latest results on photoelectrochemical water splitting are summarized in Table 2. Most of the research has been conducted on the photoanode, where the O_2 evolution reaction takes place, since this reaction is kinetically slower than the H_2 evolution reaction [129]. Recently, employing a heterometallic CoNi-MOF modified $BiVO_4$ as photanode (BDC as ligand), a significantly high charge injection efficiency of 66.3 % (1.23 V vs RHE), charge separation efficiency *ca* 50 % (1.2 V vs RHE), incident photon-to-current conversion efficiency (IPCE) *ca* 30 % (450 nm) and absorbed photon to current efficiency (APCE) 39 % (430 nm) were achieved [131]. These parameters are much better than the semiconductor $BiVO_4$ without sensitizer [131]. The excellent photoelectrocatalytic performance was attributed to the MOF 3D nanostructure. The improved interface of CoNi-MOFs/$BiVO_4$ catalyst brought about effective charge separation and transport and afforded an enhanced photocurrent [131].

Table 2. Some recent results on photoelectrochemical water splitting.

	Semiconductor	Co- catalyst	Electrolyte	On set potential V vs RHE	IPCE	Current density	Ref.
Photoanode	TiO_2 nanowires	NH_2-MIL-125(Ti)/Au	0.5 M Na_2SO_4	0.35	20 %, 400 nm	30 µA cm $^{-2}$ at 0.75 V vs RHE	[132]
	α-Fe_2O_3 nanorods	Co-MeIm nanosheets	1.0 M NaOH	0.60	25 %, 375 nm	2.0 mA cm^{-2} at 1.23 V vs RHE	[133]
	Ti-doped Fe_2O_3	NH_2-MIL-101(Fe)	1.0 M NaOH	1.0	40 %, 375 nm	2.27 mA cm^{-2} at 1.23 V vs. RHE	[129]
	ZnO nanowires	Zn-Ni BDC	0.5 M Na_2SO_4	0.40		1.40 mA cm^{-2} at 1.0 V vs RHE	[134]
	TiO_2 nanorod	CoTCPP (Zr)	0.2 M Na_2SO_4	0.2	75 %, 380 nm	2.93 mA cm^{-2} at 1.23 V vs Ag/AgCl	[135]
	Fe-doped $BiVO_4$	MIL-53 (Fe)	0.1 M Na_2SO_4	0.44		3.5 mA cm^{-2} at 1.4V vs SCE	[136]
	Co-DPPP		1 M Na_2SO_4 pH 10	1.70		5.89 mA cm^{-2} at 1.65 V vs. RHE	[137]
	$BiVO_4$	CoNi- BDC	0.5 M Na_2SO_4	0.65	30%, 450 nm	3.2 mA cm^{-2} at 1.23 V vs. RHE	[131]
	Mo: $BiVO_4$	MIL-53(Fe)	0.2 M Na_2SO_4	0.5		2.2 mA cm^{-2} at 1.23 V vs.RHE	[138]
	TiO_2 nanotube	NH_2-MIL-125(Ti)	Sea water	0.5	90 % , 350 nm	3.04 mA cm^{-2} at 1.21 V vs. RHE	[130]
	TiO_2 nanorods	NH_2-MIL-125(Ti)	1 M NaOH	0.2	85 %, 350 nm	1.63 mA cm^{-2} at 1.23 V vs.RHE	[139]
	TiO_2 nanorods	MIL-100(Fe)	0.5 M Na_2SO_4	0.6	41 %, 390 nm	0.9 mA cm^{-2} at 1.6 V	[140]
	TiFe oxides nano structure	MOF-74 (Co)	1 M NaOH	0.9		1.74 mA cm^{-2} at 1.43 V vs. RHE	[141]
	$BiVO_4$	NiOOH /FeOOH	pH 7	0.2		2.73mA cm^{-2} at 0.6 V vs. RHE	[142]
Photo cathode	p-Si	Cobalt Dithiolene	pH 1.3 H_2SO_4	0.2		3.8 mA cm^{-2} at 0 V vs. RHE	[143]
	F-doped s glass	Ir/Pt (Zr porphyrinic MOF) hollow nanotubes				0.2 mmol g^{-1} h^{-1}	[144]
	FTO	MOF-525	11 M H_2O in acetonitrile	0.25	0.6 %, 425 nm	8 µmA cm^{-2} at -0.06 V vs. NHE	[145]
	p-Si	Mo_3S_4	pH 0	0.1	75 %, 620 nm	10 mA cm^{-2} at 0 V vsRHE	[142]

Note: IPCE = incident photon-to-current conversion efficiency, MeIm = methylimidazolate, BDC = benzenedicarboxylate, TCPP = tetrakis-carboxyphenylporphyrin, Co-DPPP = $([Co_5(HL)_4(dpp)_2(H_2O)_2(\mu\text{-}OH)_2]\cdot 21H_2O)_n$ where H_3L = 5-(2 carboxybenzyloxy) isophthalic acid, dpp= 1,3-di(4-pyridyl)propane).

Photocathodic H_2 evolution has been studied employing p-doped Si electrodes coated by noble and non-noble metals as catalysts for H_2 evolution reaction [146]. A few reports employing MOFs are available. Downes and Marinescu reported on the deposition of a cobalt dithiolene polymer on p-type Si to construct a photocathode. They achieved photocurrents of 3.8 mA cm^{-2} at 0 V vs RHE under simulated 1 Sun illumination [143]. The performance of the MOF thin film was better than the corresponding one for the molecular complex, suggesting that immobilization provides a significant increase in efficiency and stability [143]. More recently, the construction of a photocathode employing Pt/Ir ions quelated within a Zr–Porphyrin MOF was reported. A suspension of the obtained hollow nanotubes was drop-casted on a F-doped s glass to construct a photocathode. The H_2 generation was about 27 - 4 times higher than bulk Ir- or Pt-porphyrin (respectively) and also higher than Ir or Pt nanoparticles. The higher catalytic activity could be attributed to the unique hollow structure, which is beneficial for the mass transport and the presence of single atom catalytic sites [144]. This is an example of taking advantage of the complexity and the synergism derived from the presence of different metal ions in the structure of MOFs, which is reflected in the superior performance of the MOF as catalyst [74].

More recently, a MOF film with a switchable anodic and cathodic behaviour in a photoelectrochemical cell was reported [145]. The Zr-porphyrin-based MOF-525 was solvothermally synthesized and electrophoretically deposited onto FTO substrates. The photoelectrodes thus constructed could act as anodes oxidizing triethanolamine (0.25 M) dissolved in a 0.1 M $LiClO_4$ acetonitrile electrolyte solution. Alternatively, these electrodes could reduce water (11 M) to H_2 in the same electrolyte. This switchable anodic and cathodic behaviour was also observed with UiO-66@Hemin as photoelectrode. The authors concluded, in this way, that the photo-anodic and photo-cathodic switching behaviour would be a general phenomenon for MOF-based photoelectrochemical cells. Additionally, this photo-anodic and photo-cathodic switching behaviour was suppressed upon mounting the MOF on top of a

semiconducting electrode, i.e.: the MOF-525 modified TiO_2 electrode worked solely as a photo-anode, due to the intrinsic n-type nature of the last compound. In table 2, data on photoelectrocatalytic water O_2 and H_2 evolution reactoions are shown. Some results on inorganic materials are also included for comparison, showing that MOFs are competitive catalysts for water splitting.

Another environmentally relevant process is CO_2 reduction to fuels (CO, methanol, CH_4, etc) [113]. There are several reports on the employment of MOFs or derivatives as electrocatalysts for CO_2 reduction [147]. In these cases, MOFs were deposited on the electrode surfaces employing different techniques. They have been also used as photocatalysts for the reduction of CO_2 following the same principles as the photocatalytic H_2 generation explained above. Most of the experiments were conducted with catalyst suspensions employing some sacrificial reducing agent [148]. However, there are very few cases where photocatalytic CO_2 reduction was performed employing MOF films. Recently, a ZIF-8 decorated TiO_2 grid-like film with high CO_2 adsorption was reported as photocatalyst [149] (see Figure 25). The supported catalyst was placed inside the reactor, with a mixture of CO_2 and water as reacting gas flowing during the entire process. Water worked as electron source and no sacrificial agents were applied. Both CO and CH_4 were detected as products. Photoexcited electrons were transferred from TiO_2 to ZIF-8, where reduction took place. Compared with a pure TiO_2 film, ZIF-8/TiO_2, improved CO yield by 38% (0.53 mmol $g^{-1}\cdot h^{-1}$) and CH_4 yield by 157% (0.18 mmol $g^{-1}\cdot h^{-1}$). For traditional semiconductor photocatalysts, the majority of CO leaves the photocatalyst surface and only a small amount of CO remains on the surface to continue the subsequent reduction to CH_4 [149]. The high gas absorption capacity (selective in some cases) and the presence of metallic sites (unsaturated in many cases), allow MOFs to behave like nanoreactors. Thus, reactants may have longer residence periods and can be further reduced.

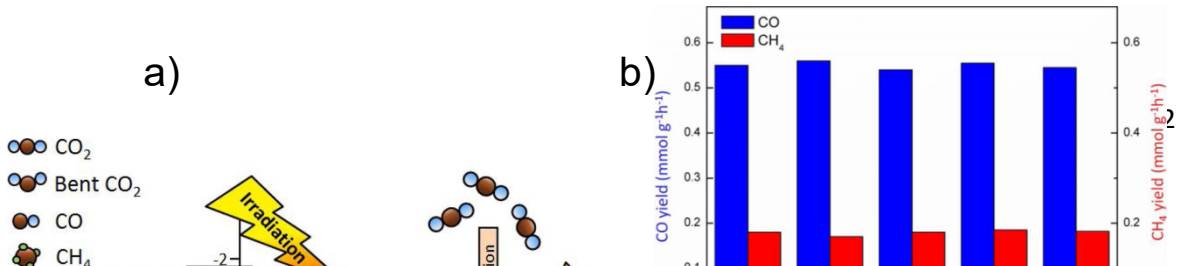

Figure 25. a) Scheme of proposed photocatalytic CO_2 reduction mechanism on TiO_2/ZIF-8. **b)** The mean production rate of a sample of TiO_2/ZIF-8 for different recycle times. **c)** CO and CH_4 yields with TiO_2, and different TiO_2/ZIF-8 samples. Reprinted with permission from [149]. Copyright 2019 Elsevier.

2.4. Solar Cells

Although most commercially spread solar cells consist in a junction of n- and p-doped silicon, MOFs could find application to other types of solar cells, like Dye Sensitized Solar Cells (DSSCs) and Perovskite Solar Cells (PVSCs), due to their crystalline structure, long range order, intense UV-vis absorption and relatively long range exciton diffusion [150]. The contribution of MOFs to solar cells has been recently reviewed [151]. DSSCs were pioneered by Grätzel and O'Regan [152], and they show some similarities with the photoelectrocatalytic cells employed for water splitting described above (see Figure 24). They are composed of a transparent anode, i.e. FTO or ITO (fluorine tin oxide, indium tin oxide) covered by a semiconductor, typically nanostructured TiO_2 or ZnO. A sensitizer (organic dye, Qdot, transition metal complex, MOF, etc) is deposited on the semiconductor. Upon visible light absorption, an electron

from the HOMO of the sensitizer is promoted to the LUMO and injected into de conduction band of the semiconductor. This electron is eventually transferred to the FTO or ITO, following its way through the external circuit to the counter electrode or cathode (see Figure 26). The cathode or counter electrode is made of Pt deposited on a conductive glass (FTO or ITO). The counter electrode reduces a mediator, typically I^-/I_3^- (also tris(2,2′-bipyridine) cobalt(II)/(III) complex) dissolved in an electrolyte. Finally, the mediator reduces the sensitizer, which remained oxidized after light absorption and electron injection into the semiconductor [153]. DSSCs have reached efficiencies up to 14 % [153]. In Figure 26 b) (right), it is possible to notice the importance of the relative energies of the involved bands or orbitals, in order to produce a photocurrent. Due to their crystalline structure, porosity, presence of light absorbing ligands or intense electronic transitions, MOFs have been applied to several components of the DSSCs in order to improve the efficiency. For example: after modification of the TiO_2 surface in the anode with ZIF-8, as electron barrier layer, an improvement in the short circuit current (Jsc) was observed due to increase in dye (sensitizer) loading [154]. The open cell voltage (Voc) was also enhanced due to the retardation of charge recombination [154], leading to a 9.42% energy conversion efficiency (tris(2,2′-bipyridine) cobalt(II)/(III) redox mediator). Allendorf *et al.* constructed a simplified planar DSSC where isolated MOF crystals were used as sensitizers. The MOF was the pillared porphyrin framework (PPF-4), solvothermally synthesized from zinc(II) nitrate, Zn-meso-tetrakis(4-carboxyphenyl)porphyrin (Zn-TCPP) and 4,4′-bipyridine as pillar. Although the efficiency was low, this study revealed that the photocurrent generation was clearly ascribable to the PPF-4 [155]. Wöll and coworkers employed the liquid epitaxy technique to grow a highly oriented, crystalline surface-grafted porphyrin MOF film (Zn-SURMOF 2). I^-/I_3^- in acetonitrile was the redox mediator. The efficiency of the device (0.2 %) was ascribed to indirect electronic band formation as a consequence of the ordered arrays of porphyrins presented in the SURMOF [156]. Later, a series of $Ru(II)L_2DCBPY$ (L = 2,2´-bipyridyl, DCBPY = 2,2´-bipyridine-5,5´-dicarboxylate),

incorporated in a zirconium(IV) MOF were solvothermally grown on TiO_2-coated FTO glass as thin films and tested as sensitizing materials in DSSCs, reaching an efficiency of 0.12 %. RuL_2DCBPY centers located at the MOF–TiO_2 interface were sensitized either directly upon absorption of the incident irradiation or indirectly via resonance energy transfer processes initiated up to 25 nm away from the interface [157]. Recently, the solvothermal growth of precisely [100]-oriented pillared porphyrin framework-11 (PPF-11) films featuring vertically aligned Zn-tetrakis(4-carboxyphenyl)porphyrin (ZnTCPP) walls and horizontally aligned 2,2′-dimethyl-4,4′-bipyridine beams attached to annealed ZnO–FTO surfaces was reported (Figure 26). The [100]-oriented PPF-11/ZnO–FTO photoanode exhibited a short-circuit current (J_{SC}): 4.65 mA/cm^2, open-circuit voltage (V_{OC}): 470 mV, power conversion efficiency: 0.86%, due to improved charge separation, transport, and injection capabilities [158].

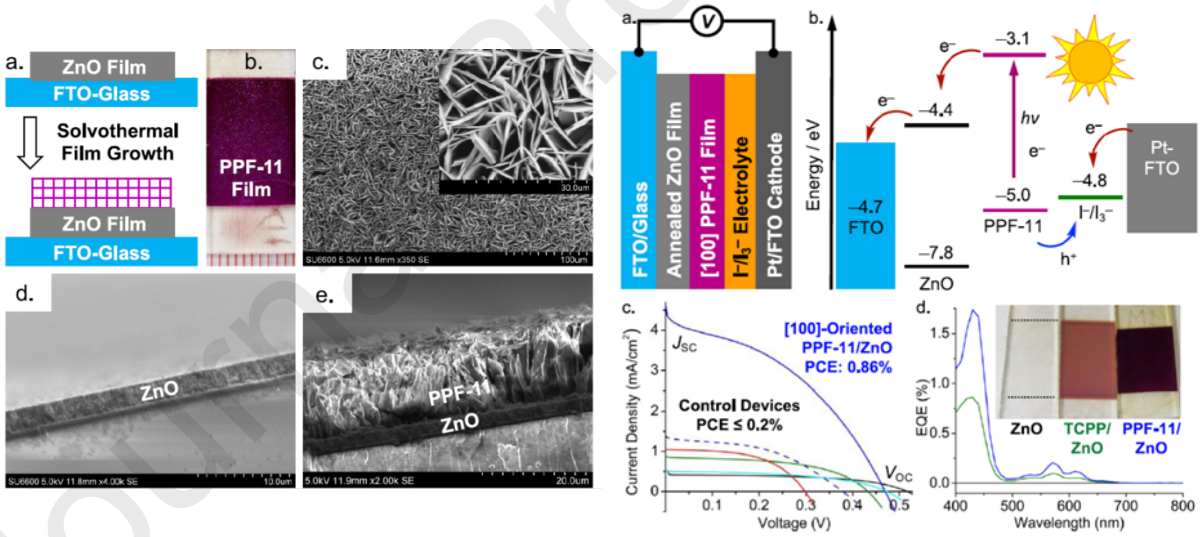

Figure 26. Left: a) Scheme of the solvothermal growth of a PPF-11 film on ZnO to contruct a DSSC. b) Photography of the PPF-11/ZnO film. c) SEM image of the PPF-11/ZnO film. d-e) Cross section SEM images of the film. **Right**: a) Scheme of a MOF-sensitized solar cell: PPF-11/ZnO−FTO photoanode, Pt-FTO counter electrode, and

I^-/I_3^- electrolyte. b) Simplified energy-level diagram of different components described in a). c) J−V plots of the studied devices. d) The external quantum efficiency (EQE) spectra of [100]-oriented PPF-11/ZnO (blue), TCPP/ZnO (green), and blank ZnO films. Inset: photographs of corresponding films used as photoanodes. Reprinted with permission from [158]. Copyright 2019 American Chemical Society.

MOF derived materials have been successfully used in the photoanode (oxides) and in the counter electrode to replace Pt (doped carbons) [151]. On the other hand, MOF/conductive polymer composites have been employed in the counter electrode [151]. However, MOF derived materials (nanostructured carbons or oxides) and composites will not be discussed in this review.

Perovskite solar cells (PVSCs) have emerged from DSSCs in 2009 [159], and are constituted by a light harvesting active material, i.e.: the Perovskite, typically methylammonium lead trihalide ($CH_3NH_3PbX_3$, where X is a halogen). Mesoporous TiO_2 is usually employed as electron transport layer (ETL) and Spiro-OMeTAD as hole transport layer (HTL). In a n-i-p configuration the ETL is deposited on the conductive glass and the metallic electrode (typically Au) on the HTL (see Figure 27), while in the p-i-n configuration the HTL is deposited on the conductive glass and the metallic electrode (typically Ag) is deposited on the ETL. PVSCs have reached an impressive increase in the efficiency from 3.8 % in 2009 to 27.3 % at the end of 2018 [160]. Perovskite materials exhibit long exciton diffusion length, ambipolar charge-transporting ability, and intense wide-range light absorption. Due to the low temperature, solution-based fabrication, PVSCs have much lower production costs than Si-based technology. However, PVSCs suffer from strong sensitivity towards atmospheric conditions particularly moisture, O_2, heat and light [160]. In this way, studies aiming to improve the long term stability are on the way. As stated before, MOFs properties, particularly optoelectronic ones, can be tuned by ligand design or metal center election. They can be readily obtained as films under mild conditions in

solution, what make them good candidates to improve PVSCs performance and durability. MOFs have been employed in PVSCs in the following ways: at the ETL or HTL interfaces with perovskite, as ETL or HTL or embedded within them, and mixed with the perovskite. Employing MOFs in the interlayer zone regulates the perovskite growth, improving the contact with the perovskite layer and film crystallinity. A similar effect has mixing the ETL or HTL with a MOF, with the additional benefit of better band alignment at the interface. The employ of MOFs to improve PVSCs performance has been recently review [151]. In the forthcoming part of this section, the most recent application of MOFs to PVSCs will be commented as examples. Recently, the introduction of an hybrid POM@MOF (POM = $[H_3PMo_{12}O_{40}]_2$, MOF = Cu_3(benzenetricarboxylate)$_2$ = HKUST-1) as dopant into the HTM was reported. An improved Fill Factor of 0.80, conversion efficiency of 21.44 % and a long-term stability in an ambient atmosphere was reached. The improvement was ascribed to oxidation of Spiro-OMeTAD by the POM anions, further improving the efficiency and stability of PVSCs [161]. In another recent report, a composite material with Pb_3(benzenetricarboxylate)$_2$ and Spiro-OMeTAD was used as HTL. The composite layer exhibited smoother surface, higher hydrophobicity and up-shifted energy levels. This led to 25 % higher conversion efficiency (13.1 %) and 54 % of this efficiency was kept after 9 days under atmosphere of 30 % relative humidity [162].

Zr-MOFs (MOF-808 and UiO-66) have been employed to modify the surface of the NiO_x HTL in inverted p-i-n PCSCs. The crystallization of the perovskite film was enhanced, facilitating the charge extraction at the interface, with consequent efficiency improvement from 15.8 % (control) to 17.0 and 16.6 % (MOF-808 and UiO-66 respectively). In the same work, a composite perovskite/MOF active layer allowed improving even further the performance, reaching efficiencies of 17.8 and 18.0 %, respectively. This was thanks to the MOF distribution on perovskite grain boundaries, providing grain locking effect, passivating defects and protecting against moisture invasion (70 % efficiency retention during two weeks at 60 % humidity) [163].

Nanoparticulated Ti-BDC (n-TiMOF, see Figure 27) films have been directly used as ETL in rigid and flexible n-i-p PVSCs, reaching a power conversion efficiency of 16.4 %. This could be further improved using PCBM ([6,6]-phenyl-C_{61}-butyric acid) between the Ti-BDC and perovskite films (18.9 %) (see Figure 27)[164].

The typical HTL in PVSCs is the Spiro-OMeTAD. Other materials employed are NiO_x, phthalocyanines, porphyrinoid analogues [165] and some transition metal complexes [166]. However, as far as we know, MOFs have not been directly employed as HTL. The closest example was reported employing $[In_2(1,10\text{-phen})_3Cl_6]\cdot CH_3CN\cdot 2H_2O$ which is actually a Metal-Organic Assembly [167].

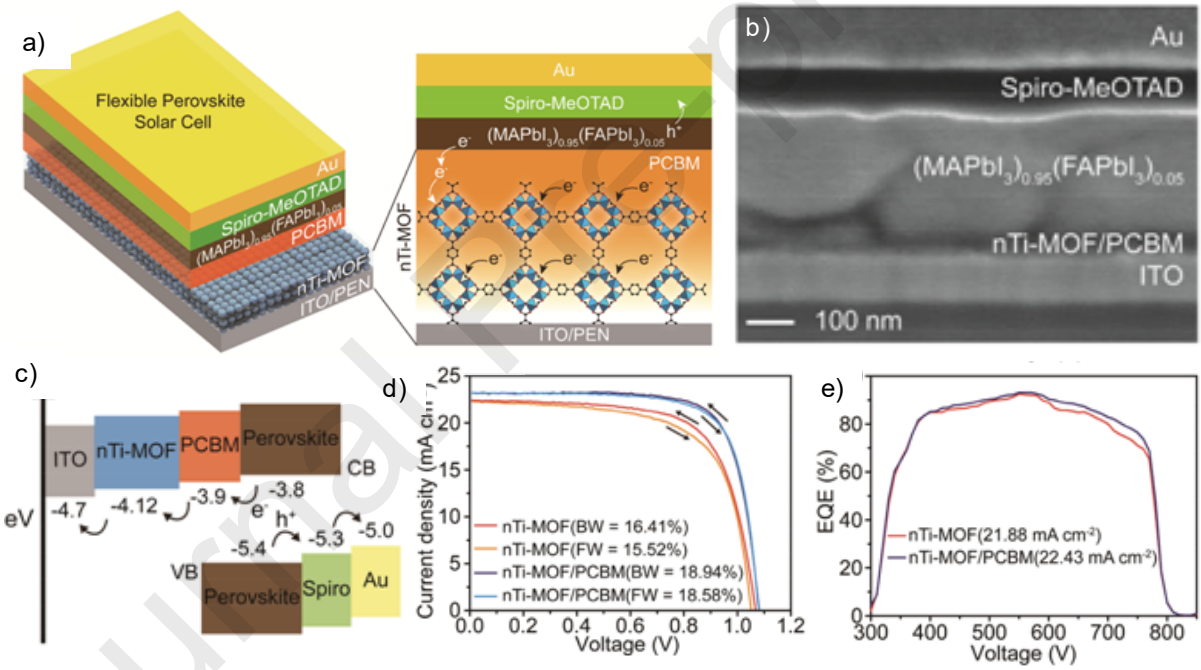

Figure 27. a) Scheme of the flexible perovskite solar cell incorporating nTi-MOF/PCBM ETL. Magnified scheme shows e^- and h^+ transfer from the perovskite toward interlayers, nTi-MOF /PCBM, and spiro-MeOTAD, respectively. b) Cross-section SEM image of the rigid PVSC employing nTi-MOF as ETL. c) Energy diagram of the deposited layers, indicating the e^- and h^+ transfer from the perovskite to the respective layers. d) J−V curves of nTi-MOF device and nTi-MOF/PCBM device. e) External quantum efficiency (EQE) spectra of the nTi-MOF device and the nTi-MOF/PCBM

device. Reprinted with permission from [164]. Copyright 2018 American Chemical Society.

Aiming to construct All-Solid-State Solar Cells, Wöll *et al* employed epitaxial porphyrin SURMOFs whose photophysical properties could be tuned by the introduction of electron-donating diphenylamine groups into the porphyrin skeleton. The porphyrin MOF films were grown on FTO and a PDEOT:PSS film was used as h^+ collector, reaching Jsc = 52.9 mA $cm^{-2}$and Voc = 0.86 V. The diphenylamine groups increased the light absorption, being responsible of extremely high photocarrier generation efficiency [168].

A solid-state solar cell based on a h^+-conducting MOF-Sensitizer was constructed employing Co-DAPV (see Figure 28). The MOF was grown by layer by layer from the coordination between Co (II) ions and a redox active di(3-diaminopropyl)-viologen (DAPV). Optimization of both the TiO_2 and the Co-DAPV thicknesses allowed reaching a Power Conversion Efficiency of 2.1%. The optimum number of layer by layer deposition cycles for Co-DAPV correlated with a minimum charge transfer resistance across the TiO_2-MOF heterojunction, as probed by electrochemical impedance spectroscopy. This efficiency value is higher than those reported for MOF-sensitized (DSSCs) liquid-junction solar cells [169].

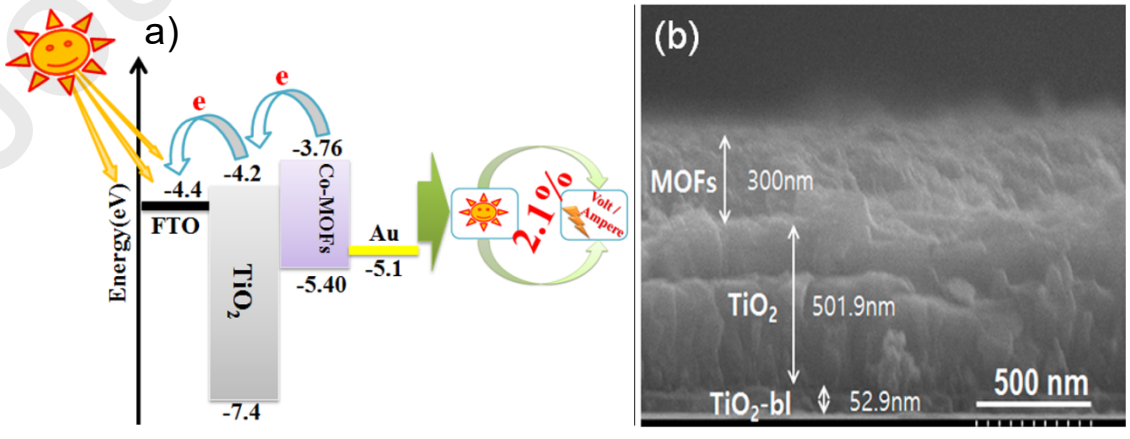

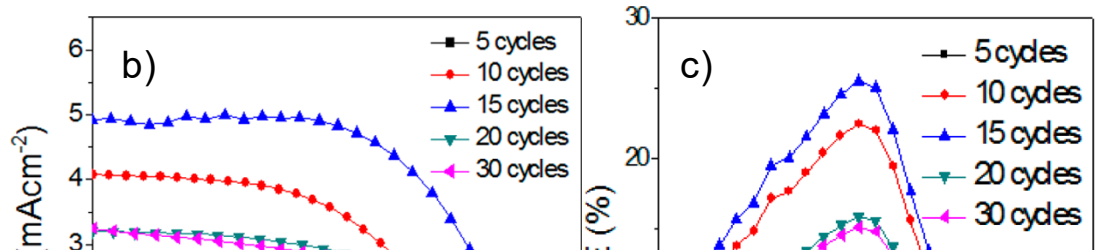

Figure 28. a) Scheme of energy levels for the All-Solid solar cell showing the band edge alignment at the TiO_2/Co-DAPV heterojunction suitable for unidirectional charge transfer. b) Cross-section SEM image of the photoanode grown at optimum conditions. c) J−V curves obtained under 1 sun illumination for the solid-state solar cell sensitized with Co-DAPV deposited at various layer by layer cycles on mesoporous TiO_2. d) Incident Photon-to-Current Conversion Efficiency (IPCE) spectra of the same solar cells. Reprinted with permission from [169]. Copyright 2017 American Chemical Society.

Extensive effort to incorporate MOFs in solar cells has been done, particularly in DSSCs and PVSCs. Although the results show significant improvement, probably the major limitation is the strong orbital localization. Although the exciton diffusion length is relatively long, it might be not enough to reach a high efficiency in a solar cell. As we commented before, RuDCBPY centers photo-excited within the Zr-MOF-bulk undergo isotropic energy migration up to 25 nm away from the point of origin [157]. On the other hand, Exciton was shown to migrate over a net distance of up to ~45 porphyrin struts within its lifetime in [5,15-bis[4-(pyridyl)ethynyl]-10,20-diphenylporphinato]zinc(II) [150]. As a comparison, electron-hole diffusion length exceeds 1mm in a perovskite ($(CH_3NH_3PbI_{3-x}Cl_x)$) [170]. In that direction, a highly efficient one-dimensional triplet exciton transport in a Palladium−Porphyrin-Based SURMOF has been recently

reported [171]. The same group reported on photo-conducting crystalline surface-mounted MOF thin films with an on–off photocurrent ratio of two orders of magnitude [172]. These films were grown using a layer-by-layer process, employing a porphyrin framework backbone and C_{60} guests loaded in the pores. It was concluded that, donor-acceptor interactions between the porphyrin of the host MOF and the C_{60} guests gave rise to an efficient photoinduced charge separation. Subsequently, e^- and h^+ were transported through separate channels formed by the porphyrin and by C_{60}. These strategies could be useful to improve e^- and h^+ transport and exciton diffusion in solar cells and increase their efficiencies.

2.5. Electroluminescence and light emitting devices.

Due to their luminescent properties and tunable intense emission in practically the whole visible spectrum, MOFs are perfect candidates for Light Emitting Devices (LEDs). Many reports have been dedicated to the use of MOFs as phosphors, i.e: coating LEDs, exploiting their photoluminescence [50]. However, fewer works report on the direct employ of MOFs as LEDs. The simplest example would be electroluminescence, where a MOF emits light as response to an electrical current flowing through it. Electrons are directly injected in the HOMO while holes are injected in the LOMO, and the recombination of the e^--h^+ pairs produces a photon. The MOF Cu-P6 ($[Cu_2(C_{39}H_{32}P_2)_2]_n$) exhibited a deep-blue electrophosphorescent behavior when solvothermally grown crystals were sandwiched between two ITO conductive glasses and connected to a direct current voltage source (CIE chromaticity: 0.1343, 0.1089) [173]. The device required a relatively large driving voltage (ca 12 V), most probably due to an inefficient thickness control (83 μm) [50].

LEDs usually are constituted by a more complex or sophisticated design in terms of layers, with the target to facilitate the e^--h^+ recombination in the active material or emissive layer and increase the efficiency. The structure is somewhat similar to the PVSCs described above (Figure 27), but the process is exactly opposite [174]. A

transparent anode (high conductivity and transmittance, FTO, ITO) injects h^+ in the device. A Hole Injection Layer (HIL), with e^- blocking capacity and high h^+ mobility, located between the anode and the emissive layer, is necessary to overcome the charge injection barrier resulting from the difference between the HOMO of the emissive material and the Fermi level of the anode material. Typical materials for HIL are: PEDOT: PSS (poly(3,4-ethylene-dioxythiophene):poly(4-styrene sulfonate)), CuPc (copper phthalocyanine), and MoO_3. The Emissive Layer (EL) is the material where the e^--h^+ recombination takes place to emit a photon. Ideally it should possess a high quantum efficiency, long emission lifetime, short excited-state lifetime and color purity [174]. The highest efficiencies reported in OLEDS were accomplished with Ir and Pt complexes, due to their high spin-orbit coupling. An Electron Transport Layer (ETL), analogously to the HIL, transports e^- from the Cathode to the emissive layer and blocks h^+. Typical materials for the ETL are PV (perylene bis-benzimidazole), Alq (8-hydroxyquinoline aluminum), Liq (8-quinolinolato lithium), and Naq (8-quinolinolato sodium). Finally, a Cathode (Al, Ag), injects e^- into the device [174].

A white light emitting device (WLED) was constructed employing a $([Sr(ntca)(H_2O)_2].H_2O)_n$ MOF film (ntca = 1,4,5,8-naphthalenetetracarboxylate) deposited between n-type ZnO and single layered graphene (see Figure 29) [175]. Several electronic transitions, assigned to LLCT), MMCT and MLCT are responsible for the broad band white emission (CIE chromaticity close to (0.333, 0.333). The device showed an efficiency of 1.2 % which is quite low compared to commercial LEDs with efficiencies around 40 %. The dependence of the quantum efficiency as a function of the film thickness had a maximum, evidencing the influence of this parameter and film quality on the electroluminescence efficiency [175].

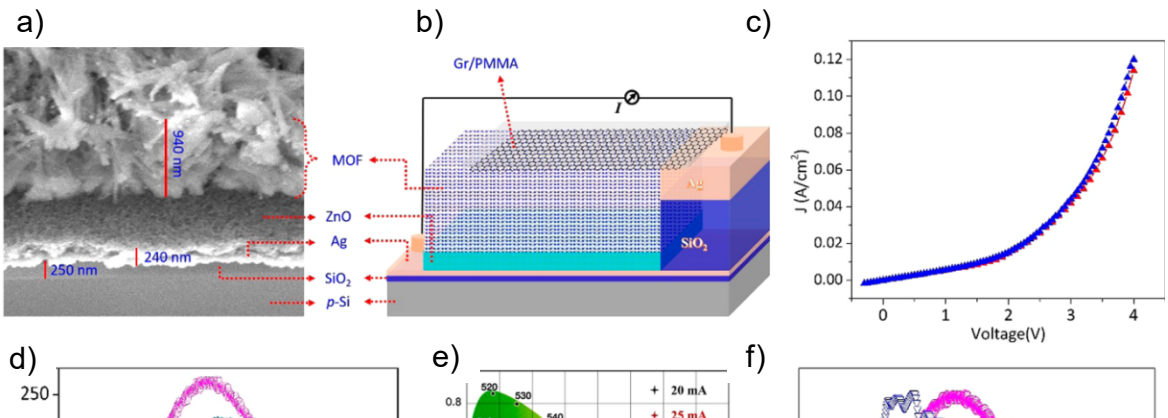

Figure 29. a-c) Structure of the MOF-based WLED (MOF = ([Sr(ntca)(H_2O)$_2$].H_2O)$_{2n}$). a) Cross section SEM image of the device where a p-n junction is formed. b) Scheme of the device. c) Room temperature J−V plot of the solid-state lighting device. d-e) Electroluminescence properties. d) Electroluminescence spectra of the device. e) CIE chromaticity diagram. The circle corresponds to the coordinate (0.333, 0.333). f) Comparison of the Electroluminiscence spectrum with natural light from the sun. Reprinted with permission from [175]. Copyright 2016 American Chemical Society.

More recently, another rare-earth free device with white light emission was constructed. In this way, Zn-ipaPy_2 Zn-MOF (ipa = 5-azidoisophthalate, Py = pyridine) was deposited between a PEDOT:PSS layer (h^+ conducting), and a (8-hydroxyquinolinato)aluminum (Alq_3) layer (e^- transport) [176]. After 6 V application white light emission was observed. The spectrum consisted in three bands (445, 537, 602 nm), which were assigned to π-π*, π-n and a charge transfer transition from the pyridine group to the linker, which produced the white light emission (CIE index (0.31, 0.33).

Finally, materials with high luminescence quantum yields, like the recently reported blue-light-emitting Cd coordination polymer (75.4% yield), would be promising materials to constitute emissive layers in LEDs [177].

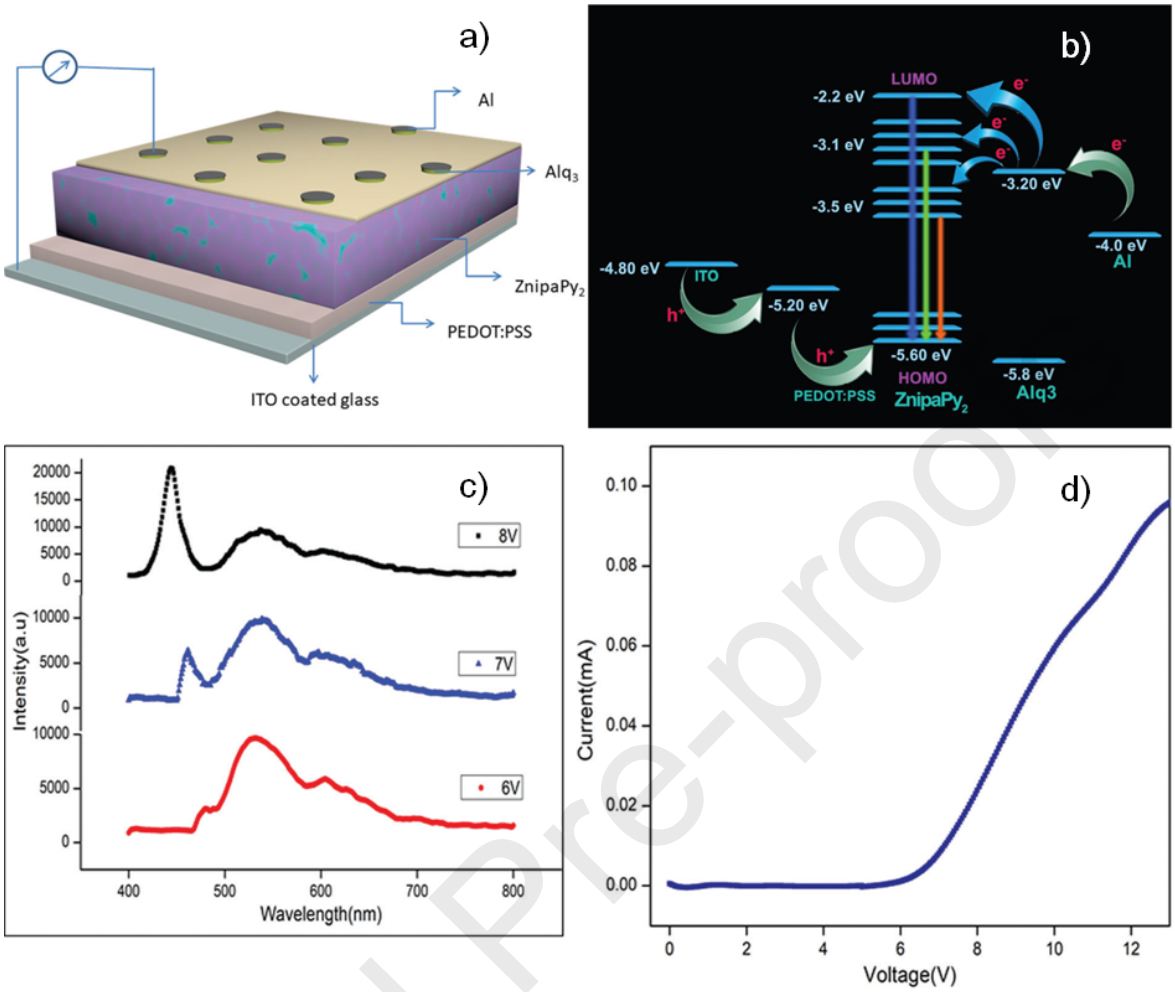

Figure 30. a) Scheme of the WLED. b) DFT-calculated energy level diagram of the components employed in the device. c) Electroluminescence spectra of Zn-ipaPy_2 obtained at different voltages. d) I–V plot of the corresponding device. From reference [176] Reproduced by permission of The Royal Society of Chemistry.

2.6. Non linear optics, up conversion and lasing

Usually, when a material is exposed to electromagnetic radiation, it can emit photons of equal or lower frequency than the incident light (Stokes shift). However, there are cases when emission with higher frequency (anti Stokes) is possible. Such phenomena have been observed in inorganic and organic materials, as well as hybrid

ones like MOFs. They can be separated in two major mechanisms: Non Linear Optical effects (NLO) and the Up Conversion of Luminescence (UC) [178-180].

The interaction of matter with an electric field (E) induces a polarization (P) or electric dipole. Light has an oscillating electric field, hence induces an oscillating polarization within the material. Under low intensity light, the strength of P is proportional to the intensity of the electric field of light (E). However, under high intensity of illumination (for example: LASERs), P and E exhibit higher order terms (second, third order, etc.) and a non linear relationship (quadratic, cubic, etc. respectively). Some examples of NLO phenomena in MOFs are two or three photon absorption [181, 182] and second or third harmonic generation [183, 184] (see Figure 31). Second harmonic generation implies the simultaneous absorption of two photons of frequency ω and emission of photon of frequency 2ω (see Figure 31). This phenomenon can be observed in non-centrosymmetric crystal materials having high polarizability. Chiral or acentric diamondoid-like nets have been employed as alternative strategies. Second order NLO properties depend not only on the nature of the material, ligands, etc. but also on the fulfillment of phase-matching conditions (i.e. when the induced polarization and the generated electric field are in phase). In other words, appropriate crystal lengths and shapes are necessary to obtain detectable intensities in NLO emission. For this reason, second order NLO properties have been widely explored with crystal and microcrystal materials and not with films. They have been reviewed in detail in the literature [178-180].

Multiphoton absorption corresponds to the simultaneous absorption of two, three, etc. photons of the same or different energy to excite a molecule to a higher electronic state (see Figure 31). The energy needed for the transition equals the energy of all absorbed photons. The exited state can relax to the ground state through emission. This mechanism has been exploited for NLO anti stokes emission in several MOFs [179, 180].

Third order NLO processes do not require non-centrosymmetric structures. The presence of metal centers with un-occupied *d* orbitals, delocalized π orbitals or donor-acceptor couples in the ligands, are some strategies to obtain third order NLO materials. The phase-matching conditions are not necessary for third order NLO. In this way, many studies on MOFs have been performed employing suspensions in organic solvents (i.e. DMF, DMSO) [180]. Two photon absorption and third harmonic generation are both third order processes [185]. A few examples of third order NLO have been conducted on films supported on quartz, obtained upon evaporation of MOF suspensions in ethanol [186, 187].

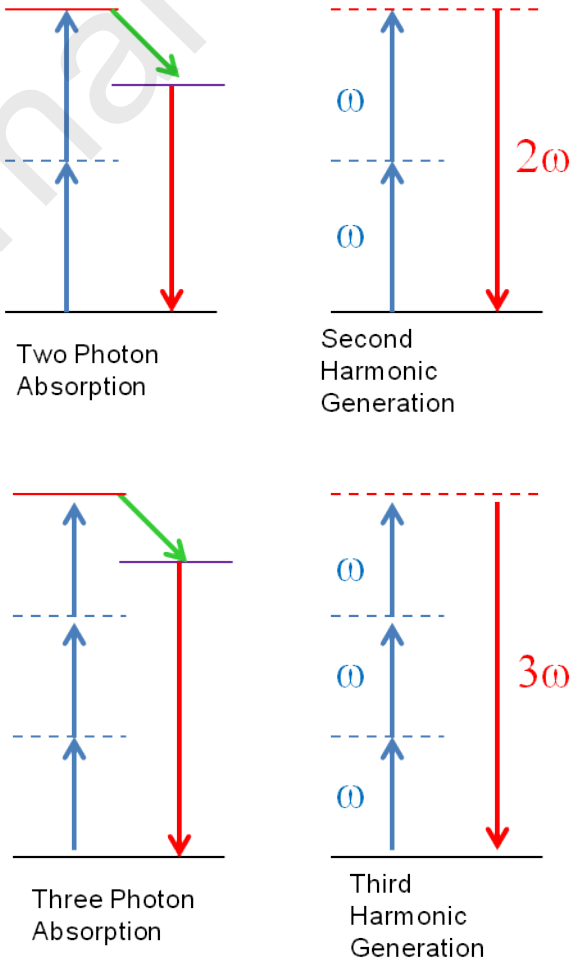

Figure 31. Non linear optical processes investigated with MOFs. Virtual states are shown in dotted lines.

Multiphoton absorption of MOF nanoparticles has possible application in bioimaging and photo-therapies, employing infrared radiation [180]. In a extensively cited paper of Yu et al., 3D two-photon patterning and imaging inside a Zn-MOF crystal was reported, employing lasers of 710 nm and 900 nm (write and read respectively) [188]. The reached resolution was 1 × 1 × 5 μm^3. The 710 nm induced a two photon reaction of the ligand 2,5-bis(3,5-dicarboxyphenyl)-1-methylpyridinium, which produced a shift in the emission spectrum from 450 nm to 540 nm. This technology for 3D patterning and 3D data storage could be further developed if two-photon responsive MOFs could be grown as flexible, printable and roll-up films.

Other mechanisms for anti-stokes emission, i.e. with higher energy or frequency than incident light, involve the sequential absorption of two or more photons (not simultaneous absorption as in NLO) [13, 180]. These processes are known as Up Conversion (UC) and have as advantage that much lower intensities than in NLO can be employed.

Lantanide based up conversion is a strategy extensively exploited due long luminescence lifetimes, long lived excited states and high photostability of lanthanide ions [179, 189]. The different mechanisms involved in lantanide up conversion will not be discussed in this review, and the reader is refered to more specialized literature [190]. Another mechanism is Triplet-Triplet Annihilation Up Conversion (TTA-UC) and has the following steps (see Figure 32): photon absorption by a donor (or sensitizer) to drive it to an excited singlet state which upon Inter-System Crossing (ISC) gives a triplet state. This triplet energy is transferred to an acceptor molecule (emitter) via

Triplet–Triplet Energy Transfer (TTET). Two emitter molecules in triplet state (or excitons in a solid) meet upon diffusion, and the Triplet-Triplet Annihilation occurs generating an emitter molecule or chromophore in an excited singlet state and other in the ground singlet state. Finally, the emitter in the resultant excited state emits the up converted photon with anti-stokes shift respect to the incident light [180].

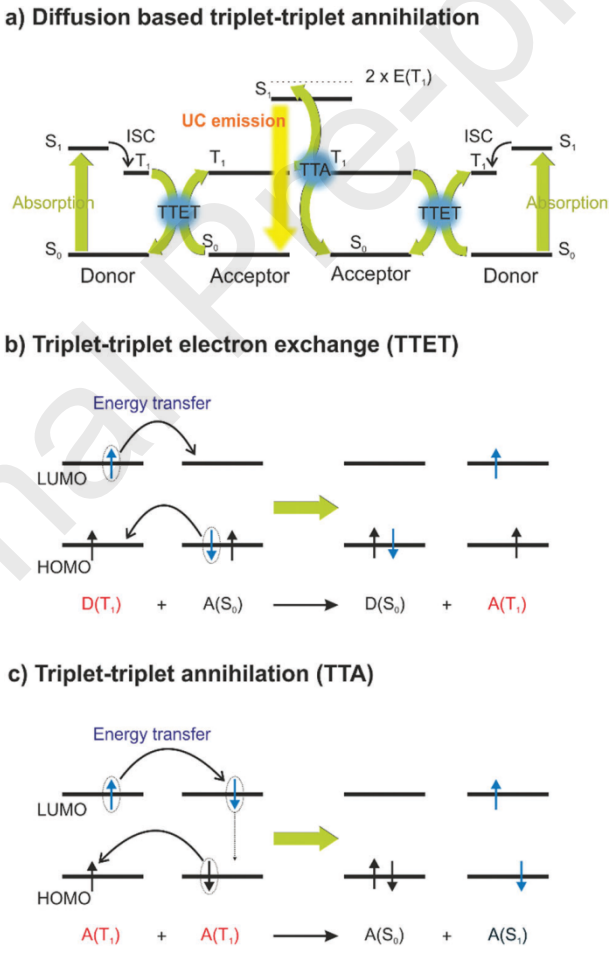

Figure 32. a) Scheme of the energy-level diagram of diffusion based Triplet-Triplet Annihilation. b) Non-radioactive triplet-triplet electron exchange (Dexter electron

transfer). c) Triplet-triplet annihilation. For details see text. From reference [180]. Reproduced by permission of The Royal Society of Chemistry.

As examples of TTA-UC in films we present the following reports. Richards, Howard *et al.* constructed a series of A–B–A hetero-structures, highly orientated in the [001]-axis perpendicular to the substrate (Si) (A = emitter, B = sensitizer layers) employing the layer by layer technique. The sensitizer (B) layer was Pd(II) 5,15-diphenyl-10,20-di(4-carboxyphenyl) porphyrin and the emitter (A) was 4,4′-(anthracene-9,10-diyl)dibenzoate, in both cases linked by paddle wheel Zn^{2+} nodes. The chromophores within B were excited with green (532 nm) photons, to which the emitter A layer was transparent. The singlet lifetime of the sensitizer B layer was bellow 10 ps, what allowed concluding that almost all absorbed photons initially generated triplet states in B through fast intersystem-crossing. Triplets which reached and crossed the B–A heterojunction, were collected in the A layer. Once trapped in the A layer, pairs of triplets decayed through TTA-UC generating emission of higher-energy blue photons. This finding demonstrated that the heterojunctions were of sufficient quality to allow electron (Triplet) transfer across a SURMOF heterojunction. However, the UC threshold (i.e. minium power to observe UC) did not decrease with increasing B layer thickness as would be expected for increased light absorption. This unexpected finding suggested that triplets were trapped in the sensitizer layer as thickness increased. An strategy to improve the layer quality employing sonication during rinsing after deposition and growing B–A bilayers, permitted to reach an UC threshold lower than 1 mW cm^{-2}, better than the previous A–B–A devices [191].

More recently, the TTA-UC mechanism was employed to increase the efficiency of a DSSC. The SURMOF (Zn-3,9-perpylenedicarboxylate) epitaxially grown along the [001] direction on a mesoporous TiO_2 substrate was employed as emitter. Platinum(II) octaethylporphyrin (PtOEP) was used as sensitizer dissolved in a $[Co(bpy)_3]^{2+/3+}$ (mediator) acetonitrile solution [192]. Upon excitation at 530 nm of the Zn-perylene

SURMOF in the presence of PtOEP, emission centered at *ca* 460 nm and 643 nm (weak) was observed (see Figure 33), in agreement with the emission spectra of the separated compounds (460 nm for Zn-perylene SURMOF, λ_{ex}= 430 nm and 643 nm for PtOEP λ_{ex}= 530 nm). Remarkably, the Zn-perylene SURMOF did not emit at 460 nm upon excitation at 530 nm. The emission signal at 460 nm observed in the Zn-perylene SURMOF + PtOEP spectrum was attributed to direct triplet energy transfer (TET) from PtOEP to the Zn-perylene SURMOF at the interface, followed by TTA-UC between the neighboring perylene molecules within the SURMOF. DSSCs were assembled using TiO_2-Zn-perylene + PtOEP, or TiO_2-Zn-perylene, or TiO_2 + PtOEP as working electrodes. Upon irradiation at 530 nm, the following photocurrents: 2.0, 0.1 and 0.2 $\mu A \cdot cm^{-2}$ were measured respectively, evidencing that a TTC-UC mechanism was responsible for the higher photocurrent. In order to further prove that the photocurrent enhancement was due to a TTA-UC mechanism, measurements of the photocurrent at different power densities (530 nm) were done for the TiO_2-Zn-perylene SURMOF + PtOEP (see Figure 32). At low power densities a quadratic dependence was observed (slope = 2), followed by a linear dependence at higher current densities (slope = 1). This behavior was not observed irradiating at 430 nm, where only the perylene groups absorbed while the sensitizer (PtOEP) did not, further confirming the operation of a TTA-UC mechanism [192]. In this way, TTA-UP was employed to increase the efficiency of a solar cell. Up conversion could help the construction of infrared solar cells and infrared sensitive photodetectors [189].

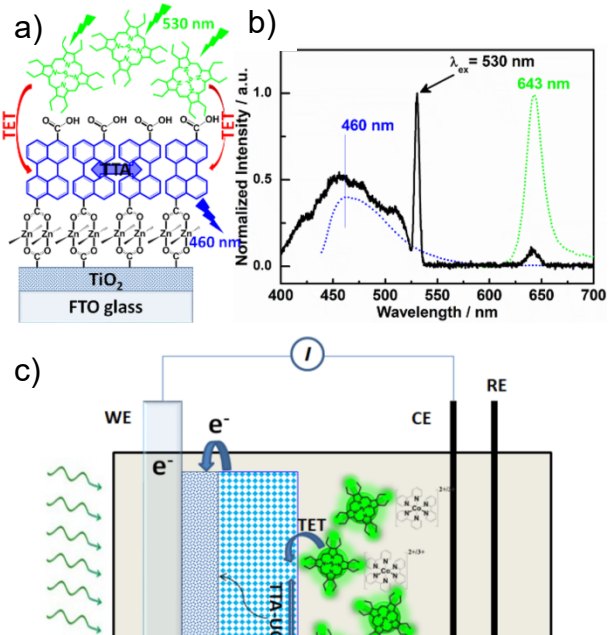

Figure 33. a) Schematic representation of the molecular structure of Zn-perylene SURMOF + PtOEP on the TiO_2 surface. b) Emission spectra of PtOEP (dotted green, λ_{ex} = 530 nm), FTO/TiO_2-Zn-perylene SURMOF (dotted blue, λ_{ex} = 430 nm), and FTO/TiO_2-Zn-perylene SURMOF + PtOEP (solid black line, λ_{ex}= 530 nm). c) Schematic illustration of the DSSC using TiO_2-Zn-perylene + PtOEP as working electrode, Ag/$AgNO_3$ as reference electrode, and platinum wire as counter electrode in 0.01 μM $[Co(bpy)_3]^{2+/3+}$ acetonitrile solution (mediator). d) The i−t curves for the employed photoanodes under AM1.5 solar irradiation passing through a 530 nm long-pass filter (power density = 35 mW cm^{-2}) at external applied potential 0 V vs Ag/$AgNO_3$. e) Photocurrent density from photoelectrochemical cell (TiO_2-Zn-perylene SURMOF + PtEOP) vs power density (λ_{ex} = 530 nm) (external applied potential 0 V vs Ag/$AgNO_3$). Reprinted with permission from [192]. Copyright 2018 American Chemical Society.

LASERs play uncountable functions in our everyday life. The construction requires principally three main components: a gain material, a resonator or optical feedback and a pumping source. MOFs are also materials which have shown application to these devices, particularly contributing with the gain material [180]. MOFs can be synthesized with highly luminescent ligands. Alternatively, highly luminescent organic dyes can be absorbed within their pores, as guests. Broad wavelength tunability, characteristics for solution dye LASERs, can be obtained with MOF LASERs, but the later ones prevent aggregation of the chromophores avoiding non radiative pathways (quenching, intramollecular charge transfer, etc), what hinders population inversion. On the other hand, MOFs are usually obtained as single crystal with smooth surfaces and highly ordered chromophores, which act themselves as resonant cavities, allowing obtaining microLASERs with low lasing threshold [180, 193, 194]. Two- and three-photon-pumped dye@MOF LASERs have great present and potential relevance due to their application in up-conversion, optical data storage, biological imaging and photodynamic therapy [180, 193, 194]. Aggregation and quenching prevents the construction of such LASER employing dyes in the solid state [52, 180, 194, 195]. Stimulated emission is the fundamental property on which LASERs are based. It is evidenced through the pumping power dependence of the fluorescence intensity, the fluorescence spectrum (see Figure 34 a), and its lifetime as well. Upon increasing pumping power, a change in the slope of the fluorescence dependence is observed (threshold power) where stimulated emission starts (see Figure 34 a inset). Stimulated emission also leads to narrowing of the fluorescence spectra, which usually show feedback effects (see Figures 34 a, b) [52, 180, 194, 195].

Recently, reversible switching of the dual wavelength lasing of MOF microwires was demonstrated employing Cd-tpbe (tpbe = 1,1,2,2-Tetrakis(4′-(pyridin-4-yl)-[1,1′-biphenyl]-4-yl)-ethane) [196] (Figure 34). Desorption of guest molecules like dimethylacetamide or acetone allowed rotation of the phenyl groups with red shifted gain behavior. The lasing emission could be reversibly switched between two distinct

wavelengths ($\lambda_{acetone}$ = 489 nm; λ_{air} = 508 nm) through alternating plugs of air and acetone [196].

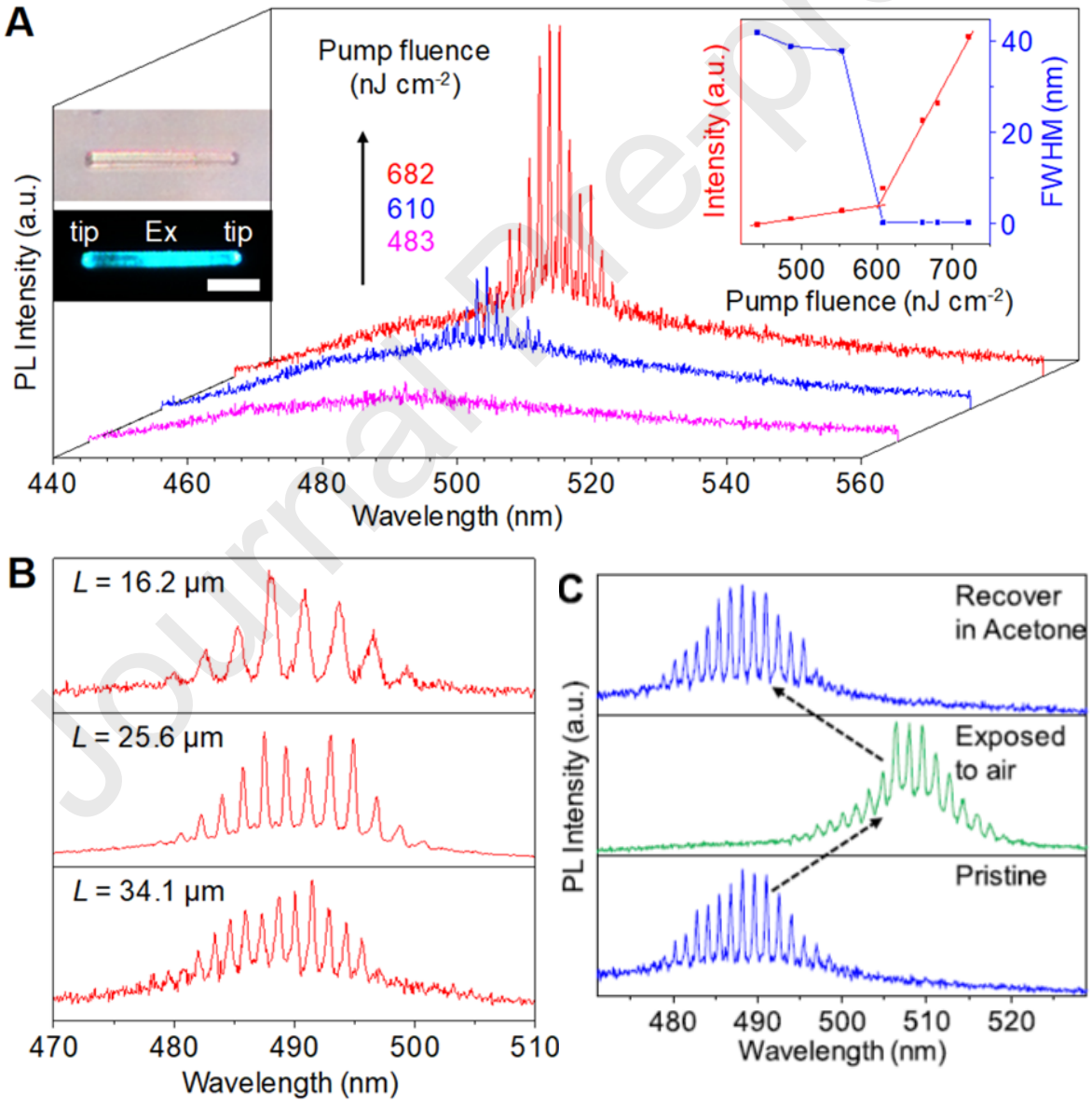

Figure 34. A) Photoluminescence spectra of a tpbe-Cd microwire as a function of pump energy. Left inset: Bright-field and Photoluminescence images of a tpbe-Cd microwire under excitation. Scale bar: 10 μm. Right inset: Plots of photoluminescence peak intensities and full width at half maximum (fwhm) vs pump fluence. B) Photoluminescence spectra of tpbe-Cd microwires with different lengths. C) Wavelength shift of lasing modes in the tpbe-Cd microwire under alternate exposure to air and acetone. Reprinted with permission from [196]. Copyright 2019 American Chemical Society.

Lasing studies with MOFs have been mostly conducted with microcrystalline samples, even with isolated microcrystals which provided resonating cavity. Lasing is, in principle, possible without a strictly defined cavity, i.e.: if the feedback is provided by random scattering in a highly disordered medium [180]. However, as far as we know, no reports are available employing MOF films. This would allow incorporating them in devices with possible application in communications or optical computing.

2.7. Photoswitching MOFs

Photoswitching materials are compounds which suffer changes in their structure or physical properties upon interaction with light as a consequence of a switcht between two different stable forms. [197, 198]. Typical compounds which exhibit this property are: azobencene, spiropyrane and diarylethene, which undergo reversible cis/-trans isomerization or ring opening/closing. MOF phtotoswitches have been recently reviewed [13]. There are mainly two strategies to obtain MOF photoswitches: absorption of photoswitchable molecules within the pores or employing ligands with photoswitchable groups to synthesize the MOFs. In the case the photoswitchable group is not pendant (side group) but forms part of the MOF backbone, significant structural changes are expected upon light irradiation. The most important properties

that have been switched upon light illumination are: color and fluorescence, electrical conductivity, magnetization, up take and release of guest molecules, membrane permeance and selectivity, proton conduction and catalytic activity [13].

SURMOF, with all their advantages i.e.: highly ordered and orientated thin films, supported on suitable substrates, have been employed as photoswitches using specially designed ligands. They found application as remote-controlled release of guest molecules, photoswitching of proton and electronic conduction, membrane permeation and separation [199, 200]. Recently, a photonic crystal composed of alternating layers of TiO_2 and a SURMOF with azobenzene side groups was constructed. Cu^{2+} ions were used as nodes, the organic linkers was (E)-2-((2,6-difluorophenyl)diazenyl)terephthalic acid and dabco (1,4-diazabicyclo[2.2.2]octane) was used as pillar (see Figure 35). The refractive index of this device was photomodulated, since the rigid MOF lattice was unaffected, but the optical density was reversibly modified by the light-induced trans−cis-azobenzene isomerization of pendant group. In this way the Bragg reflexes could be reversibly shifted by more than 4 nm [201].

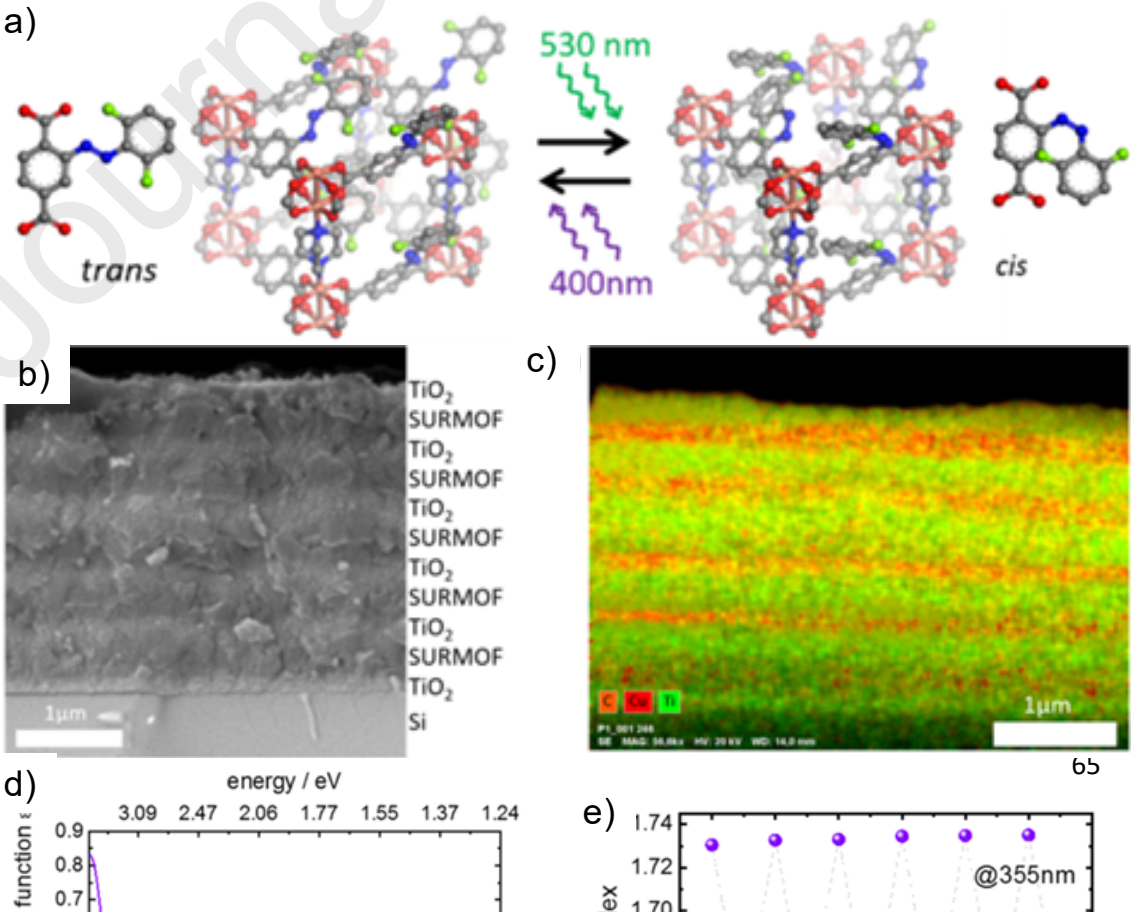

Figure 35. Photoswitchable $Cu_2(F_2AzoBDC)_2(dabco)$ SURMOF. a) Structure of the SURMOF and the photoswitchable ligand in *trans* conformation (left) and *cis* conformation (right). b-c) Photonic structure: b) SEM image of the cross section of the SURMOF−TiO_2 sample. c) EDX mapping showing Cu (red), C (orange), and Ti (green) distribution. d) Imaginary part of the refractive index (ε_2) of the photoswitchable SURMOF determined by ellipsometry. e) Reversible-switching of the refractive index at 600 nm and at 355 nm for five cycles of irradiation with green light (cis, green spheres) and with violet light (trans, violet spheres). Reprinted with permission from [201]. Copyright 2019 American Chemical Society.

3. Conclusions and Perspectives.

MOFs, those mesmerizing materials, have attracted the attention of many groups of synthetic chemistry around the world due their intricate structures and endless potential applications. Because of the great impulse in MOFs research in many fields, it is possible to find excellent reports and reviews regarding to photophysical and photochemical properties of MOF powder samples, microcrystals and suspensions, or alternatively on thin films implementations. The careful selection of the building blocks along with the corresponding synthesis methodology is vital for the design a

photofunctional MOF to explore a particular application. A summary of the latest results on photofunctional applications of MOF films is presented. It is remarkable that some areas like photoswitchable MOFs have experienced a great advance. Significant advance in sensing employing MOFs platforms is seen in the literature, principally in powders form and secondly in composites and thin films. In this sense, by elaborating luminescent MOFs with specific fluorescent transitions, it is possible to detect a variety of molecules not only of environmental and security importance, but also of biomedical relevance. These researches could open the possibilities to elaborate new methodologies that require stable and reliable platforms with robust sensing performance in many areas.

The thermal sensing is an example of exponential interest during the last decade, where dozens of powder MOF thermometers were synthesized employing the correct building blocks. This area will have new type of MOF platforms in a near future, such as novel SURMOFs or even new type of composites in order to detect the temperature under extreme conditions or even in living organisms. Moreover, studies regarding the role of photofunctional MOFs, it is important the use of computational techniques in order to support the experimental data as well as to get key parameters such HOMO and LUMO energies and also, predict molecular interactions in diverse media

H_2 and O_2 evolution reactions as well as CO_2 reduction to fuels has been extensively studied employing MOF suspensions with sacrificial reagents, electrically driven or photo-electrocatalyzed. In these cases other organic chemicals or electricity are consumed to get solar fuels like H_2, reducing the sustainability of these processes. However, practically no reports are available where overall light driven water splitting or artificial photosynthesis are observed employing MOFs films. The basic knowledge of these reactions is mature enough to construct in the near future devices which photocatalyze the overall water splitting or the artificial photosynthesis, for example in a Z-scheme photocatalysts [202]. These mimic the natural photosynthesis system and are basically constituted by two coupled catalysts: one for the H_2 evolution and the

other for the O_2 evolution reaction, i.e. spatially separated reductive and oxidative active sites. Holes generated during the H_2 production by the first catalyst are consumed by the second catalyst which catalyzes the O_2 evolution. Vice versa, electrons generated during the O_2 production are consumed by the second catalyst. In this way, the photogenerated e^- with strong reduction abilities and h^+ with strong oxidation abilities are employed to produce H_2 and O_2 respectively. As a result, a Z-scheme photocatalyst simultaneously has the strong redox ability, which can also be exploited for CO_2 reduction and organic transformations [202].

Many reports have been devoted to MOF sensitized solar cells and several others to the application of MOFs to Perovskite Solar cells. Recent papers reporting the application of MOF to all-solid-state solar cells evidence the difficulties and challenges in growing MOFs films with the quality and specification for such solar cells. As proposed in the corresponding section, efforts to obtain films with higher e^- and h^+ mobilities, and longer exciton diffusion lengths would contribute to improve the solar cell efficiencies and develop a competitive technology.

MOFs have been proved to be useful as emissive layers in LEDs. These reports highlighted the necessity of a control of the film thickness and quality in order to improve the device performance (lower the emission threshold and higher efficiency). Several reported devices were constructed employing grinded crystalline samples. MOF LEDs would improve in terms of efficiency, if films were grown employing techniques which allow crystal order and thickness control, like liquid film epitaxy. In an ideal case, lasing conditions could be met and MOF diode LASERs could be constructed.

This review has summarized recent developments on photofunctional MOFs, showing important advances in fields like sensing, catalysis, solar energy, light emission, non linear optics, lasing and switching. MOFs thin films could have a promising and bright future, related to their incorporation to optoelectronic devices, sensors and catalysts.

Acknowledgements

This work was supported by the Agencia Nacional de Promoción Científica y Tecnológica (project PICT-2016-3017), the Commission for Atomic Energy of Argentina (CNEA), and the Research Council of Argentina (CONICET). G. E. G. and F. R. are permanent staff of the National Research Council of Argentina (CONICET).

Declarations of interests

The authors declare no competing interests.

Author Biography

Dr. Germán E. Gomez completed his Ph.D in Chemistry at Universidad Nacional de San Luis (UNSL) in research topics related to study Lanthanide-MOFs with luminescent and catalytic properties with the supervision of Dra. Griselda Narda and Dra. Elena Brusau. After that, he made postdoc stays in Nano-Chemistry group in CAC-CNEA (2015-2017, at the Dr. G. J. A. A. Soler-Illia group), College de France (2016, Dr. Clément Sanchez group) and Ghent University (2016, Dr. R. van Deun group) studying MOFs for chemical and thermal sensing. In 2018 he joined the group of Prof. C. Cahill at George Washington University as a Fulbright fellow, for the development of actinide MOFs. Also, in 2018 he visited the group of Prof. Muralee Murugesu in Ottawa University to work in the project “MOFs and MMPFs for opto/magnetic applications”. In 2019 Gomez made a SURMOF research in Karlsruhe Institution of Technology (KIT) with the supervision of Dr. Christof Wöll. Nowadays Gomez is researcher of CONICET in INTEQUI (UNSL) for the research of MOFs for sensing, photoluminescence and photocatalysis fields.

Dr. Federico Roncaroli graduated as a chemist in 2000 at the University of Buenos Aires (Argentina), where he obtained a PhD (2004) studying the reactivity and spectroscopic properties of metal–nitrosyl complexes under the direction of Professor José Olabe. In 2005 he was awarded a *Dr. rer. nat.* at the Universty of Erlangen-Nürnberg (Germany), working on the reactions of nitric oxide with biologically relevant models, under the supervision of Professor Rudi van Eldik. After post doctoral work in the Commission for Atomic Energy of Argentina (CNEA) with Professor Miguel Blesa, he obtained a postdoctoral fellowship from the Alexander von Humboldt foundation, to perform pulse EPR studies on Hydrogenases, at the Max Plank Institute for Chemical Energy Conversion under the supervision of Professor Wolfgang Lubitz. Since 2013 FR is researcher of CONICET at CNEA. His current interests are application of MOFs to sustainable energy conversion and storage.

References

[1] S.R. Batten, N.R. Champness, X.-M. Chen, J. Garcia-Martinez, S. Kitagawa, L. Öhrström, M. O'Keeffe, M.P. Suh, J. Reedijk, Terminology of metal-organic frameworks and coordination polymers (IUPAC recomendations 2013), Pure Applied Chemistry, 85 (2013) 1715–1724.
[2] L.R. MacGillivray, Metal Organic Framework Materials, John Wiley & Sons Ltd, Chichester, UK, 2014.
[3] D. Farrusseng, Metal-Organic Frameworks Applications from Catalysis to Gas Storage, Wiley-VCH Verlag & Co, Weinheim, Germany, 2011.
[4] M. Eddaoudi, D.B. Moler, H. Li, B. Chen, T.M. Reineke, M. O'Keeffe, O.M. Yaghi, Modular Chemistry: Secondary Building Units as a Basis for the Design of Highly Porous and Robust Metal–Organic Carboxylate Frameworks, Accounts of Chemical Research, 34 (2001) 319-330.
[5] J.-R. Li, J. Sculley, H.-C. Zhou, Metal–Organic Frameworks for Separations, Chemical Reviews, 112 (2012) 869-932.
[6] J. Liu, G.-P. Yang, J. Jin, D. Wu, L.-F. Ma, Y.-Y. Wang, A first new porous d–p HMOF material with multiple active sites for excellent CO2 capture and catalysis, Chemical Communications, 56 (2020) 2395-2398.

[7] P. Horcajada, C. Serre, G. Maurin, N.A. Ramsahye, F. Balas, M. Vallet-Regí, M. Sebban, F. Taulelle, G. Férey, Flexible Porous Metal-Organic Frameworks for a Controlled Drug Delivery, Journal of the American Chemical Society, 130 (2008) 6774-6780.
[8] B. Liu, Metal–organic framework-based devices: separation and sensors, Journal of Materials Chemistry, 22 (2012) 10094-10101.
[9] A.E. Baumann, D.A. Burns, B. Liu, V.S. Thoi, Metal-organic framework functionalization and design strategies for advanced electrochemical energy storage devices, Communications Chemistry, 2 (2019) 86.
[10] Y.-P. Wu, J.-W. Tian, S. Liu, B. Li, J. Zhao, L.-F. Ma, D.-S. Li, Y.-Q. Lan, X. Bu, Bi-Microporous Metal–Organic Frameworks with Cubane [M4(OH)4] (M=Ni, Co) Clusters and Pore-Space Partition for Electrocatalytic Methanol Oxidation Reaction, Angewandte Chemie International Edition, 58 (2019) 12185-12189.
[11] A. Dhakshinamoorthy, S. Navalon, A.M. Asiri, H. Garcia, Metal organic frameworks as solid catalysts for liquid-phase continuous flow reactions, Chemical Communications, 56 (2020) 26-45.
[12] A. Dhakshinamoorthy, A.M. Asiri, H. García, Metal–Organic Frameworks as Multifunctional Solid Catalysts, Trends in Chemistry, 2 (2020) 454-466.
[13] R. Haldar, L. Heinke, C. Wöll, Advanced Photoresponsive Materials Using the Metal–Organic Framework Approach, Advanced Materials, n/a (2019) 1905227.
[14] P. Falcaro, R. Ricco, C.M. Doherty, K. Liang, A.J. Hill, M.J. Styles, MOF positioning technology and device fabrication, Chemical Society Reviews, 43 (2014) 5513-5560.
[15] M.W. Logan, S. Langevin, Z. Xia, Reversible Atmospheric Water Harvesting Using Metal-Organic Frameworks, Scientific Reports, 10 (2020) 1492.
[16] K. Biradha, A. Ramanan, J.J. Vittal, Coordination Polymers Versus Metal−Organic Frameworks, Crystal Growth & Design, 9 (2009) 2969-2970.
[17] N. Stock, S. Biswas, Synthesis of Metal-Organic Frameworks (MOFs): Routes to Various MOF Topologies, Morphologies, and Composites, Chemical Reviews, 112 (2012) 933-969.
[18] P. Silva, S.M.F. Vilela, J.P.C. Tomé, F.A. Almeida Paz, Multifunctional metal–organic frameworks: from academia to industrial applications, Chemical Society Reviews, 44 (2015) 6774-6803.
[19] O.M. Yaghi, US Pat., (1997) US5648508A.
[20] O.M. Yaghi, G. Li, H. Li, Selective binding and removal of guests in a microporous metal–organic framework, Nature, 378 (1995) 703-706.
[21] O.M. Yaghi, H. Li, Hydrothermal Synthesis of a Metal-Organic Framework Containing Large Rectangular Channels, Journal of the American Chemical Society, 117 (1995) 10401-10402.
[22] H. Li, M. Eddaoudi, M. O'Keeffe, O.M. Yaghi, Design and synthesis of an exceptionally stable and highly porous metal-organic framework, Nature, 402 (1999) 276-279.
[23] S.S.Y. Chui, S.M.F. Lo, J.P.H. Charmant, A.G. Orpen, I.D. Williams, A Chemically Functionalizable Nanoporous Material [Cu3(TMA)2(H2O)3]n, Science, 283 (1999) 1148.
[24] K. Barthelet, J. Marrot, D. Riou, G. Férey, A Breathing Hybrid Organic–Inorganic Solid with Very Large Pores and High Magnetic Characteristics, Angewandte Chemie International Edition, 41 (2002) 281-284.
[25] C. Serre, F. Millange, C. Thouvenot, M. Noguès, G. Marsolier, D. Louër, G. Férey, Very Large Breathing Effect in the First Nanoporous Chromium(III)-Based Solids: MIL-53 or CrIII(OH)·{O2C−C6H4−CO2}·{HO2C−C6H4−CO2H}x·H2Oy, Journal of the American Chemical Society, 124 (2002) 13519-13526.
[26] J.H. Cavka, S. Jakobsen, U. Olsbye, N. Guillou, C. Lamberti, S. Bordiga, K.P. Lillerud, A New Zirconium Inorganic Building Brick Forming Metal Organic Frameworks with Exceptional Stability, Journal of the American Chemical Society, 130 (2008) 13850-13851.
[27] Y.-Q. Tian, C.-X. Cai, Y. Ji, X.-Z. You, S.-M. Peng, G.-H. Lee, [Co5(im)10·2 MB]∞: A Metal-Organic Open-Framework with Zeolite-Like Topology, Angewandte Chemie International Edition, 41 (2002) 1384-1386.

[28] T. Tsuruoka, S. Furukawa, Y. Takashima, K. Yoshida, S. Isoda, S. Kitagawa, Nanoporous Nanorods Fabricated by Coordination Modulation and Oriented Attachment Growth, Angewandte Chemie International Edition, 48 (2009) 4739-4743.
[29] P. Horcajada, T. Chalati, C. Serre, B. Gillet, C. Sebrie, T. Baati, J.F. Eubank, D. Heurtaux, P. Clayette, C. Kreuz, J.-S. Chang, Y.K. Hwang, V. Marsaud, P.-N. Bories, L. Cynober, S. Gil, G. Férey, P. Couvreur, R. Gref, Porous metal–organic-framework nanoscale carriers as a potential platform for drug delivery and imaging, Nature Materials, 9 (2010) 172-178.
[30] W.J. Rieter, K.M.L. Taylor, H. An, W. Lin, W. Lin, Nanoscale Metal−Organic Frameworks as Potential Multimodal Contrast Enhancing Agents, Journal of the American Chemical Society, 128 (2006) 9024-9025.
[31] W.J. Rieter, K.M. Pott, K.M.L. Taylor, W. Lin, Nanoscale Coordination Polymers for Platinum-Based Anticancer Drug Delivery, Journal of the American Chemical Society, 130 (2008) 11584-11585.
[32] K.K. Tanabe, S.M. Cohen, Postsynthetic modification of metal–organic frameworks—a progress report, Chemical Society Reviews, 40 (2011) 498-519.
[33] O. Shekhah, H.K. Arslan, K. Chen, M. Schmittel, R. Maul, W. Wenzel, C. Wöll, Post-synthetic modification of epitaxially grown, highly oriented functionalized MOF thin films, Chemical Communications, 47 (2011) 11210-11212.
[34] W. Yin, C.-a. Tao, X. Zou, F. Wang, T. Qu, J. Wang, The Tuning of Optical Properties of Nanoscale MOFs-Based Thin Film through Post-Modification, Nanomaterials, 7 (2017) 242.
[35] M.D. Allendorf, A. Schwartzberg, V. Stavila, A.A. Talin, A Roadmap to Implementing Metal–Organic Frameworks in Electronic Devices: Challenges and Critical Directions, Chemistry – A European Journal, 17 (2011) 11372-11388.
[36] J. Liu, C. Wöll, Surface-supported metal–organic framework thin films: fabrication methods, applications, and challenges, Chemical Society Reviews, 46 (2017) 5730-5770.
[37] S. Qiu, M. Xue, G. Zhu, Metal–organic framework membranes: from synthesis to separation application, Chemical Society Reviews, 43 (2014) 6116-6140.
[38] I. Stassen, M. Styles, G. Grenci, Hans V. Gorp, W. Vanderlinden, Steven D. Feyter, P. Falcaro, D.D. Vos, P. Vereecken, R. Ameloot, Chemical vapour deposition of zeolitic imidazolate framework thin films, Nature Materials, 15 (2016) 304-310.
[39] A.M. Spokoyny, D. Kim, A. Sumrein, C.A. Mirkin, Infinite coordination polymer nano- and microparticle structures, Chemical Society Reviews, 38 (2009) 1218-1227.
[40] R. Ameloot, L. Stappers, J. Fransaer, L. Alaerts, B.F. Sels, D.E. De Vos, Patterned Growth of Metal-Organic Framework Coatings by Electrochemical Synthesis, Chemistry of Materials, 21 (2009) 2580-2582.
[41] I. Stassen, D. De Vos, R. Ameloot, Vapor-Phase Deposition and Modification of Metal–Organic Frameworks: State-of-the-Art and Future Directions, Chemistry – A European Journal, 22 (2016) 14452-14460.
[42] R. Ameloot, L. Pandey, M.V.d. Auweraer, L. Alaerts, B.F. Sels, D.E. De Vos, Patterned film growth of metal–organic frameworks based on galvanic displacement, Chemical Communications, 46 (2010) 3735-3737.
[43] S. Hermes, F. Schröder, R. Chelmowski, C. Wöll, R.A. Fischer, Selective Nucleation and Growth of Metal−Organic Open Framework Thin Films on Patterned COOH/CF3-Terminated Self-Assembled Monolayers on Au(111), Journal of the American Chemical Society, 127 (2005) 13744-13745.
[44] Y. Cui, Y. Yue, G. Qian, B. Chen, Luminescent Functional Metal–Organic Frameworks, Chemical Reviews, 112 (2012) 1126-1162.
[45] W.P. Lustig, S. Mukherjee, N.D. Rudd, A.V. Desai, J. Li, S.K. Ghosh, Metal–organic frameworks: functional luminescent and photonic materials for sensing applications, Chemical Society Reviews, 46 (2017) 3242-3285.

[46] L. Armelao, S. Quici, F. Barigelletti, G. Accorsi, G. Bottaro, M. Cavazzini, E. Tondello, Design of luminescent lanthanide complexes: From molecules to highly efficient photo-emitting materials, Coordination Chemistry Reviews, 254 (2010) 487-505.
[47] Y. Cui, J. Zhang, H. He, G. Qian, Photonic functional metal–organic frameworks, Chemical Society Reviews, 47 (2018) 5740-5785.
[48] J. Liu, Z.-D. Luo, Y. Pan, A. Singh, M. Trivedi, A. Kumar, Recent developments in luminescent coordination polymers: Designing strategies, sensing application and theoretical evidences, Coordination Chemistry Reviews, 406 (2019) 213145.
[49] J. Heine, K. Müller-Buschbaum, Engineering metal-based luminescence in coordination polymers and metal–organic frameworks, Chemical Society Reviews, 42 (2013) 9232-9242.
[50] W.P. Lustig, J. Li, Luminescent metal–organic frameworks and coordination polymers as alternative phosphors for energy efficient lighting devices, Coordination Chemistry Reviews, 373 (2018) 116-147.
[51] M.D. Allendorf, C.A. Bauer, R.K. Bhakta, R.J.T. Houk, Luminescent metal–organic frameworks, Chemical Society Reviews, 38 (2009) 1330-1352.
[52] J. Yu, Y. Cui, H. Xu, Y. Yang, Z. Wang, B. Chen, G. Qian, Confinement of pyridinium hemicyanine dye within an anionic metal-organic framework for two-photon-pumped lasing, Nature Communications, 4 (2013) 2719.
[53] J. An, C.M. Shade, D.A. Chengelis-Czegan, S. Petoud, N.L. Rosi, Zinc-Adeninate Metal–Organic Framework for Aqueous Encapsulation and Sensitization of Near-infrared and Visible Emitting Lanthanide Cations, Journal of the American Chemical Society, 133 (2011) 1220-1223.
[54] G. Lu, S. Li, Z. Guo, O.K. Farha, B.G. Hauser, X. Qi, Y. Wang, X. Wang, S. Han, X. Liu, J.S. DuChene, H. Zhang, Q. Zhang, X. Chen, J. Ma, S.C.J. Loo, W.D. Wei, Y. Yang, J.T. Hupp, F. Huo, Imparting functionality to a metal–organic framework material by controlled nanoparticle encapsulation, Nature Chemistry, 4 (2012) 310-316.
[55] K. Binnemans, Lanthanide-Based Luminescent Hybrid Materials, Chemical Reviews, 109 (2009) 4283-4374.
[56] M.-L. Gao, W.-J. Wang, L. Liu, Z.-B. Han, N. Wei, X.-M. Cao, D.-Q. Yuan, Microporous Hexanuclear Ln(III) Cluster-Based Metal–Organic Frameworks: Color Tunability for Barcode Application and Selective Removal of Methylene Blue, Inorganic Chemistry, 56 (2017) 511-517.
[57] L. Liu, X.-N. Zhang, Z.-B. Han, M.-L. Gao, X.-M. Cao, S.-M. Wang, An InIII-based anionic metal–organic framework: sensitization of lanthanide (III) ions and selective absorption and separation of cationic dyes, Journal of Materials Chemistry A, 3 (2015) 14157-14164.
[58] A.A. Godoy, G.E. Gomez, A.M. Kaczmarek, R. Van Deun, O.J. Furlong, F. Gándara, M.A. Monge, M.C. Bernini, G.E. Narda, Sensing properties, energy transfer mechanism and tuneable particle size processing of luminescent two-dimensional rare earth coordination networks, Journal of Materials Chemistry C, 5 (2017) 12409-12421.
[59] C. Daiguebonne, N. Kerbellec, O. Guillou, J.-C. Bünzli, F. Gumy, L. Catala, T. Mallah, N. Audebrand, Y. Gérault, K. Bernot, G. Calvez, Structural and Luminescent Properties of Micro- and Nanosized Particles of Lanthanide Terephthalate Coordination Polymers, Inorganic Chemistry, 47 (2008) 3700-3708.
[60] G.E. Gomez, M.C. Bernini, E.V. Brusau, G.E. Narda, W.A. Massad, A. Labrador, Two Sets of Metal Organic Frameworks along the Lanthanide Series Constructed by 2,3-Dimethylsuccinate: Structures, Topologies, and Strong Emission without Ligand Sensitization, Crystal Growth & Design, 13 (2013) 5249-5260.
[61] G.E. Gomez, M.C. Bernini, E.V. Brusau, G.E. Narda, D. Vega, A.M. Kaczmarek, R. Van Deun, M. Nazzarro, Layered exfoliable crystalline materials based on Sm-, Eu- and Eu/Gd-2-phenylsuccinate frameworks. Crystal structure, topology and luminescence properties, Dalton Transactions, 44 (2015) 3417-3429.
[62] G.E. Gomez, E.V. Brusau, A.M. Kaczmarek, C. Mellot-Draznieks, J. Sacanell, G. Rousse, R. Van Deun, C. Sanchez, G.E. Narda, G.J.A.A. Soler Illia, Flexible Ligand-Based Lanthanide Three-

Dimensional Metal–Organic Frameworks with Tunable Solid-State Photoluminescence and OH-Solvent-Sensing Properties, European Journal of Inorganic Chemistry, 2017 (2017) 2321-2331.
[63] R.G. Denning, Electronic Structure and Bonding in Actinyl Ions and their Analogs, The Journal of Physical Chemistry A, 111 (2007) 4125-4143.
[64] G.E. Gomez, J.A. Ridenour, N.M. Byrne, A.P. Shevchenko, C.L. Cahill, Novel Heterometallic Uranyl-Transition Metal Materials: Structure, Topology, and Solid State Photoluminescence Properties, Inorganic Chemistry, 58 (2019) 7243-7254.
[65] H. Guo, Y. Zhu, S. Qiu, J.A. Lercher, H. Zhang, Coordination Modulation Induced Synthesis of Nanoscale Eu1-xTbx-Metal-Organic Frameworks for Luminescent Thin Films, Advanced Materials, 22 (2010) 4190-4192.
[66] D.-H. Chen, R. Haldar, B.L. Neumeier, Z.-H. Fu, C. Feldmann, C. Wöll, E. Redel, Tunable Emission in Heteroepitaxial Ln-SURMOFs, Advanced Functional Materials, 29 (2019) 1903086.
[67] G.E. Gomez, R.F. D'Vries, D.F. Lionello, L.M. Aguirre-Díaz, M. Spinosa, C.S. Costa, M.C. Fuertes, R.A. Pizarro, A.M. Kaczmarek, J. Ellena, L. Rozes, M. Iglesias, R. Van Deun, C. Sanchez, M.A. Monge, G.J.A.A. Soler-Illia, Exploring physical and chemical properties in new multifunctional indium-, bismuth-, and zinc-based 1D and 2D coordination polymers, Dalton Transactions, 47 (2018) 1808-1818.
[68] R.F. D'Vries, G.E. Gomez, D.F. Lionello, M.C. Fuertes, G.J.A.A. Soler-Illia, J. Ellena, Luminescence, chemical sensing and mechanical properties of crystalline materials based on lanthanide–sulfonate coordination polymers, RSC Advances, 6 (2016) 110171-110181.
[69] Q.-R. Fang, G.-S. Zhu, Z. Jin, Y.-Y. Ji, J.-W. Ye, M. Xue, H. Yang, Y. Wang, S.-L. Qiu, Mesoporous Metal–Organic Framework with Rare etb Topology for Hydrogen Storage and Dye Assembly, Angewandte Chemie International Edition, 46 (2007) 6638-6642.
[70] H. Mieno, R. Kabe, N. Notsuka, M.D. Allendorf, C. Adachi, Long-Lived Room-Temperature Phosphorescence of Coronene in Zeolitic Imidazolate Framework ZIF-8, Advanced Optical Materials, 4 (2016) 1015-1021.
[71] N. Baroni, A. Turshatov, M. Adams, E.A. Dolgopolova, S. Schlisske, G. Hernandez-Sosa, C. Wöll, N.B. Shustova, B.S. Richards, I.A. Howard, Inkjet-Printed Photoluminescent Patterns of Aggregation-Induced-Emission Chromophores on Surface-Anchored Metal–Organic Frameworks, ACS Applied Materials & Interfaces, 10 (2018) 25754-25762.
[72] S. SeethaLekshmi, A.R. Ramya, M.L.P. Reddy, S. Varughese, Lanthanide complex-derived white-light emitting solids: A survey on design strategies, Journal of Photochemistry and Photobiology C: Photochemistry Reviews, 33 (2017) 109-131.
[73] Y. Zhao, Y.-J. Wang, N. Wang, P. Zheng, H.-R. Fu, M.-L. Han, L.-F. Ma, L.-Y. Wang, Tetraphenylethylene-Decorated Metal–Organic Frameworks as Energy-Transfer Platform for the Detection of Nitro-Antibiotics and White-Light Emission, Inorganic Chemistry, 58 (2019) 12700-12706.
[74] M.Y. Masoomi, A. Morsali, A. Dhakshinamoorthy, H. Garcia, Mixed-Metal MOFs: Unique Opportunities in Metal–Organic Framework (MOF) Functionality and Design, Angewandte Chemie International Edition, 58 (2019) 15188-15205.
[75] N. Kerbellec, D. Kustaryono, V. Haquin, M. Etienne, C. Daiguebonne, O. Guillou, An Unprecedented Family of Lanthanide-Containing Coordination Polymers with Highly Tunable Emission Properties, Inorganic Chemistry, 48 (2009) 2837-2843.
[76] X.-L. Qu, B. Yan, Ln(III)-Functionalized Metal–Organic Frameworks Hybrid System: Luminescence Properties and Sensor for trans,trans-Muconic Acid as a Biomarker of Benzene, Inorganic Chemistry, 57 (2018) 7815-7824.
[77] C.D.S. Brites, P.P. Lima, N.J.O. Silva, A. Millán, V.S. Amaral, F. Palacio, L.D. Carlos, Thermometry at the nanoscale, Nanoscale, 4 (2012) 4799-4829.
[78] V.B. Mykhaylyk, A. Wagner, H. Kraus, Non-contact luminescence lifetime cryothermometry for macromolecular crystallography, Journal of Synchrotron Radiation, 24 (2017) 636-645.

[79] C.D.S. Brites, P.P. Lima, N.J.O. Silva, A. Millán, V.S. Amaral, F. Palacio, L.D. Carlos, A Luminescent Molecular Thermometer for Long-Term Absolute Temperature Measurements at the Nanoscale, Advanced Materials, 22 (2010) 4499-4504.
[80] S.A. Wade, S.F. Collins, G.W. Baxter, Fluorescence intensity ratio technique for optical fiber point temperature sensing, Journal of Applied Physics, 94 (2003) 4743-4756.
[81] Y. Cui, H. Xu, Y. Yue, Z. Guo, J. Yu, Z. Chen, J. Gao, Y. Yang, G. Qian, B. Chen, A Luminescent Mixed-Lanthanide Metal–Organic Framework Thermometer, Journal of the American Chemical Society, 134 (2012) 3979-3982.
[82] G.E. Gomez, A.M. Kaczmarek, R. Van Deun, E.V. Brusau, G.E. Narda, D. Vega, M. Iglesias, E. Gutierrez-Puebla, M.Á. Monge, Photoluminescence, Unconventional-Range Temperature Sensing, and Efficient Catalytic Activities of Lanthanide Metal–Organic Frameworks, European Journal of Inorganic Chemistry, 2016 (2016) 1577-1588.
[83] X. Rao, T. Song, J. Gao, Y. Cui, Y. Yang, C. Wu, B. Chen, G. Qian, A Highly Sensitive Mixed Lanthanide Metal–Organic Framework Self-Calibrated Luminescent Thermometer, Journal of the American Chemical Society, 135 (2013) 15559-15564.
[84] Y. Cui, W. Zou, R. Song, J. Yu, W. Zhang, Y. Yang, G. Qian, A ratiometric and colorimetric luminescent thermometer over a wide temperature range based on a lanthanide coordination polymer, Chemical Communications, 50 (2014) 719-721.
[85] Y. Cui, R. Song, J. Yu, M. Liu, Z. Wang, C. Wu, Y. Yang, Z. Wang, B. Chen, G. Qian, Dual-Emitting MOF⊃Dye Composite for Ratiometric Temperature Sensing, Advanced Materials, 27 (2015) 1420-1425.
[86] A. Cadiau, C.D.S. Brites, P.M.F.J. Costa, R.A.S. Ferreira, J. Rocha, L.D. Carlos, Ratiometric Nanothermometer Based on an Emissive Ln3+-Organic Framework, ACS Nano, 7 (2013) 7213-7218.
[87] Z. Wang, D. Ananias, A. Carné-Sánchez, C.D.S. Brites, I. Imaz, D. Maspoch, J. Rocha, L.D. Carlos, Lanthanide–Organic Framework Nanothermometers Prepared by Spray-Drying, Advanced Functional Materials, 25 (2015) 2824-2830.
[88] M. Ren, C.D.S. Brites, S.-S. Bao, R.A.S. Ferreira, L.-M. Zheng, L.D. Carlos, A cryogenic luminescent ratiometric thermometer based on a lanthanide phosphonate dimer, Journal of Materials Chemistry C, 3 (2015) 8480-8484.
[89] R.F. D'Vries, S. Álvarez-García, N. Snejko, L.E. Bausá, E. Gutiérrez-Puebla, A. de Andrés, M.Á. Monge, Multimetal rare earth MOFs for lighting and thermometry: tailoring color and optimal temperature range through enhanced disulfobenzoic triplet phosphorescence, Journal of Materials Chemistry C, 1 (2013) 6316-6324.
[90] K. Miyata, Y. Konno, T. Nakanishi, A. Kobayashi, M. Kato, K. Fushimi, Y. Hasegawa, Chameleon Luminophore for Sensing Temperatures: Control of Metal-to-Metal and Energy Back Transfer in Lanthanide Coordination Polymers, Angewandte Chemie International Edition, 52 (2013) 6413-6416.
[91] Y. Zhou, B. Yan, F. Lei, Postsynthetic lanthanide functionalization of nanosized metal–organic frameworks for highly sensitive ratiometric luminescent thermometry, Chemical Communications, 50 (2014) 15235-15238.
[92] S.-N. Zhao, L.-J. Li, X.-Z. Song, M. Zhu, Z.-M. Hao, X. Meng, L.-L. Wu, J. Feng, S.-Y. Song, C. Wang, H.-J. Zhang, Lanthanide Ion Codoped Emitters for Tailoring Emission Trajectory and Temperature Sensing, Advanced Functional Materials, 25 (2015) 1463-1469.
[93] Y. Wei, R. Sa, Q. Li, K. Wu, Highly stable and sensitive LnMOF ratiometric thermometers constructed with mixed ligands, Dalton Transactions, 44 (2015) 3067-3074.
[94] X. Shen, Y. Lu, B. Yan, Lanthanide Complex Hybrid System for Fluorescent Sensing as Thermometer, European Journal of Inorganic Chemistry, 2015 (2015) 916-919.
[95] Y. Zhou, B. Yan, Ratiometric detection of temperature using responsive dual-emissive MOF hybrids, Journal of Materials Chemistry C, 3 (2015) 9353-9358.

[96] X. Liu, S. Akerboom, M.d. Jong, I. Mutikainen, S. Tanase, A. Meijerink, E. Bouwman, Mixed-Lanthanoid Metal–Organic Framework for Ratiometric Cryogenic Temperature Sensing, Inorganic Chemistry, 54 (2015) 11323-11329.
[97] B. Chen, L. Wang, F. Zapata, G. Qian, E.B. Lobkovsky, A Luminescent Microporous Metal−Organic Framework for the Recognition and Sensing of Anions, Journal of the American Chemical Society, 130 (2008) 6718-6719.
[98] Y. Yu, J.-P. Ma, Y.-B. Dong, Luminescent humidity sensors based on porous Ln3+-MOFs, CrystEngComm, 14 (2012) 7157-7160.
[99] W.-G. Lu, L. Jiang, X.-L. Feng, T.-B. Lu, Three-Dimensional Lanthanide Anionic Metal−Organic Frameworks with Tunable Luminescent Properties Induced by Cation Exchange, Inorganic Chemistry, 48 (2009) 6997-6999.
[100] H. Xu, X. Rao, J. Gao, J. Yu, Z. Wang, Z. Dou, Y. Cui, Y. Yang, B. Chen, G. Qian, A luminescent nanoscale metal–organic framework with controllable morphologies for spore detection, Chemical Communications, 48 (2012) 7377-7379.
[101] J.-H. Wei, J.-W. Yi, M.-L. Han, B. Li, S. Liu, Y.-P. Wu, L.-F. Ma, D.-S. Li, A Water-Stable Terbium(III)–Organic Framework as a Chemosensor for Inorganic Ions, Nitro-Containing Compounds and Antibiotics in Aqueous Solutions, Chemistry – An Asian Journal, 14 (2019) 3694-3701.
[102] C.-X. Yu, F.-L. Hu, J.-G. Song, J.-L. Zhang, S.-S. Liu, B.-X. Wang, H. Meng, L.-L. Liu, L.-F. Ma, Ultrathin two-dimensional metal-organic framework nanosheets decorated with tetra-pyridyl calix[4]arene: Design, synthesis and application in pesticide detection, Sensors and Actuators B: Chemical, 310 (2020) 127819.
[103] S. Pramanik, C. Zheng, X. Zhang, T.J. Emge, J. Li, New Microporous Metal−Organic Framework Demonstrating Unique Selectivity for Detection of High Explosives and Aromatic Compounds, Journal of the American Chemical Society, 133 (2011) 4153-4155.
[104] Z. Hu, B.J. Deibert, J. Li, Luminescent metal–organic frameworks for chemical sensing and explosive detection, Chemical Society Reviews, 43 (2014) 5815-5840.
[105] J.C. Sanchez, W.C. Trogler, Efficient blue-emitting silafluorene–fluorene-conjugated copolymers: selective turn-off/turn-on detection of explosives, Journal of Materials Chemistry, 18 (2008) 3143-3156.
[106] G.E. Gomez, M. Dos Santos Afonso, H.A. Baldoni, F. Roncaroli, G.J.A.A. Soler-Illia, Luminescent Lanthanide Metal Organic Frameworks as Chemosensing Platforms towards Agrochemicals and Cations, Sensors (Basel), 19 (2019) 1260.
[107] C.Tao, J. Wang, R. Chen, Metal Organic Frameworks-Based Optical Thin Films, Multilayer Thin Films - Versatile Applications for Materials Engineering, IntechOpen (2020).
[108] G. Lu, J.T. Hupp, Metal−Organic Frameworks as Sensors: A ZIF-8 Based Fabry−Pérot Device as a Selective Sensor for Chemical Vapors and Gases, Journal of the American Chemical Society, 132 (2010) 7832-7833.
[109] Z. Hu, C.-a. Tao, H. Liu, X. Zou, H. Zhu, J. Wang, Fabrication of an NH2-MIL-88B photonic film for naked-eye sensing of organic vapors, Journal of Materials Chemistry A, 2 (2014) 14222-14227.
[110] A. Dhakshinamoorthy, Z. Li, H. Garcia, Catalysis and photocatalysis by metal organic frameworks, Chemical Society Reviews, 47 (2018) 8134-8172.
[111] M.C. Bernini, G.E. Gomez, E.V. Brusau, G.E. Narda, Reviewing Rare Earth Succinate Frameworks from the Reticular Chemistry Point of View: Structures, Nets, Catalytic and Photoluminescence Applications, Israel Journal of Chemistry, 58 (2018) 1044-1061.
[112] T. Zhang, W. Lin, Metal–organic frameworks for artificial photosynthesis and photocatalysis, Chemical Society Reviews, 43 (2014) 5982-5993.
[113] A. Dhakshinamoorthy, A.M. Asiri, H. García, Metal–Organic Framework (MOF) Compounds: Photocatalysts for Redox Reactions and Solar Fuel Production, Angewandte Chemie International Edition, 55 (2016) 5414-5445.

[114] X. Yu, L. Wang, S.M. Cohen, Photocatalytic metal–organic frameworks for organic transformations, CrystEngComm, 19 (2017) 4126-4136.
[115] A. Dhakshinamoorthy, A.M. Asiri, H. Garcia, 2D Metal–Organic Frameworks as Multifunctional Materials in Heterogeneous Catalysis and Electro/Photocatalysis, Advanced Materials, 31 (2019) 1900617.
[116] C.-C. Wang, J.-R. Li, X.-L. Lv, Y.-Q. Zhang, G. Guo, Photocatalytic organic pollutants degradation in metal–organic frameworks, Energy & Environmental Science, 7 (2014) 2831-2867.
[117] A.A. Talin, A. Centrone, A.C. Ford, M.E. Foster, V. Stavila, P. Haney, R.A. Kinney, V. Szalai, F. El Gabaly, H.P. Yoon, F. Léonard, M.D. Allendorf, Tunable Electrical Conductivity in Metal-Organic Framework Thin-Film Devices, Science, 343 (2014) 66.
[118] Y. Horiuchi, T. Toyao, M. Takeuchi, M. Matsuoka, M. Anpo, Recent advances in visible-light-responsive photocatalysts for hydrogen production and solar energy conversion – from semiconducting TiO2 to MOF/PCP photocatalysts, Physical Chemistry Chemical Physics, 15 (2013) 13243-13253.
[119] W. Wang, X. Xu, W. Zhou, Z. Shao, Recent Progress in Metal-Organic Frameworks for Applications in Electrocatalytic and Photocatalytic Water Splitting, Advanced Science, 4 (2017) 1600371.
[120] Q.-L. Zhu, Q. Xu, Metal–organic framework composites, Chemical Society Reviews, 43 (2014) 5468-5512.
[121] J.-D. Xiao, L. Han, J. Luo, S.-H. Yu, H.-L. Jiang, Integration of Plasmonic Effects and Schottky Junctions into Metal–Organic Framework Composites: Steering Charge Flow for Enhanced Visible-Light Photocatalysis, Angewandte Chemie International Edition, 57 (2018) 1103-1107.
[122] H. Luo, Z. Zeng, G. Zeng, C. Zhang, R. Xiao, D. Huang, C. Lai, M. Cheng, W. Wang, W. Xiong, Y. Yang, L. Qin, C. Zhou, H. Wang, Y. Zhou, S. Tian, Recent progress on metal-organic frameworks based- and derived-photocatalysts for water splitting, Chemical Engineering Journal, 383 (2020) 123196.
[123] H.-F. Wang, L. Chen, H. Pang, S. Kaskel, Q. Xu, MOF-derived electrocatalysts for oxygen reduction, oxygen evolution and hydrogen evolution reactions, Chemical Society Reviews, 49 (2020) 1414-1448.
[124] C. Guizard, A. Princivalle, Preparation and characterization of catalyst thin films, Catalysis Today, 146 (2009) 367-377.
[125] Q. Zuo, T. Liu, C. Chen, Y. Ji, X. Gong, Y. Mai, Y. Zhou, Ultrathin Metal–Organic Framework Nanosheets with Ultrahigh Loading of Single Pt Atoms for Efficient Visible-Light-Driven Photocatalytic H2 Evolution, Angewandte Chemie International Edition, 58 (2019) 10198-10203.
[126] G. Paille, M. Gomez-Mingot, C. Roch-Marchal, M. Haouas, Y. Benseghir, T. Pino, M.-H. Ha-Thi, G. Landrot, P. Mialane, M. Fontecave, A. Dolbecq, C. Mellot-Draznieks, Thin Films of Fully Noble Metal-Free POM@MOF for Photocatalytic Water Oxidation, ACS Applied Materials & Interfaces, 11 (2019) 47837-47845.
[127] S. Fang, Y.H. Hu, Recent progress in photocatalysts for overall water splitting, International Journal of Energy Research, 43 (2019) 1082-1098.
[128] G. Paille, M. Gomez-Mingot, C. Roch-Marchal, B. Lassalle-Kaiser, P. Mialane, M. Fontecave, C. Mellot-Draznieks, A. Dolbecq, A Fully Noble Metal-Free Photosystem Based on Cobalt-Polyoxometalates Immobilized in a Porphyrinic Metal–Organic Framework for Water Oxidation, Journal of the American Chemical Society, 140 (2018) 3613-3618.
[129] Y.-J. Dong, J.-F. Liao, Z.-C. Kong, Y.-F. Xu, Z.-J. Chen, H.-Y. Chen, D.-B. Kuang, D. Fenske, C.-Y. Su, Conformal coating of ultrathin metal-organic framework on semiconductor electrode for boosted photoelectrochemical water oxidation, Applied Catalysis B: Environmental, 237 (2018) 9-17.

[130] H. Song, Z. Sun, Y. Xu, Y. Han, J. Xu, J. Wu, T. Sun, H. Meng, X. Zhang, Fabrication of NH2-MIL-125(Ti) incorporated TiO2 nanotube arrays composite anodes for highly efficient PEC water splitting, Separation and Purification Technology, 228 (2019) 115764.
[131] S. Zhou, K. Chen, J. Huang, L. Wang, M. Zhang, B. Bai, H. Liu, Q. Wang, Preparation of heterometallic CoNi-MOFs-modified BiVO4: a steady photoanode for improved performance in photoelectrochemical water splitting, Applied Catalysis B: Environmental, 266 (2020) 118513.
[132] L. Zhang, P. Cui, H. Yang, J. Chen, F. Xiao, Y. Guo, Y. Liu, W. Zhang, F. Huo, B. Liu, Metal–Organic Frameworks as Promising Photosensitizers for Photoelectrochemical Water Splitting, Advanced Science, 3 (2016) 1500243.
[133] Q. Zhang, H. Wang, Y. Dong, J. Yan, X. Ke, Q. Wu, S. Xue, In situ growth of ultrathin Co-MOF nanosheets on α-Fe2O3 hematite nanorods for efficient photoelectrochemical water oxidation, Solar Energy, 171 (2018) 388-396.
[134] Z. Peng, S.C. Abbas, J. Lv, R. Yang, M. Wu, Y. Wang, Mixed-metal organic framework-coated ZnO nanowires array for efficient photoelectrochemical water oxidation, International Journal of Hydrogen Energy, 44 (2019) 2446-2453.
[135] H. Yang, J. Bright, S. Kasani, P. Zheng, T. Musho, B. Chen, L. Huang, N. Wu, Metal–organic framework coated titanium dioxide nanorod array p–n heterojunction photoanode for solar water-splitting, Nano Research, 12 (2019) 643-650.
[136] G. Liu, Y. Li, Y. Xiao, D. Jia, C. Li, J. Zheng, X. Liu, Nanoporous Fe-doped BiVO4 Modified with MIL-53 (Fe) for Enhanced Photoelectrochemical Stability and Water Splitting Perfromances, Catalysis Letters, 149 (2019) 870-875.
[137] K. Natarajan, A.K. Gupta, S.N. Ansari, M. Saraf, S.M. Mobin, Mixed-Ligand-Architected 2D Co(II)-MOF Expressing a Novel Topology for an Efficient Photoanode for Water Oxidation Using Visible Light, ACS Applied Materials & Interfaces, 11 (2019) 13295-13303.
[138] B. Zhang, G. Dong, L. Wang, Y. Zhang, Y. Ding, Y. Bi, Efficient hydrogen production from MIL-53(Fe) catalyst-modified Mo:BiVO4 photoelectrodes, Catalysis Science & Technology, 7 (2017) 4971-4976.
[139] J.W. Yoon, D.H. Kim, J.-H. Kim, H.W. Jang, J.-H. Lee, NH2-MIL-125(Ti)/TiO2 nanorod heterojunction photoanodes for efficient photoelectrochemical water splitting, Applied Catalysis B: Environmental, 244 (2019) 511-518.
[140] W. Cui, H. Bai, K. Qu, F. Wang, P. Guan, D. Xu, W. Fan, W. Shi, In Situ Decorating Coordinatively Unsaturated Fe Sites for Boosting Water Oxidation Performance of TiO2 Photoanode, Energy Technology, 7 (2019) 1801128.
[141] L. Li, H. Zhang, C. Liu, P. Liang, N. Mitsuzaki, Z. Chen, Effect of Co-Based Metal–Organic Framework Prepared by an In Situ Growth Method on the Photoelectrochemical Performance of Electrodeposited Hematite Photoanode, Energy Technology, 7 (2019) 1801069.
[142] I. Roger, M.A. Shipman, M.D. Symes, Earth-abundant catalysts for electrochemical and photoelectrochemical water splitting, Nature Reviews Chemistry, 1 (2017) 0003.
[143] C.A. Downes, S.C. Marinescu, Efficient Electrochemical and Photoelectrochemical H2 Production from Water by a Cobalt Dithiolene One-Dimensional Metal–Organic Surface, Journal of the American Chemical Society, 137 (2015) 13740-13743.
[144] T. He, S. Chen, B. Ni, Y. Gong, Z. Wu, L. Song, L. Gu, W. Hu, X. Wang, Zirconium–Porphyrin-Based Metal–Organic Framework Hollow Nanotubes for Immobilization of Noble-Metal Single Atoms, Angewandte Chemie International Edition, 57 (2018) 3493-3498.
[145] R. Ifraemov, R. Shimoni, W. He, G. Peng, I. Hod, A metal–organic framework film with a switchable anodic and cathodic behaviour in a photo-electrochemical cell, Journal of Materials Chemistry A, 7 (2019) 3046-3053.
[146] Z. Luo, T. Wang, J. Gong, Single-crystal silicon-based electrodes for unbiased solar water splitting: current status and prospects, Chemical Society Reviews, 48 (2019) 2158-2181.
[147] N. Corbin, J. Zeng, K. Williams, K. Manthiram, Heterogeneous molecular catalysts for electrocatalytic CO2 reduction, Nano Research, 12 (2019) 2093-2125.

[148] S. Wang, X. Wang, Multifunctional Metal–Organic Frameworks for Photocatalysis, Small, 11 (2015) 3097-3112.
[149] Z. Huang, P. Dong, Y. Zhang, X. Nie, X. Wang, X. Zhang, A ZIF-8 decorated TiO2 grid-like film with high CO2 adsorption for CO2 photoreduction, Journal of CO2 Utilization, 24 (2018) 369-375.
[150] H.-J. Son, S. Jin, S. Patwardhan, S.J. Wezenberg, N.C. Jeong, M. So, C.E. Wilmer, A.A. Sarjeant, G.C. Schatz, R.Q. Snurr, O.K. Farha, G.P. Wiederrecht, J.T. Hupp, Light-Harvesting and Ultrafast Energy Migration in Porphyrin-Based Metal–Organic Frameworks, Journal of the American Chemical Society, 135 (2013) 862-869.
[151] C.-C. Chueh, C.-I. Chen, Y.-A. Su, H. Konnerth, Y.-J. Gu, C.-W. Kung, K.C.W. Wu, Harnessing MOF materials in photovoltaic devices: recent advances, challenges, and perspectives, Journal of Materials Chemistry A, 7 (2019) 17079-17095.
[152] B. O'Regan, M. Grätzel, A low-cost, high-efficiency solar cell based on dye-sensitized colloidal TiO2 films, Nature, 353 (1991) 737-740.
[153] N.A. Karim, U. Mehmood, H.F. Zahid, T. Asif, Nanostructured photoanode and counter electrode materials for efficient Dye-Sensitized Solar Cells (DSSCs), Solar Energy, 185 (2019) 165-188.
[154] A. Gu, W. Xiang, T. Wang, S. Gu, X. Zhao, Enhance photovoltaic performance of tris(2,2'-bipyridine) cobalt(II)/(III) based dye-sensitized solar cells via modifying TiO2 surface with metal-organic frameworks, Solar Energy, 147 (2017) 126-132.
[155] E.D. Spoerke, L.J. Small, M.E. Foster, J. Wheeler, A.M. Ullman, V. Stavila, M. Rodriguez, M.D. Allendorf, MOF-Sensitized Solar Cells Enabled by a Pillared Porphyrin Framework, The Journal of Physical Chemistry C, 121 (2017) 4816-4824.
[156] J. Liu, W. Zhou, J. Liu, I. Howard, G. Kilibarda, S. Schlabach, D. Coupry, M. Addicoat, S. Yoneda, Y. Tsutsui, T. Sakurai, S. Seki, Z. Wang, P. Lindemann, E. Redel, T. Heine, C. Wöll, Photoinduced Charge-Carrier Generation in Epitaxial MOF Thin Films: High Efficiency as a Result of an Indirect Electronic Band Gap?, Angewandte Chemie International Edition, 54 (2015) 7441-7445.
[157] W.A. Maza, A.J. Haring, S.R. Ahrenholtz, C.C. Epley, S.Y. Lin, A.J. Morris, Ruthenium(ii)-polypyridyl zirconium(iv) metal–organic frameworks as a new class of sensitized solar cells, Chemical Science, 7 (2016) 719-727.
[158] M.A. Gordillo, D.K. Panda, S. Saha, Efficient MOF-Sensitized Solar Cells Featuring Solvothermally Grown [100]-Oriented Pillared Porphyrin Framework-11 Films on ZnO/FTO Surfaces, ACS Applied Materials & Interfaces, 11 (2019) 3196-3206.
[159] A. Kojima, K. Teshima, Y. Shirai, T. Miyasaka, Organometal Halide Perovskites as Visible-Light Sensitizers for Photovoltaic Cells, Journal of the American Chemical Society, 131 (2009) 6050-6051.
[160] P. Roy, N. Kumar Sinha, S. Tiwari, A. Khare, A review on perovskite solar cells: Evolution of architecture, fabrication techniques, commercialization issues and status, Solar Energy, 198 (2020) 665-688.
[161] Y. Dong, J. Zhang, Y. Yang, L. Qiu, D. Xia, K. Lin, J. Wang, X. Fan, R. Fan, Self-Assembly of Hybrid Oxidant POM@Cu-BTC for Enhanced Efficiency and Long-Term Stability of Perovskite Solar Cells, Angewandte Chemie International Edition, 58 (2019) 17610-17615.
[162] L. Huang, X. Zhou, R. Wu, C. Shi, R. Xue, J. Zou, C. Xu, J. Zhao, W. Zeng, Oriented haloing metal-organic framework providing high efficiency and high moisture-resistance for perovskite solar cells, Journal of Power Sources, 433 (2019) 226699.
[163] C.-C. Lee, C.-I. Chen, Y.-T. Liao, K.C.W. Wu, C.-C. Chueh, Enhancing Efficiency and Stability of Photovoltaic Cells by Using Perovskite/Zr-MOF Heterojunction Including Bilayer and Hybrid Structures, Advanced Science, 6 (2019) 1801715.
[164] U. Ryu, S. Jee, J.-S. Park, I.K. Han, J.H. Lee, M. Park, K.M. Choi, Nanocrystalline Titanium Metal–Organic Frameworks for Highly Efficient and Flexible Perovskite Solar Cells, ACS Nano, 12 (2018) 4968-4975.

[165] M. Urbani, G. de la Torre, M.K. Nazeeruddin, T. Torres, Phthalocyanines and porphyrinoid analogues as hole- and electron-transporting materials for perovskite solar cells, Chemical Society Reviews, 48 (2019) 2738-2766.
[166] Z. Yu, A. Hagfeldt, L. Sun, The application of transition metal complexes in hole-transporting layers for perovskite solar cells: Recent progress and future perspectives, Coordination Chemistry Reviews, 406 (2020) 213143.
[167] M. Li, D. Xia, Y. Yang, X. Du, G. Dong, A. Jiang, R. Fan, Doping of [In2(phen)3Cl6]·CH3CN·2H2O Indium-Based Metal–Organic Framework into Hole Transport Layer for Enhancing Perovskite Solar Cell Efficiencies, Advanced Energy Materials, 8 (2018) 1800552.
[168] J. Liu, W. Zhou, J. Liu, Y. Fujimori, T. Higashino, H. Imahori, X. Jiang, J. Zhao, T. Sakurai, Y. Hattori, W. Matsuda, S. Seki, S.K. Garlapati, S. Dasgupta, E. Redel, L. Sun, C. Wöll, A new class of epitaxial porphyrin metal–organic framework thin films with extremely high photocarrier generation efficiency: promising materials for all-solid-state solar cells, Journal of Materials Chemistry A, 4 (2016) 12739-12747.
[169] D.Y. Ahn, D.Y. Lee, C.Y. Shin, H.T. Bui, N.K. Shrestha, L. Giebeler, Y.-Y. Noh, S.-H. Han, Novel Solid-State Solar Cell Based on Hole-Conducting MOF-Sensitizer Demonstrating Power Conversion Efficiency of 2.1%, ACS Applied Materials & Interfaces, 9 (2017) 12930-12935.
[170] S.D. Stranks, G.E. Eperon, G. Grancini, C. Menelaou, M.J.P. Alcocer, T. Leijtens, L.M. Herz, A. Petrozza, H.J. Snaith, Electron-Hole Diffusion Lengths Exceeding 1 Micrometer in an Organometal Trihalide Perovskite Absorber, Science, 342 (2013) 341.
[171] M. Adams, M. Kozlowska, N. Baroni, M. Oldenburg, R. Ma, D. Busko, A. Turshatov, G. Emandi, M.O. Senge, R. Haldar, C. Wöll, G.U. Nienhaus, B.S. Richards, I.A. Howard, Highly Efficient One-Dimensional Triplet Exciton Transport in a Palladium–Porphyrin-Based Surface-Anchored Metal–Organic Framework, ACS Applied Materials & Interfaces, 11 (2019) 15688-15697.
[172] X. Liu, M. Kozlowska, T. Okkali, D. Wagner, T. Higashino, G. Brenner-Weiß, S.M. Marschner, Z. Fu, Q. Zhang, H. Imahori, S. Bräse, W. Wenzel, C. Wöll, L. Heinke, Photoconductivity in Metal–Organic Framework (MOF) Thin Films, Angewandte Chemie International Edition, 58 (2019) 9590-9595.
[173] Z. You, H. Li, L. Zhang, B. Yu, J. Zhang, X. Wu, A Host Material for Deep-Blue Electrophosphorescence Based on a Cuprous Metal–Organic Framework, The Journal of Physical Chemistry C, 121 (2017) 23072-23079.
[174] H. Kaur, S. Sundriyal, V. Pachauri, S. Ingebrandt, K.-H. Kim, A.L. Sharma, A. Deep, Luminescent metal-organic frameworks and their composites: Potential future materials for organic light emitting displays, Coordination Chemistry Reviews, 401 (2019) 213077.
[175] G. Haider, M. Usman, T.-P. Chen, P. Perumal, K.-L. Lu, Y.-F. Chen, Electrically Driven White Light Emission from Intrinsic Metal–Organic Framework, ACS Nano, 10 (2016) 8366-8375.
[176] T. Mondal, S. Mondal, S. Bose, D. Sengupta, U.K. Ghorai, S.K. Saha, Pure white light emission from a rare earth-free intrinsic metal–organic framework and its application in a WLED, Journal of Materials Chemistry C, 6 (2018) 614-621.
[177] J.A. do Nascimento Neto, A.K.S.M. Valdo, C.C. da Silva, F.F. Guimarães, L.H.K. Queiroz Júnior, L.J.Q. Maia, R.C. de Santana, F.T. Martins, A Blue-Light-Emitting Cadmium Coordination Polymer with 75.4% Photoluminescence Quantum Yield, Journal of the American Chemical Society, 141 (2019) 3400-3403.
[178] L.R. Mingabudinova, V.V. Vinogradov, V.A. Milichko, E. Hey-Hawkins, A.V. Vinogradov, Metal–organic frameworks as competitive materials for non-linear optics, Chemical Society Reviews, 45 (2016) 5408-5431.
[179] T.N. Nguyen, F.M. Ebrahim, K.C. Stylianou, Photoluminescent, upconversion luminescent and nonlinear optical metal-organic frameworks: From fundamental photophysics to potential applications, Coordination Chemistry Reviews, 377 (2018) 259-306.

[180] R. Medishetty, J.K. Zaręba, D. Mayer, M. Samoć, R.A. Fischer, Nonlinear optical properties, upconversion and lasing in metal–organic frameworks, Chemical Society Reviews, 46 (2017) 4976-5004.
[181] D.C. Mayer, A. Manzi, R. Medishetty, B. Winkler, C. Schneider, G. Kieslich, A. Pöthig, J. Feldmann, R.A. Fischer, Controlling Multiphoton Absorption Efficiency by Chromophore Packing in Metal–Organic Frameworks, Journal of the American Chemical Society, 141 (2019) 11594-11602.
[182] J.K. Zaręba, M. Nyk, J. Janczak, M. Samoć, Three-Photon Absorption of Coordination Polymer Transforms UV-to-VIS Thermometry into NIR-to-VIS Thermometry, ACS Applied Materials & Interfaces, 11 (2019) 10435-10441.
[183] Z. Chen, G. Gallo, V.A. Sawant, T. Zhang, M. Zhu, L. Liang, A. Chanthapally, G. Bolla, H.S. Quah, X. Liu, K.P. Loh, R.E. Dinnebier, Q.-H. Xu, J.J. Vittal, Giant Enhancement of Second Harmonic Generation Accompanied by the Structural Transformation of 7-Fold to 8-Fold Interpenetrated Metal–Organic Frameworks (MOFs), Angewandte Chemie International Edition, 59 (2020) 833-838.
[184] M. Liu, H.S. Quah, S. Wen, Z. Yu, J.J. Vittal, W. Ji, Efficient Third Harmonic Generation in a Metal–Organic Framework, Chemistry of Materials, 28 (2016) 3385-3390.
[185] R. Antoine, Atomically precise clusters of gold and silver: A new class of nonlinear optical nanomaterials, Frontier Research Today, 1 (2018) 1001.
[186] P. Liu, Q. Liu, N. Zhao, C. An, Z. Lian, Structure and third-order nonlinear optical properties of the two-dimensional CoII coordination polymer [Co(1,2-BIB)(PA)]n {1,2-BIB is 1,2-bis[(1H-imidazol-1-yl)methyl]benzene and H2PA is phthalic acid}, Acta Crystallographica Section C, 72 (2016) 890-894.
[187] R.-Q. Liu, N. Zhao, F.-X. Yang, A.-R. Wang, P. Liu, C.-X. An, Z.-X. Lian, Enhanced third-order nonlinear optical properties of three 2D coordination polymers based on bis(imidazole) ligands and dicarboxylic ligands, Polyhedron, 111 (2016) 16-25.
[188] J. Yu, Y. Cui, C.-D. Wu, Y. Yang, B. Chen, G. Qian, Two-Photon Responsive Metal–Organic Framework, Journal of the American Chemical Society, 137 (2015) 4026-4029.
[189] Q.-C. Sun, Y.C. Ding, D.M. Sagar, P. Nagpal, Photon upconversion towards applications in energy conversion and bioimaging, Progress in Surface Science, 92 (2017) 281-316.
[190] X.-Z. Song, S.-Y. Song, H.-J. Zhang, Luminescent Lanthanide Metal–Organic Frameworks, 2014, pp. 109-144.
[191] M. Oldenburg, A. Turshatov, D. Busko, S. Wollgarten, M. Adams, N. Baroni, A. Welle, E. Redel, C. Wöll, B.S. Richards, I.A. Howard, Photon Upconversion at Crystalline Organic–Organic Heterojunctions, Advanced Materials, 28 (2016) 8477-8482.
[192] S. Ahmad, J. Liu, C. Gong, J. Zhao, L. Sun, Photon Up-Conversion via Epitaxial Surface-Supported Metal–Organic Framework Thin Films with Enhanced Photocurrent, ACS Applied Energy Materials, 1 (2018) 249-253.
[193] Y. Liu, H. Dong, K. Wang, Z. Gao, C. Zhang, X. Liu, Y.S. Zhao, F. Hu, Suppressing Nonradiative Processes of Organic Dye with Metal–Organic Framework Encapsulation toward Near-Infrared Solid-State Microlasers, ACS Applied Materials & Interfaces, 10 (2018) 35455-35461.
[194] H. He, H. Li, Y. Cui, G. Qian, MOF-Based Organic Microlasers, Advanced Optical Materials, 7 (2019) 1900077.
[195] H. He, E. Ma, Y. Cui, J. Yu, Y. Yang, T. Song, C.-D. Wu, X. Chen, B. Chen, G. Qian, Polarized three-photon-pumped laser in a single MOF microcrystal, Nature Communications, 7 (2016) 11087.
[196] Y. Lv, Z. Xiong, Z. Yao, Y. Yang, S. Xiang, Z. Zhang, Y.S. Zhao, Steric-Hindrance-Controlled Laser Switch Based on Pure Metal–Organic Framework Microcrystals, Journal of the American Chemical Society, 141 (2019) 19959-19963.
[197] M.-M. Russew, S. Hecht, Photoswitches: From Molecules to Materials, Advanced Materials, 22 (2010) 3348-3360.

[198] A. Schneemann, V. Bon, I. Schwedler, I. Senkovska, S. Kaskel, R.A. Fischer, Flexible metal–organic frameworks, Chemical Society Reviews, 43 (2014) 6062-6096.
[199] L. Heinke, C. Wöll, Surface-Mounted Metal–Organic Frameworks: Surface-Mounted Metal–Organic Frameworks: Crystalline and Porous Molecular Assemblies for Fundamental Insights and Advanced Applications (Adv. Mater. 26/2019), Advanced Materials, 31 (2019) 1970184.
[200] S. Garg, H. Schwartz, M. Kozlowska, A.B. Kanj, K. Müller, W. Wenzel, U. Ruschewitz, L. Heinke, Conductance Photoswitching of Metal–Organic Frameworks with Embedded Spiropyran, Angewandte Chemie International Edition, 58 (2019) 1193-1197.
[201] Z. Zhang, K. Müller, S. Heidrich, M. Koenig, T. Hashem, T. Schlöder, D. Bléger, W. Wenzel, L. Heinke, Light-Switchable One-Dimensional Photonic Crystals Based on MOFs with Photomodulatable Refractive Index, The Journal of Physical Chemistry Letters, 10 (2019) 6626-6633.
[202] Q. Xu, L. Zhang, J. Yu, S. Wageh, A.A. Al-Ghamdi, M. Jaroniec, Direct Z-scheme photocatalysts: Principles, synthesis, and applications, Materials Today, 21 (2018) 1042-1063.

MOFs consist in metallic ions bridged by organic ligands generating porous structures

Their properties can be tuned by ligand design and metallic ion selection

MOF films exhibit unique properties allowing the fabrication of devices

Latest results on sensing, catalylsis, photovoltaics, up conversion and LED fabrication

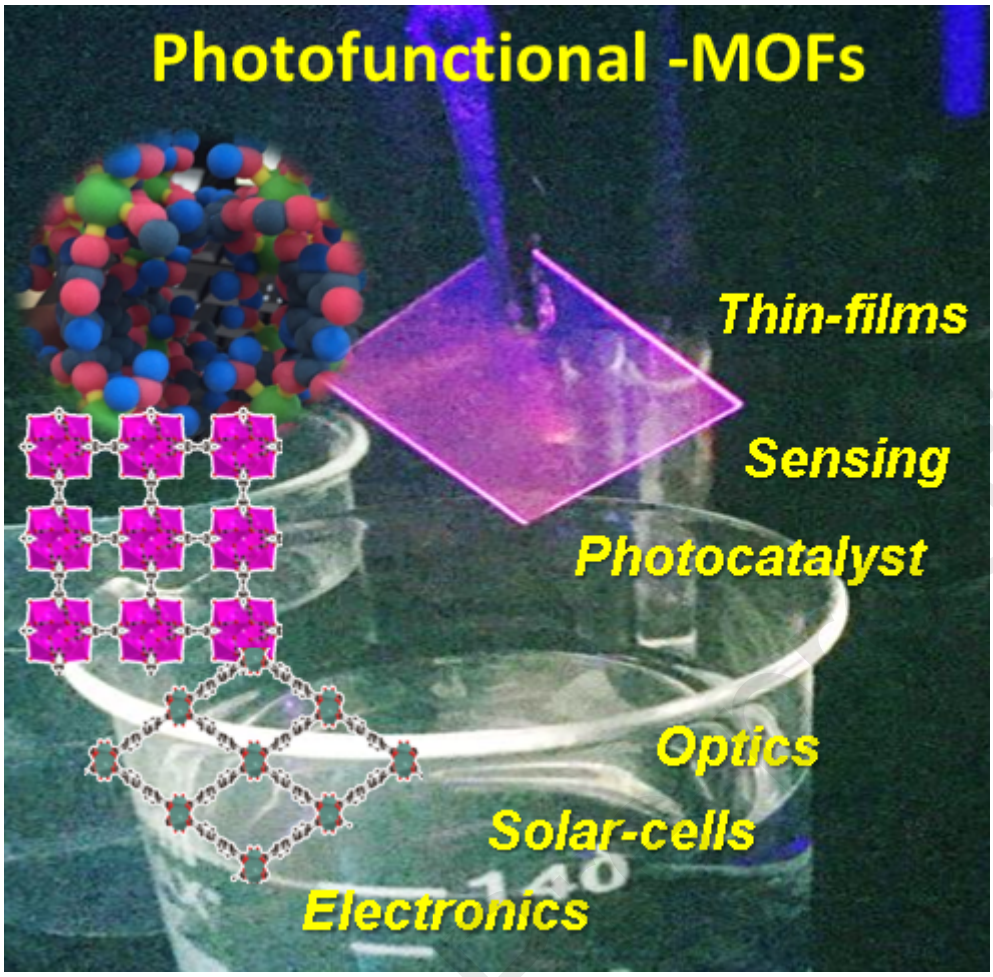

Dr. Germán E. Gomez completed his Ph.D in Chemistry at Universidad Nacional de San Luis (UNSL) in research topics related to study Lanthanide-MOFs with luminescent and catalytic properties with the supervision of Dra. Griselda Narda and Dra. Elena Brusau. After that, he made postdoc stays in Nano-Chemistry group in CAC-CNEA (2015-2017, at the Dr. G. J. A. A. Soler-Illia group), College de France (2016, Dr. Clément Sanchez group) and Ghent University (2016, Dr. R. van Deun group) studying MOFs for chemical and thermal sensing. In 2018 he joined the group of Prof. C. Cahill at George Washington University as a Fulbright fellow, for the development of actinide MOFs. Also, in 2018 he visited the group of Prof. Muralee Murugesu in Ottawa University to work in the project “MOFs and MMPFs for opto/magnetic applications”. In 2019 Gomez made a SURMOF research in Karlsruhe Institution of Technology (KIT) with the supervision of Dr. Christof Wöll. Nowadays

Gomez is researcher of CONICET in INTEQUI (UNSL) for the research of MOFs for sensing, photoluminescence and photocatalysis fields.

Dr. Federico Roncaroli graduated as a chemist in 2000 at the University of Buenos Aires (Argentina), where he obtained a PhD (2004) studying the reactivity and spectroscopic properties of metal–nitrosyl complexes under the direction of Professor José Olabe. In 2005 he was awarded a *Dr. rer. nat.* at the Universty of Erlangen-Nürnberg (Germany), working on the reactions of nitric oxide with biologically relevant models, under the supervision of Professor Rudi van Eldik. After post doctoral work in the Commission for Atomic Energy of Argentina (CNEA) with Professor Miguel Blesa, he obtained a postdoctoral fellowship from the Alexander von Humboldt foundation, to perform pulse EPR studies on Hydrogenases, at the Max Plank Institute for Chemical Energy Conversion under the supervision of Professor Wolfgang Lubitz. Since 2013 FR is researcher of CONICET at CNEA. His current interests are application of MOFs to sustainable energy conversion and storage.

Declaration of interests

X The authors declare that they have no known competing financial interests or personal relationships that could have appeared to influence the work reported in this paper.

☐The authors declare the following financial interests/personal relationships which may be considered as potential competing interests:

Dr Federico Roncaroli and Dr Germán E. Gomez